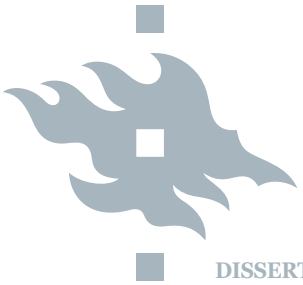

DISSERTATIONES SCHOLAE DOCTORALIS AD SANITATEM INVESTIGANDAM
UNIVERSITATIS HELSINKIENSIS

18/2018

PATRICK VINGADAS ALMEIDA

Multifunctional Porous Silicon Based Nanocomposites for Cancer Targeting and Drug Delivery

DRUG RESEARCH PROGRAM
DIVISION OF PHARMACEUTICAL CHEMISTRY AND TECHNOLOGY
FACULTY OF PHARMACY
DOCTORAL PROGRAMME IN DRUG RESEARCH
UNIVERSITY OF HELSINKI

Division of Pharmaceutical Chemistry and Technology
Faculty of Pharmacy
University of Helsinki
Finland

Multifunctional Porous Silicon Based Nanocomposites for Cancer Targeting and Drug Delivery

by

Patrick Vingadas Almeida

ACADEMIC DISSERTATION

To be presented, with the permission of the Faculty of Pharmacy of the University of Helsinki, for public examination in Auditorium 1, Infocenter Korona (Viikinkaari 11, Helsinki), on 6th of April 2018, at 12:00 noon.

Helsinki 2018

Supervisors

Associate Professor Dr. Hélder A. Santos
Drug Research Program
Faculty of Pharmacy
University of Helsinki
Finland

Professor and Dean Dr. Jouni Hirvonen
Drug Research Program
Faculty of Pharmacy
University of Helsinki
Finland

Reviewers

Professor Dr. Caitriona O'Driscoll
School of Pharmacy
University College Cork
Ireland

Dr. Frédérique Cunin
Advanced Materials for Catalysis and Health
Institute Charles Gerhardt Montpellier
France

Opponent

Professor Dr. Tambet Teesalu
Institute of Biomedicine and Translational Medicine
University of Tartu
Estonia

ISBN 978-951-51-4149-1 (Paperback)
ISBN 978-951-51-4150-7 (PDF)
ISSN 2342-3161 (Print)
ISSN 2342-317X (Online)

Helsinki University Printing House
Helsinki 2018

Abstract

Recent breakthroughs in nanotechnology have paved the way for a new era in cancer medicine. Among the myriad of nanotechnology-based systems that have been revolutionizing the field of cancer nanomedicine, porous silicon (PSi) nanoparticles have recently emerged as a promising nanoplatform, owing to advantageous physicochemical and biological properties. Nevertheless, the successful establishment of PSi nanoparticulate systems as effective cancer nanomedicines is challenged by several shortcomings associated with the instability in biological fluids, the poor tumour targeting efficiency and unfavourable pharmacokinetics, the limited capacity to overcome extra and intracellular biological barriers, and the ubiquitous and uncontrolled release of the therapeutic payloads.

This dissertation aimed at designing and developing novel strategies, including the surface modification of PSi nanoparticles with biofunctional polymers and the engineering of advanced multifunctional PSi-based nanocomposites, in order to overcome some of the aforementioned deadlocks, improving the tumour targeting and drug delivery efficiencies, and ultimately potentiating the application of PSi nanomaterials in cancer nanomedicine.

First, the biofunctionalization of PSi nanoparticles with a hyaluronic acid (HA) derivative was proven to improve the colloidal and plasma stabilities and to significantly enhance the cellular internalization of the nanosystems in breast cancer cells. The HA-modified PSi nanoplatforms exhibited higher affinity and endocytic activity in the cells overexpressing the CD44 receptor, thus evidencing a great potential for further development as active targeted drug delivery systems to CD44-overexpressing tumours.

Next, a bilayered zwitterionic PSi nanocomposite was fabricated by successive conjugation of poly(ethyleneimine) and poly(methyl vinyl ether-*alt*-maleic acid) polymers on the surface of PSi nanoparticles. In addition to satisfactory cytocompatibility, and high colloidal and plasma stabilities, the designed polymeric surface modification was shown to enhance the non-specific cellular association and uptake, and to improve the intracellular trafficking of the PSi nanoparticles in breast cancer cells. Moreover, this strategy contributed to increase the drug loading of methotrexate (MTX), sustain the release of the drug and potentiate the *in vitro* antiproliferative effect of the MTX-loaded PSi nanocarriers.

In addition, PSi nanoplatforms were used to engineer multifunctional PSi-based nanocomposites, envisioned for cancer therapeutic and theranostic applications. In one approach, both sorafenib-loaded PSi and gold nanoparticles were simultaneously encapsulated into a self-assembling polymeric nanocomplex. In another study, the same nanocomplexes were used to encapsulate DNA-capped PSi nanoparticles, as an innovative strategy to bioresponsively deliver hydrophilic and hydrophobic drug molecules into the cytosolic compartment of cancer cells. The potential of the fabricated multifunctional PSi-based nanocomposites stemmed from the versatility to incorporate a combination of nanosystems, hydrophilic or hydrophobic drug molecules, and fluorescent dyes within a single nanostructure, and the capability to enhance the cellular interactions, endocytosis and cytoplasmic delivery of the encapsulated nanoparticles and therapeutics.

In conclusion, the developed PSi-based nanocomposites exhibited great potential for cancer targeting and drug delivery, representing an advanced contribution for the successful implementation of PSi nanomaterials as the next generation of cancer nanomedicines.

Acknowledgements

First of all, I acknowledge the Doctoral Program in Drug Research of the University of Helsinki for granting me the opportunity to pursue my doctoral studies in this prestigious University. The scientific work of this dissertation was carried out at the Division of Pharmaceutical Chemistry and Technology, Faculty of Pharmacy, University of Helsinki, during the years 2013–2018. In addition, I acknowledge all the funding sources that financially supported this work and that allowed me to participate and present my research in national and international conferences and scientific meetings, namely the Finnish Cultural Foundation, the European Research Council under the European Union's Seventh Framework Programme, the University of Helsinki Research Funds, the Doctoral School in Health Sciences, and the Finnish Pharmaceutical Society.

I express my deepest gratitude to my main supervisor, Associate Professor Dr. Hélder A. Santos. I usually say that I have the best supervisor one could ever wish for, but the truth is that you are and have always been much more than a supervisor, and no words can fairly express how grateful I am for everything you have done for me. As a scientist, your ambition, enthusiasm, passion and dedication to science are a true source of inspiration for me. As a supervisor, your constant guidance and support, endless patience and encouragement, and belief in my capacities have always kept me moving forward when I most doubted of myself and, without you, none of these accomplishments would have been possible. As a friend, your kindness, support, comprehension and positive attitude have helped me overcoming some of the most difficult phases of my life and largely contributed for the person I am today. I dedicate this thesis to my family and, therefore, also to you, as part of it.

I extend my sincerest gratefulness to my supervisor, Professor and Dean Dr. Jouni Hirvonen, not only for giving me the opportunity to join this outstanding research team and to pursue my doctoral studies at this prestigious institution, but also for his inestimable and unwavering scientific contribution for this work. Dear Professor, it has been an hounour and privilege to have been supervised by you, and I will always be grateful for your kindheartedness, your positive and joyful attitude, your words of support and understanding, and all the enthusiasm you have always demonstrated towards my achievements.

A special acknowledgment is dedicated to all the co-authors and collaborators, for their invaluable help and scientific input, productive cooperation, and sharing of knowledge and expertise, which represents one the basal stones of this research work and this dissertation. In particular, I would like to thank Professor Dr. Jarno Salonen, Ermei Mäkilä and Dr. Martti Kaasalainen for our fruitful collaboration and discussions that were fundamental for this work, as well as for the numerous scientific and non-scientific encounters, conversations and moments of laughter.

I extend my honest gratitude to Dr. Richard Harbottle and all the group members of the DNA Vector Lab at the German Cancer Research Center (DKFZ) in Heidelberg, for our collaboration and for giving me the opportunity to join and pursue my future scientific career in this fantastic research group. Thank you all for sharing your scientific knowledge and expertise with me, for your support, motivation, enthusiasm demonstrated towards my research, and, most of all, for your warm welcome and great friendship.

I sincerely acknowledge Professor Dr. Catriona O'Driscoll (University of Cork, Ireland) and Dr. Frédérique Cunin (Institute Charles Gerhardt Montpellier, France) for reviewing this work and providing their positive, valuable and constructive comments, which greatly helped me to improve this thesis. A word of appreciation is also given to Adjunct Professor Dr. Vincenzo Cerullo and Adjunct Professor Dr. Tapani Viitala for accepting the invitation to constitute the Grading Committee of this doctoral dissertation.

I am also endlessly thankful to all my friends and colleagues from the Division of Pharmaceutical Chemistry and Technology, not only for providing me the best working environment and unreservedly sharing their knowledge, but also for their friendship, their countless words of motivation, their thoughtfulness, the unforgettable moments we have shared and the everlasting memories we have created. I would like to specially thank (in alphabetical order), Alexandra Correia, Dr. Antti Rahikkala, Dr. Bárbara Herranz-Blanco, Dr. Dongfei Liu, Eloy Ginestar, Flavia Fontana, Dr. Francisca Araújo, Jernej Štukelj, João Pedro Martins, Dr. Jukka Saarinen, Dr. Mohammad-Ali Shahbazi, Dr. Mónica Ferreira, Dr. Neha Shrestha, Patrícia Figueiredo, Dr. Sami Svanbäck, Tomás Ramos, and Dr. Vimalkumar Balasubramanian. Alexandra, your dedication to work is unbelievable and also reflected in this thesis. Thank you for your kindness, and for all the help and assistance throughout these years. Jukka, you have the two sides of a coin. On one side, the shyness, calmness, and trustfulness, typical of a Finn. On the other side, the contagious passion and excitement for everything that thrills you, being science, music or running. Thank you for sharing both sides with me, for all the kilometres we ran, in the darkness, rain, snow and ice, and all the conversations that came along. Ali, I cannot find words to express how important you have been in my life. You were my closest colleague, my right arm throughout my studies, an example of a scientist that I look up to, and one of the persons that contributed the most for the realization of this thesis. Although I miss you deeply since you left Finland, you have always been a constant presence in my life and you have shown me that our friendship is boundless in space and time. Thank you Ali, for everything. I have started this long journey of higher education ten years ago and, Mónica, you have been there since the very first day. Thank you for everything you have always done for me, for your friendship and words of encouragement, and for contributing so much for the person I am today. Some people pass through our lives and take peace of us. Some people pass and leave a peace of themselves. And some people simply do not pass, but remain forever. João, Sami and Tomás, you are those people, my best friends. I cannot thank you enough for everything you guys did for me in the past years, for your friendship, your kindheartedness, for the countless moments of laughter, hilarity, and tears of joy and sadness. You have always been there to listen to me, to help me, to encourage me, but also to bring me to my senses and reason when I was terribly wrong. You will always have a place in my heart and in my life.

I extend my gratitude to all my friends in Helsinki, particularly to Dr. Elisa Lazaro-Ibañes, Riccardo Provenzani and Miia Viinamäki for their friendship and for all the moments we spent together. I also thank all the members of my handball team, HC Kiffen, for their spirit of camaraderie, their friendship, the way they integrated me as a foreigner in their core. It was in handball that many times I sought refuge and abstracted myself from my daily problems and the stressful life of a doctoral student.

In the last phase of my doctoral studies, I travelled to Heidelberg, Germany, for a research visit and it was there that I found some of the greatest people I have ever met. Margareta, João, Verónica, Manuel, Márcia, Oriana, Gonçalo, Vanessa, Francisco, Ana Marta, and also Martin and Paul from Munich, I feel so grateful for having met all of you. Thank you for your friendship, for pushing me forward and for the motivation you gave me, for making me feel like Germany can be my next home, and for the numerous happy moments that I am so much looking forward to multiply in the near future.

I could not finish these acknowledgements without expressing my deepest gratefulness to my family for everything they have done for me my entire life, for their unconditional love and support, and for being the best family in the world. First, I leave a special word of gratitude to my cousin Sérgio Almeida, for being my partner in Finland, for everything we shared while living together, for his patience and support, for all the moments of laughter, and for standing by my side through some of the happiest and toughest moments I had during these past years in Finland. I extend my sincerest thankfulness to my cousin Joel Esteves. "O gajo não fala" ("The dude doesn't talk") is one of the infinite episodes that marked our childhood. The "dude" wished, at this moment, to find words that describe the importance you have in his life. We grew up together, you were there since I can remember, we became men side by side, you are my older brother and my best friend, and you will forever be. Nico, my little brother, you are the most precious person I have in my life. Despite your young age, your maturity, sense of responsibility, tenderness and capacity to overcome every single obstacle in life are a true source of admiration and inspiration for me. I am absolutely certain that you will accomplish everything in your life, if you keep on fighting as you always do. "However far way, I will always love you", little brother. I am forever indebted to my parents, António and Ustilina. Pai, Mãe, lembram-se quando sempre me diziam que um dia vos iria agradecer? Pois, eu acho que nunca vou encontrar forma de vos demonstrar o quão eternamente grato sou por tudo o que fizeram por mim toda a minha, pelo vosso infinito amor e apoio, e pelos valores familiares e de educação que sempre me incutiram. É a vós quem devo tudo o que sou e sempre serei. To my entire family, my grandparents, uncles and cousins. Minha família, nunca vou conseguir agradecer por tudo o que sempre fizeram por mim e por fazerem de mim o homem que sou hoje. Vocês são o pilar da minha vida e é a todos vós que dedico esta tese de Doutoramento.

Last, but not least, I express my deepest gratitude and love to my beloved Martina, my girlfriend, mein bester Freund, meine Liebe. You entered my life when I less expected and, since the very first day, you have always stood by my side, giving me your hand when I most needed. I would not be in the privileged position of writing these final words if it was not for you, and you cannot imagine how blessed and grateful I feel for having found you and for everything you brought into my life. Your constant beautiful smile, your endless patience and support, and your unconditional love have been essential and have pushed me to the finish line of this long journey. "Happiness is only real when shared", and there is no better person in the world with whom I could share this and all the happiness of my life.

Helsinki, April 2018.

Patrick Vingadas Almeida

"*Every mountain top is within reach if you just keep climbing*" – Barry Finlay

To my family

Table of contents

List of original publications

This thesis is based on the following publications, which are referred to in the text by their respective roman numerals (**I–IV**):

I **Almeida P.A.**, Shahbazi M.A., Mäkilä E., Kaasalainen M., Salonen J., Hirvonen J., Santos H.A., 2014. Amine-modified hyaluronic acid-functionalized porous silicon nanoparticles for breast cancer targeting. Nanoscale, 6: 10377–10387.

II Shahbazi M.A., **Almeida, P.V.**, Mäkilä E., Kaasalainen M., Salonen J., Hirvonen J., Santos H.A., 2014. Augmented cellular trafficking and endosomal escape of porous silicon nanoparticles via zwitterionic bilayer polymer surface engineering. Biomaterials, 35: 7488–7500.

III **Almeida P.V.***, Shahbazi M.A.*, Correia A., Mäkilä E., Kemell M., Salonen J., Hirvonen J., Santos H.A., 2017. A multifunctional nanocomplex for enhanced cell uptake, endosomal escape and improved cancer therapeutic effect. Nanomedicine (Lond.), 12: 1401–1420.

IV Shahbazi M.A., **Almeida P.V.**, Correia A., Herranz-Blanco B., Shrestha N., Mäkilä E., Salonen J., Hirvonen J., Santos H.A., 2017. Intracellular responsive dual delivery by endosomolytic polyplexes carrying DNA anchored porous silicon nanoparticles. Journal of Controlled Release, 249: 111−122.

*In publication **III**, the first two authors contributed equally to the work.

List of additional publications

The list below presents additional publications, which are not included in the experimental section of this thesis:

1. Shahbazi, M.A., Hamidi, M., Mäkilä, E., Zhang, H., **Almeida, P.V.**, Salonen, J., Hirvonen, J., Santos, H.A., 2013. The mechanisms of surface chemistry effects of mesoporous silicon nanoparticles on immunotoxicity and biocompatibility. Biomaterials, 34(31): 7776−7789.

2. Shahbazi, M.A., **Almeida, P.V.**, Mäkilä, E., Kaasalainen, M., Salonen, J., Hirvonen, J., Santos, H.A., 2014. Poly(methyl vinyl ether–co–maleic acid) conjugated to porous silicon nanoparticles for enhanced stability and internalization. Macromol. Rapid Comm., 35(6): 624–629.

3. Mori, M., **Almeida, P.V.**, Cola, M., Anselmi, G., Mäkilä, E., Correia, A., Salonen, J., Hirvonen, J., Caramella, C., Santos, H.A., 2014. *In vitro* assessment of biopolymer-modified porous silicon microparticles for wound healing applications. Eur. J. Pharm. Biopharm., 88(3): 635–642.

4. Ferreira, M.P., Ranjan, S., Correia, A., Mäkilä, E., Kinnunen, S.M., Zhang, H., Shahbazi, M.A., **Almeida, P.V.**, Salonen, J., Ruskoaho, H.J., Airaksinen, A.J., Hirvonen, J., Santos, H.A., 2016. *In vitro* and *in vivo* assessment of heart-homing porous silicon nanoparticles, Biomaterials, 94: 93–104.

5. Balasubramanian, V., Herranz-Blanco, B., **Almeida, P.V.**, Hirvonen, J., Santos, H.A., 2016. Multifaceted polymersome platforms: spanning from self-assembly to drug delivery and protocells. Prog. Polym. Sci., 60: 51–85.

6. Santos, H.A., Mäkilä, E., Bimbo, L.M., **Almeida, P.V.**, Hirvonen, J., 2013. Porous silicon nanoparticles for biomedical imaging and drug delivery. In: Fundamentals of Pharmaceutical Nanoscience, I.J. Uchegbu (Ed.), Springer Science + Business Media, 235–275.

7. Zhang, H., Shahbazi, M.A., **Almeida, P.V.**, Santos, H.A., 2014. Mucus as a barrier for biopharmaceuticals and drug delivery systems. In: Mucosal Delivery of Biopharmaceuticals: Biology, Challenges and Strategies, B. Sarmento and J. das Neves (Eds.), Springer Science + Business Media, 59–97.

8. Ferreira, M.P., **Almeida, P.V.**, Shahbazi, M.A., Correia, A., Santos, H.A., 2015. Chapter 5: Current trends and developments for nanotechnology in cancer. In: Biomedical Chemistry: Current Trends and Developments, N. Vale (Ed.), De Gruyter Open, 290–342.

Abbreviations and symbols

AcDex	Acetalated dextran
AF488	Alexa Fluor® 488
APSTCPSi	3-aminopropyltrietoxysilane modified TCPSi
ATR	Attenuated total reflectance
Au	Gold
BET	Brunauer-Emmett-Teller
CPP	L-cysteine-poly(ethylenimine)-poly(methyl vinyl ether-*alt*-maleic acid)
DAPI	4',6-diamidino-2-phenylindole
DCs	Dendritic cells
DLS	Dynamic light scattering
DIPA	*N*-ethyldiisopropylamine
DMEM	Dulbecco's Modified Eagle's Medium
DMSO	Dimethylsulfoxide
DOX	Doxorubicin
D-PBS	Dulbecco's phosphate buffered saline
ECM	Extracellular matrix
EDC	1-ethyl-3-[3-dimethylaminopropyl]carbodiimide
EDTA	Ethylenediaminetetraacetic acid
EDX	Energy dispersive X-ray
ELS	Electrophoretic light scattering
EPR	Enhanced permeation and retention
FBS	Fetal bovine serum
FDA	Food and Drug Administration
FITC	Fluorescein isothiocyanate
FTIR	Fourier transform infrared
GALA	Glutamic acid-alanine-leucine-alanine
GI	Gastrointestinal
GSH	Glutathione
HA	Hyaluronic acid
HA^+	Amine modified hyaluronic acid
HA2	Influenza virus hemagglutinin 2
HBSS	Hank's balanced salt solution
HCl	Hydrochloric acid
HEPES	4(-2-hydroxyethyl)-1-piperazineethanesulfonic acid
HF	Hydrofluoric acid
HGP	HIV gp41-derived peptide
HIV	Human immunodeficiency virus
HPLC	High pressure liquid chromatography
IFP	Interstitial fluid pressure

iRGD	Internalizing RGD
L240	Papilloma virus L2 minor capsid protein-derived peptide
LD	Loading degree
MAA	Maleic acid amide
MDGI	Mammary-derived growth inhibitor
MDR	Multidrug resistance
MeOH	Methanol
MES	2-(*N*-morpholino)ethanesulfonic acid
MPS	Mononuclear phagocytic system
miRNA	microRNA
MTX	Methotrexate
MTX@UnP	MTX-loaded UnP
MTX@UnPP	MTX-loaded UnPP
MTX@UnTHCSi	MTX-loaded UnTHCPSi
NaCac	Sodium cacodylate buffer
NaOH	Sodium hydroxide
NEAA	Non-essential amino acids
NHS	*N*-hydroxysuccinimide
PAA	Poly(aminoamide)
PBS	Phosphate buffer solution
PdI	Polydispersity index
PEG	Polyethylene glycol
PEI	Poly(ethylenimine)
PFA	Paraformaldehyde
PK	Pharmacokinetics
PMVE-MA	Poly(methyl vinyl ether-*alt*-maleic acid)
PMVE-MAh	Poly(methyl vinyl ether-*alt*-maleic anhydrate)
PSi	Porous silicon
Pt	Platinum
PTX	Paclitaxel
RBCs	Red blood cells
RES	Reticuloendothelial system
RGD	Arginine-glycine-aspartic acid sequence
RNAi	RNA interference
RPMI	Roswell Park Memorial Institute
SEM	Scanning electron microscopy
SFB	Sorafenib
SFB@UnTHCSi	SFB-loaded UnTHCPSi
SFB@UnCPP	SFB-loaded UnCPP
SFB@UnAuCPP	SFB-loaded UnAuCPP
Si	Silicon
siRNA	Small interfering RNA

SPECT/CT	Single photon emission computed tomography
SPION	Superparamagnetic iron oxide nanoparticle
SSC	Side scatter
Sulfo-NHS	Sulfo-*N*-hydroxysulfosuccinimide
TAT	HIV transactivator of transcription
TB	Trypan blue
TCPSi	Thermally carbonized porous silicon
TEM	Transmission electron microscopy
TFA	Trifluoroacetic acid
THCPSi	Thermally hydrocarbonized porous silicon
TOPSi	Thermally oxidized porous silicon
TME	Tumor microenvironment
UnAuCPP	UnTHCPSi and Au nanoparticles encapsulated in CPP
UnC	UnTHCPSi-cystine
UnCA	UnTHCPSi-cystine-acridine
UnCAD	UnTHCPSi-cystine-acridine-DNA
UnCAD@CPP	UnCAD nanoparticles encapsulated in CPP
UnCPP	UnTHCPSi nanoparticles encapsulated in CPP
$UnHA^+$	UnTHCPSi-HA^+
UnP	UnTHCPSi-PEI
UnPP	UnTHCPSi-PEI-PMVE-MA
UnTHCPSi	Undecylenic acid modified THCPSi
WHO	World Health Organization
ζ	Zeta

1 Introduction

Cancer still stands as a global burden and one of the leading causes of morbidity and mortality worldwide. The World Health Organization (WHO) estimated that 32.6 million cases, 14.1 million new cancer cases and 8.2 million cancer deaths occurred globally in the year 2012.[1] The same demographic and epidemiologic report pointed out to lung cancer as the most frequent and mortal cancer in both men and women, owing to the high fatality rate, followed by breast cancer as the second most common cancer overall. Although breast cancer presents a substantially higher incidence in women comparatively to other cancer sites, its mortality rate is significantly lower due to the relatively favourable prognosis. Colorectal, prostate, stomach and liver cancers complete the list of six cancer types with higher incidence, which represent more than 50% of the global burden.[1]

In general, cancer defines a group of diseases that progressively evolve from the initial genetic mutation of normal cells into tumorigenic cells, which are characterized by a rapid and uncontrolled proliferation, ultimately leading to the formation of a malignant tumour. In advanced pathological stages, some malignant cells can acquire the capacity to penetrate the lymphatic or blood circulation and, consequently, invade and replicate in other organs, originating secondary or metastatic tumours.[2] The multistage and complex process of tumour pathogenesis is highly dependent on the interaction between individual's factors (*i.e.*, genetic factors and ageing), lifestyle factors (*e.g.*, nutrition, tobacco consumption and physical activity), and the exposure to external factors, including physical (*e.g.*, ultraviolet and ionizing irradiation), chemical (*e.g.*, asbestos, food and water contaminants) and biological (*e.g.*, viral, bacterial and parasitic infections) carcinogenic agents. Therefore, modifying or avoiding these risk factors can contribute to a significant reduction of the cancer incidence and prevalence. In addition, the screening and early diagnosis of cancer can play a determinant role on treatment's response and effectiveness and, consequently, on the patient survival rates and reduction of the global burden of cancer.[3]

The current clinical treatment of cancer diseases generally relies on local interventions, including surgery and radiotherapy, chemotherapy, alternative therapeutic approaches, such as targeted therapy and immunotherapy, or a combination of these therapeutic modalities. In principle, the administration of potent chemotherapeutic regimens to oncological patients can have effective therapeutic outcomes on tumour ablation, by pharmacologically targeting the molecular mechanisms and hallmark capabilities of mutant cells involved in the tumorigenic process.[2] However, the non-specific delivery and ubiquitous biodistribution of the chemotherapeutic drugs also induces cytotoxicity to normal cells, consequently resulting in severe damages on healthy tissues and organs, and deleterious adverse effects to the patients. Another complication arising from multiple chemotherapeutic cycles, which may significantly impair the therapeutic efficacy of anticancer drugs, is the development of multidrug resistance (MDR) mechanisms by the tumour cells.[4,5] A common approach to overcome cancer MDR, while maximizing the efficacy and minimizing the off-target side effects of chemotherapy, consisting on the combined administration of anticancer drugs with complementary mechanisms of action.[6,7] In addition, from the perspective of pharmaceutical development, the formulation and delivery of chemotherapeutics to the pharmacological target in the optimal dose range, can be considerably challenged by the intrinsic

physicochemical properties of these drug molecules, particularly when considered for combination chemotherapy. On one hand, the majority of drugs currently in clinical use or in drug development for cancer treatment are hydrophobic, thus presenting low solubility and tendency to aggregate in the aqueous biological fluids and, consequently, requiring the use of organic solvents to solubilize them prior to administration.[8,9] On the other hand, hydrophilic drug molecules, including biomacromolecules (*e.g.*, peptides, proteins and nucleic acids), suffer from limited capacity to overcome biological barriers, lability to proteolytic and hydrolytic degradation and short circulatory half-life.[10] Therefore, there is demanding need to develop new therapeutic approaches that circumvent the abovementioned inherent limitations of conventional chemotherapeutic drug formulations.

Recent exciting breakthroughs in nanotechnology have promised to revolutionize the current paradigms of cancer therapy and diagnostics, paving the way for a new era in cancer medicine.[11-14] In fact, a first generation of cancer nanomedicines has already been approved for clinical use, while numerous others are currently under clinical or pre-clinical evaluation, with successful outcomes expected in a foreseeable future.[14,15] In general, the tremendous potential of cancer nanomedicine stems from: (1) improving the therapeutic index of therapeutics by maximizing the efficacy and/or mitigating the toxicity; (2) refining the intrinsic properties of drug molecules, such as solubility, stability, and blood circulation half-life; (3) enhancing the delivery of the therapeutic drugs and biomacromolecules to the intracellular site of action at increased dose; (3) targeting the delivery of therapeutics to specific tissues, cells or intracellular compartments; (4) enabling a controlled, sustained and/or stimuli-responsive drug release; (5) co-delivering multiple drugs for combination therapy with individual spatiotemporal control over the drug release profiles, significantly improving the therapeutic efficacy and overcoming MDR; (6) increasing the sensitivity of cancer diagnostic and imaging agents; and (7) integrating both drug molecules and imaging agents into a single platform for simultaneous therapeutic and diagnostic modalities (*i.e.*, theranostics) and/or for the real-time readout of the therapeutic efficacy.[13,14]

Over the past few decades, porous silicon (PSi) nanoparticles have been highlighted and demonstrating tremendous potential for biomedical applications, with particular focus on cancer nanomedicine, owing to the remarkable and unique physicochemical and biological features.[16-21] In addition to a high biocompatibility and tuneable biodegradability,[22-24] PSi nanoparticles are characterized by a sponge-like architecture with high surface-to-volume ratio, large pore volume and surface area, and controllable pore size that allows the high loading of diverse therapeutic drug molecules and biomolecules within the porous structure.[16,17,25] Moreover, these nanomaterials present high mechanical, chemical and thermal stabilities, and surface chemical versatility, enabling the straightforward functionalization with biofunctional polymers and biomolecules for controlling the release profiles of the therapeutic payloads, targeting specific organs, tissues and cells, and/or improving the biological performance.[19,26-30] However, the successful implementation of PSi nanoparticulate systems as effective nanoplatforms for cancer medicine is still hindered by several drawbacks related to (i) the intrinsic instability in aqueous environments and biological fluids, (ii) the poor tumour targeting efficiency and unfavourable pharmacokinetic (PK) profiles, (iii) the limited capability to overcome extra

and intracellular biological barriers, and (iv) the premature and uncontrolled release of the therapeutic cargos.

This dissertation contemplates the design and development of new strategies, including the surface modification of PSi nanoparticles with biofunctional polymers and the engineering of advanced multifunctional PSi-based nanocomposites, aiming at circumventing some of the abovementioned bottlenecks inherent to PSi nanomaterials, improving the tumour targeting and drug delivery efficiencies, and ultimately potentiating the application of PSi nanoplatforms in cancer nanomedicine.

2 Review of the literature

2.1 Clinical advances in cancer nanomedicine

The recent advances in the field of nanotechnology and significant progresses in fundamental cancer research have led to an increasing interest from both the academic and industrial sectors on developing novel nanotechnology-based tools for cancer biomedical applications (**Figure 1**). As an outcome of this joint effort, a first generation of nanomedicines have successfully been approved for clinical use in cancer therapy and diagnostics (**Table 1**).[14,15] Furthermore, a vast pipeline of other promising nanotechnology-based formulations is currently under clinical evaluation for a wide range of cancer therapeutic modalities, including non-targeted, targeted, stimuli-responsive and combinatorial chemotherapy, hyperthermia, radiotherapy, gene or RNA interference (RNAi) therapy and immunotherapy (**Table 2**).[14,15]

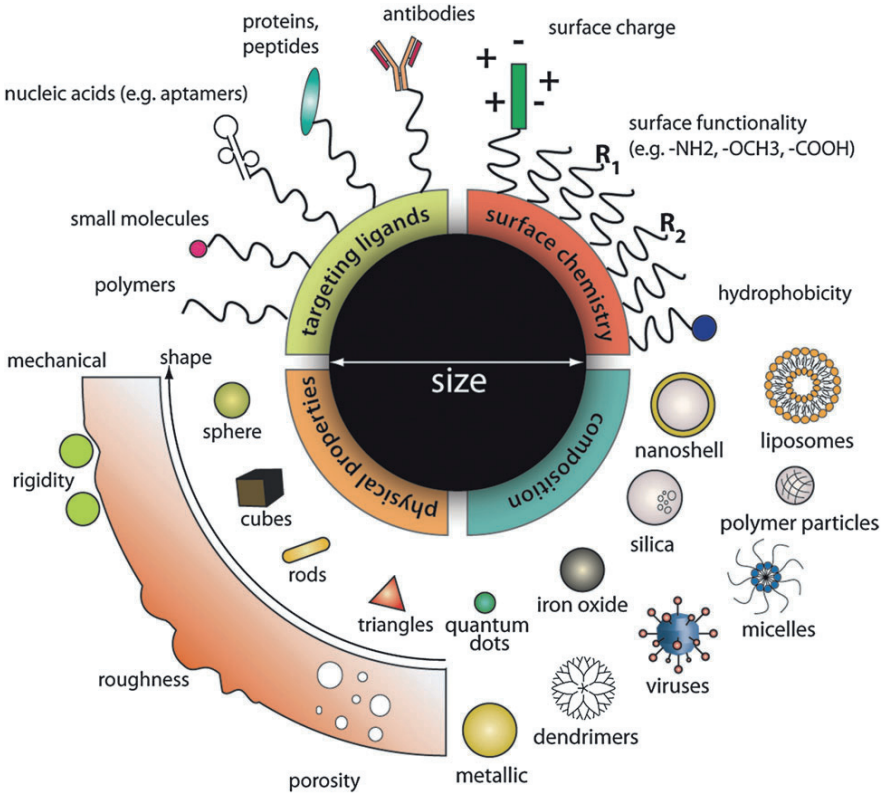

Figure 1. *The design of nanoparticles for cancer biomedical applications. Nanomedicines can be modularly assembled from different materials with different physicochemical properties and functionalized with a myriad of ligands for cancer targeting, drug delivery and diagnostics. Copyright © (2011) The Royal Chemistry Society. Reprinted with permission from ref.*[31].

Table 1. *Cancer nanomedicines approved for clinical use by one or more regulatory entities. Adapted with permission from refs.*[14,15].

Product	Nanoplatform	Drug	Indication	Status
Non-targeted chemotherapy				
Doxil	Pegylated liposome	Doxorubicin	HIV-related Kaposi sarcoma, ovarian cancer and multiple myeloma	Approved by FDA
DaunoXome	Liposome	Daunorubicin	HIV-related Kaposi sarcoma	Approved by FDA
Marqibo	Liposome	Vincristine sulphate	Acute lymphoblastic leukaemia	Approved by FDA
Onivyde or MM-398	Pegylated liposome	Irinotecan	Post-gemcitabine metastatic pancreatic cancer	Approved by FDA
Myocet	Liposome	Doxorubicin	Metastatic breast cancer	Approved in Europe and Canada
Mepact	Liposome	Muramyl tripeptide phosphatidyl-ethanolamide	Nonmetastatic, resectable osteosarcoma	Approved in Europe
Abraxane	Albumin nanoparticle	Paclitaxel	Breast, lung and pancreatic cancer	Approved by FDA
SMANCS	Polymer conjugate	Neocarzinostatin	Liver and renal cancer	Approved in Japan
Genexol-PM	Polymeric micelle	Paclitaxel	Breast cancer and NSCLC	Approved in Korea
Protein delivery				
Oncaspar	Pegylated asparaginase	Asparaginase	Acute lymphoblastic leukaemia	Approved by FDA
miRNA therapy				
Rexin-G	Targeting protein tagged phospholipid	miRNA-122	Sarcoma, osteosarcoma, pancreatic cancer and other solid tumours	Approved in Europe
Hyperthermia				
NanoTherm	Iron oxide nanoparticle	NA	Glioblastoma	Approved in Europe
Diagnostics/Imaging				
Feridex	Dextran-coated iron oxide nanoparticles	NA	Liver lesion imaging	Approved by FDA

Resovist	Carboxydextran-coated iron oxide nanoparticles	NA	Liver lesion imaging	Approved in Europe
Endoderm	Dextran-coated iron oxide nanoparticles	NA	Liver lesion imaging	Approved by FDA and in Europe

Abbreviations: FDA, US Food and Drug Administration; HIV, human immunodeficiency virus; miRNA, micro-RNA; NA, not applicable; NSCLC, non-small-cell lung cancer.

Since the initial clinical approval of Doxil®, a pegylated liposomal formulation of doxorubicin (DOX), by the Food and Drug Administration (FDA) in 1995,[32] lipid-based nanoparticles, particularly liposomes, still represent the major class of nanotherapeutics in the market or under clinical evaluation for cancer treatment.[33] The attractiveness and recognized clinical success of lipid-based nanodrugs reside on their high biocompatibility and biodegradability, low immunogenicity, and capability of improving the PK and biodistribution of the encapsulated therapeutic agents.[34] However, these advantages have mainly contributed to improve the toxicological profile and enlarge the therapeutic window of the formulated drugs, rather than enhancing the therapeutic efficacy and increasing overall patient survival.[35] Taking Doxil® as an example, the benefits of this drug-liposome formulation, in comparison with the free DOX, arise from prolonging the blood half-life of the drug from ~5 min to up to 72 h and, consequently, increasing the tumour accumulation, decreasing the volume of distribution nearly to the plasma volume, and reducing the dose-limiting inherent cardiotoxicity.[36-39]

Abraxane® or nab-paclitaxel, consisting of albumin-bound paclitaxel (PTX), was the second nanomedicine clinically approved for cancer treatment. Although the albumin-PTX nanoconjugate has not shown to significantly affect the PK profile and biodistribution of PTX, it has demonstrated an improved therapeutic efficacy in patients with advanced breast cancer,[40,41] most likely by increasing the drug's transport from the intravascular space and the intratumoral uptake.[42] Equally important, this nanoformulation has also revealed to significantly decrease the acute adverse effects of the conventional PTX formulations, which were typically caused by the toxic organic solvents used for solubilizing the hydrophobic drug.[42]

Furthermore, polymer-based nanotechnologies, particularly polymeric micelles and polymeric nanoparticles, have also been applied for improving the delivery of new and potent hydrophobic chemotherapeutics, which clinical use is, however, restricted by their poor aqueous solubility or low permeability across biological barriers.[43] Genexol-PM®, a polymeric micellar nanoformulation of PTX, is a successful example of this new class of nanomedicines that has already been introduced in the market.[44] Contrarily, other polymeric nanoformulations envisioned for non-targeted (*e.g.*, NK-105[45] and CRLX-101[46]) and targeted (*e.g.*, BIND-014[47]) chemotherapy have recently shown unsatisfactory results in clinical trials.

Nanomedicines have also taken their clinical strides as promising platforms for the delivery of biomolecules, including proteins,[48] antisense oligonucleotides,[49] DNA inhibitor

oligonucleotides,[50] microRNA (miRNA)[51] and small interfering RNA (siRNA).[52,53] For example, Oncaspar®, a pegylated form of asparaginase, has been demonstrated to prolong the circulation and retention time of this enzyme, while reducing the proteolysis, renal excretion and side effects, such as hypersensitivity.[48] Moreover, the first gene therapy nanomedicine, consisting of a cancer collagen matrix targeted liposome encapsulating miRNA (Regin-G®), has already received clinical approval.[51]

In addition to the organic-based nanomedicines clinically approved for cancer therapy, a few inorganic nanosystems have also been introduced in the market. All of these nanoformulations are based on superparamagnetic iron oxide nanoparticles (SPIONs), which are coated with aminosilane (NanoTherm®) for hyperthermia therapy of solid tumours,[54] or with carboxydextran (Resovist®) and dextran (Feridex®/Endoderm®) as magnetic resonance imaging contrast agents for the diagnostics of liver lesions.[55] Furthermore, other inorganic nanomaterials, particularly silica-gold core-shell[56] and hafnium oxide nanoparticles,[57] are currently under clinical investigation for cancer hyperthermia and radiotherapy, respectively.

Table 2. *Examples of nanomedicines under clinical investigation for cancer treatment. Adapted with permission from ref.[14].*

Product	Nanoplatform	Drug(s)	Indication	Status
Non-targeted chemotherapy				
Lipoplatin	Pegylated liposome	Cisplatin	NSCLC	Phase III
NK-105	Polymeric micelle	Paclitaxel	Metastatic or recurrent breast cancer	Phase III
EndoTAG-1	Liposome	Paclitaxel	Pancreatic cancer, liver metastases, HER2-negative and triple-negative breast cancer	Phase III
CRLX-101	Cyclodextrin nanoparticle	Camptothecin	NSCLC, metastatic renal cell carcinoma and recurrent ovarian cancer	Phase II
Targeted chemotherapy				
MM-302	HER2- targeting liposome	Doxorubicin	HER2-positive breast cancer	Phase II/III
BIND-014	PSMA-targeting polymeric nanoparticle	Docetaxel	NSCLC and mCRPC	Phase II
MBP-426	TfR-targeting liposome	Oxaliplatin	Gastric, oesophageal, and gastro-oesophageal adenocarcinoma	Phase I/II
Anti-EGFR immuno-liposomes	EGFR-targeting liposome	Doxorubicin	Solid tumours	Phase I

Stimuli-responsive chemotherapy				
ThermoDox	Heat-activated liposome	Doxorubicin	Hepatocellular carcinoma	Phase III
Combinatorial chemotherapy				
CPX-351 or Vyxeos	Liposome	Cytarabine and daunorubicin (5:1)	High-risk acute myeloid leukaemia	Phase III
CPX-1	Liposome	Irinotecan and floxuridine (1:1)	Advanced colorectal cancer	Phase II
Hyperthermia				
AuroLase	Silica-gold core-shell nanoparticle	NA	Head and neck cancer, and primary and metastatic lung cancer	Pilot study
Radiotherapy				
NBTXR3	Hafnium oxide nanoparticle	NA	Adult soft tissue sarcoma	Phase II/III
Gene or RNAi therapy				
SGT53	TfR-targeting liposome	Plasmid encoding normal human wild-type p53 DNA	Recurrent glioblastoma and metastatic pancreatic cancer	Phase II
PNT2258	Liposome	DNA nucleotide against BCL-2	Relapsed or refractory non-Hodgkin lymphoma and diffuse large B-cell lymphoma	Phase II
SNS01-T	PEI nanoparticle	siRNA against eIF5A and pDNA expressing eIF5A-K50R	Relapsed or refractory B-cell malignancies	Phase I/II
Atu027	Liposome	siRNA against protein kinase N3	Advanced and metastatic pancreatic cancer	Phase I/II
Immunotherapy				
Tecetomide	Liposome	MUC1 antigen	NSCLC	Phase III
dHER2 + AS15	Liposome	Recombinant HER2 (dHER2) antigen and AS15 adjuvant	Metastatic breast cancer	Phase I/II
JVRS-100	Lipid nanoparticle	Plasmid DNA	Relapsed or refractory leukaemia	Phase I
CYT-6091	Colloidal gold nanoparticle	TNF	Advanced solid tumours	Phase I

Abbreviations: EGFR, epithelial growth factor receptor; eIF5A, eukaryotic initiation factor 5A; HER2, human epidermal growth factor receptor type-2; mCRPC, metastatic castration-resistant prostate cancer; MUC1, membrane-bound mucin 1; NA, not applicable; NSCLC, non-small-cell lung

cancer; PSMA, prostate-specific membrane receptor; RNAi, RNA interference; siRNA, small interfering RNA; TfR, transferrin receptor; TNF, tumour necrosis factor.

In spite of the aforementioned clinical advances in cancer nanomedicine, this field is still at an early stage of development and has yet to fulfil the promise to revolutionize the future of cancer medicine. Currently, there are still several challenges defying the bench-to-bedside translation of cancer nanomedicines: (1) the controlled reproducible synthesis of nanoplatforms with optimal physicochemical properties; (2) the lack of tumour models that replicate the complexity and heterogeneity of human cancers and, consequently, the discrepant therapeutic outcomes between preclinical and clinical studies; (3) the scaling-up process of innovative and complex nanomedicines, particularly the ones requiring novel manufacturing techniques, integrating biological payloads and/or targeting moieties, and theranostic/multifunctional nanosystems; and (4) the demanding regulatory guidelines and requirements for the clinical approval and commercialization of nanotechnology-based therapeutics.[14,15]

2.2 Biological barriers and strategies in cancer nanomedicine

The complexity and heterogeneity of the human body and, particularly, the tumour pathophysiology, together with an incomplete comprehension of the nano-bio interactions, represent main hurdles for the establishment of nanomedicines as a new paradigm in cancer therapy. Despite considerable efforts on developing nanomedicines for non-invasive administration (*e.g.*, oral, pulmonary, nasal and transdermal delivery routes),[58-60] most cancer nanomedicines are envisioned to be administered systemically. After intravenous injection, the nanoparticle-based therapeutics face the challenge to reach and accumulate at the targeted tumour site, in order to exert a therapeutic effect. Therefore, the *in vivo* PK and related therapeutic efficacy of newly developed nanomedicines crucially depends on their capability to overcome multiple biological barriers. Generally, the passive tumour accumulation and localization of nanomedicines is favoured by an increased leakiness of the abnormal tumour microvasculature and a defective lymphatic drainage, enabling the nanoparticulate systems to extravasate from the blood circulation into the perivascular tumour microenvironment (TME) and to be retained within the tumour tissue.[61-64] However, after intravenous administration, the *in vivo* fate and tumour accumulation of nanoparticles are highly influenced by a multiplicity of biological processes, including the adsorption of plasma proteins, the nanoparticles' opsonisation, clearance and degradation, the extravasation and interaction with the TME, the tumour tissue penetration, as well as the cellular internalization and intracellular trafficking (**Figure 2**). In turn, the physicochemical properties of nanoparticles, such as the size, morphology, composition, surface charge and chemistry, and modification with biofunctional polymers and targeting ligands, can significantly impact the aforementioned biological phenomena, thus playing a determinant role on the PK profile, therapeutic outcome and safety of the nanomedicines (**Figure 2A**).[14]

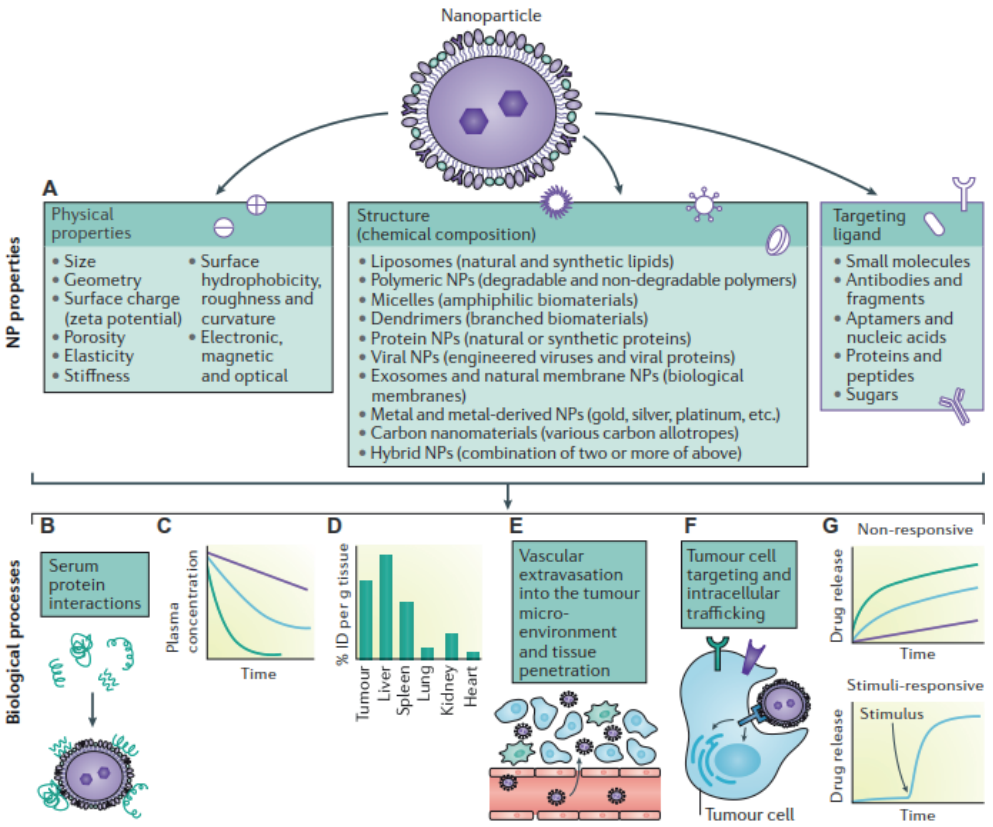

Figure 2. *The impact of nanoparticles' physicochemical properties, chemical composition and surface modification with targeting ligands (A) on the biological processes involved in the systemic delivery to tumour tissues, including the interaction with plasma proteins (B), blood circulation (C), biodistribution (D), extravasation to the tumour microenvironment (E), tumour cell targeting and intracellular trafficking (F), and release profile of payloads (G). Copyright © (2017) Nature Publishing Group. Adapted and reprinted with permission from ref.*[14].

2.2.1 Protein adsorption and protein corona formation

Once a nanoparticle enters a biological system, such as the blood, interstitial fluid or extracellular matrix (ECM), it is exposed and interacts with a variety of biomolecules, particularly proteins, which are tissue or organ specific in terms of their chemical and biological composition. These nanoparticle-protein interactions will lead to the formation of a protein layer or corona adsorbed onto the nanoparticles' surface that is constantly interacting with other proteins in the surrounding biological environment (**Figure 2B**).[65-69] The phenomena of protein adsorption and protein corona formation, as well as their composition, are highly dependent on the physicochemical properties of the nanomaterials, (*i.e.*, size, morphology, chemical composition, and surface chemistry), the composition of

biological system (blood, interstitial fluid, TME, intracellular compartment, etc.), the pathological state, and other factors such as temperature, pH, dynamic sheer stress, and exposure time.[69-73]

In turn, the protein corona formation alters the nanoparticle size, surface properties, stability, and functionality, thus providing the nanomedicines with a new entity that significantly impacts their biocompatibility, PK profile, biodistribution, tumour cellular internalization, intracellular trafficking, drug release and, consequently, their safety and therapeutic efficacy. For example, the surface adsorption of opsonins can induce the rapid recognition and phagocytosis by the mononuclear phagocytic system (MPS),[67,74] resulting in the clearance of the nanoparticles from the systemic circulation and the accumulation in the MPS associated organs (*i.e.*, liver and spleen).[75] Contrarily, the surface binding of dyopsonins, such as apolipoproteins and albumin, can render stealthy properties to the nanoparticles, avoiding the opsonisation by the MPS.[76-78]

In addition, the formation of a protein layer on the nanoparticles surface can affect their non-specific cellular interactions, uptake and the intracellular trafficking. As an example, the cellular internalization of silica nanoparticles revealed to be considerably more efficient when the particles were incubated with the cells in serum-free conditions,[79] since the proteins bound on the nanoparticles surface significantly decreased their adhesion to the cellular membrane and, consequently, lowered their cellular uptake.[80] However, the formation of a protein layer also diminishes the interaction with the cellular milieu, attenuating the acute cytotoxic effect of nanomaterials.[79] In the case of nanoparticles functionalized with targeting ligands, the formation of a protein corona can affect the function of conjugated targeting moieties by displacing, altering their orientation, disrupting their structure and conformation, or masking their recognition, thus limiting the specific interaction and internalization of the nanomedicines by the targeted cancer cells and, consequently, impacting their targeting efficiency and biofate.[69,81,82] Contrarily, the protein corona composition can also be designed for improving the targeting of nanotherapeutics. For instance, the adsorption of apolipoprotein E has recently been shown to drive the *in vivo* targeting of siRNA lipoplexes to hepatocytes.[83] Similarly, the surface modification of gold (Au) nanoparticles with apolipoprotein E and albumin has been demonstrated to prolong their blood circulation time, and to significantly increase their translocation into the brain and accumulation in the lungs.[84]

Furthermore, the protein corona can modify the dissolution rate of nanoparticles and, consequently, the release profiles of the therapeutic cargo. This is, for example, the case of Abraxane®, which tissue distribution and dissolution rate were affected by the protein corona formation and composition, thus also interfering with the tissue distribution of the formulated PTX.[73,85]

2.2.2 Opsonization, clearance and degradation of nanomedicines

Nanomedicines delivered systemically by intravenous injection are immediately subjected to rapid clearance from the blood circulation (**Figure 2C**). Although the eventual clearance and biodegradation of nanomedicines are important prerequisites from a toxicological perspective, their rapid removal from the bloodstream can result in a primary accumulation

in organs like the liver, spleen and kidneys (**Figure 2D**).[13] This unfavourable PK and biodistribution between the targeted tumour site and other tissues can not only offset the desired therapeutic effect and dramatically impair the therapeutic efficacy of nanomedicines, but also induce off-target toxicity.[86,87] Therefore, the rational design of nanomedicines that enable to circumvent the mechanisms of rapid clearance, to achieve a prolonged circulatory half-life and to preferably accumulate at the tumour site, are determinant for the overall effectiveness of nanoparticle-based therapeutics and represent some of the main focuses in cancer nanomedicine research.

The MPS and direct renal filtration are the two major physiological mechanisms responsible for the clearance of nanoparticles from the systemic circulation.[88,89] The MPS, also known as reticuloendothelial system (RES), is composed of phagocytic cells, including macrophages, monocytes and Kupffer cells that reside in MPS associated organs, such as the liver, spleen, lymph nodes and bone marrow, which are responsible for engulfing and eliminating external organisms, viruses and particles travelling in the blood circulation.[90] When entering the bloodstream, nanoparticles are immediately opsonized by plasma proteins, typically albumin, immunoglobulins, complement proteins and apolipoproteins, resulting in the formation of a protein corona onto the nanoparticles' surface.[65,91] The opsonization promotes the recognition and phagocytic clearance of the nanoparticles by the MPS, through the binding of the adsorbed opsonins to specific receptors expressed on the phagocytic cells, followed by enzymatic degradation. The nanoparticles that are not degradable by enzymatic breakdown, such as inorganic nanoparticles, will be transported by the phagocytes and accumulate in the liver and spleen.[92,93] In addition to the association with the MPS, the intrinsic physiology of the liver and spleen can contribute for the permanent excretion of nanomedicines from the body. In the liver, hepatocytes may endocytose and slowly degrade the nanoparticles, subsequently eliminating them in the biliary system.[94] In turn, nanoparticulate systems with sizes larger than 200 nm and long blood half-lives can be physically filtered from the bloodstream through the blood filtration system of the spleen.[95]

The clearance of nanomedicines by the MPS is complemented by the renal filtration system. The glomerular bed of the kidneys is characterized by a fenestrated capillary epithelium with an adjacent basement membrane and an epithelial layer of podocytes, which present a combined physiological pore size of approximately 4.5–5 nm.[96] Contrarily to the active phagocytic role of the MPS, the renal clearance is fundamentally a passive mechanism, which is predominantly affected by the particle size rather than the surface properties of nanomedicines. Moreover, upon renal filtration, nanoparticles are directly excreted from the body in the urine, instead of accumulating in the kidneys.[96]

The clearance process and *in vivo* biofate of nanomedicines is generally influenced by their physicochemical properties, particularly the size, shape, surface charge and hydrophobicity/hydrophilicity.[97,98] In general, spherical nanoparticles with a hydrodynamic diameter smaller than 6 nm are rapidly dialysed from the blood circulation through the renal filtration system, independently of their surface charge, while the renal clearance of 6–8 nm sized nanoparticles significantly depends on their surface properties. Accordingly, positively charged nanoparticles smaller than 8 nm have exhibited greater glomerular filtration than the negatively charged and neutral counterparts with similar dimensions, due to an increased interaction with the anionic moieties of the glomerular capillary wall.[88,89,99] In contrary,

nanomedicines larger than 8 nm cannot be handled by the kidneys and tend to be cleared by the MPS.[88] As mentioned above, the phenomena of opsonization and protein corona formation play critical roles in the process of MPS clearance. In this regard, ionic and/or hydrophobic nanoparticles present a higher propensity to be opsonized and phagocytosed by the MPS cells, compared to their neutral and hydrophilic counterparts, which minimally interact with the plasma proteins, owing to their sterically stabilized surface.[86,87]

Therefore, extensive efforts have been devoted to rationally engineer the surfaces of nanomedicines, with the aim of mitigating their opsonization and MPS clearance, prolonging their blood half-life and enhancing their tumour accumulation. The most widely explored strategy to achieve these goals consists of adsorbing or conjugating polyethylene glycol (PEG) or PEG derivatives onto the nanoparticles' surface, a process also known as pegylation.[100] The stealth properties of PEG arise from its hydrophilicity, neutral charge and steric repulsion, forming a hydrating shell on the nanoparticles' surface that minimizes the interaction with plasma proteins and, consequently, the recognition and internalization by the MPS cells. As a result, pegylated nanoparticles normally travel longer in the systemic circulation, giving an opportunity to accumulate more efficiently in the tumour tissues.[101,102] Additionally to PEG-based moieties, other hydrophilic polymers, including polyacrylamide, poly(vinyl alcohol), poly(*N*-vinyl-2-pyrrolidone) and polysaccharides, such as dextran, heparin, chitosan and hyaluronic acid (HA), have demonstrated similar stealth features and provided significant benefits on prolonging the blood half-lives of nanomedicines.[75] Furthermore, alternative biomimetic approaches that inhibit the phagocytic activity of the MPS and consequent hepatic and splenic clearances, have recently been exploited. Such biologically inspired strategies involve, for example, the surface modification of nanoparticulate systems with self-recognizing peptides, such as CD47 peptides,[103,104] and their coating with membranes derived from haematopoietic cells, including erythrocytes,[105] leukocytes[106] and thrombocytes.[107,108]

2.2.3 Tumour extravasation and accumulation

2.2.3.1 Enhanced permeation and retention effect and passive tumour targeting

In order to exert the envisioned therapeutic effect and reduce adverse off-target effects, cancer nanomedicines need not only to avoid the mechanisms of rapid clearance, as mentioned in the previous section, but also to extravasate from the tumour microvasculature and accumulate within the tumour tissues (**Figure 2E**). Since the concept of the "magic bullet" was idealized almost one hundred years ago,[109] extensive research focus has been dedicated to better study and understand the tumour biology and pathophysiology and, accordingly, to design new strategies to improve the specific accumulation of cancer nanomedicines in malignant tissues.[11,110,111] Nowadays, it is well know that therapeutic macromolecules and nanoparticles administered intravenously tend to preferably accumulate and be retained in tumour lesions, as a combined result of the defective tumour vasculature and impaired tumour lymphatic drainage.[61,63,112]

During the tumorigenic process, the normal vasculature surrounding the solid tumour mass does not comply with the oxygen supply required for the frenetic and uncontrolled

proliferation of malignant cells, resulting in a hypoxic TME. In response to the hypoxic cell death, cancer cells increase the secretion of vascular epithelial growth factors and pro-angiogenic signals that promote the continuous development of new blood vessels.[2,113] Contrarily to the vasculature in normal tissues (**Figure 3**, left panel), the active tumour angiogenesis generates an irregular vascular architecture that is characterized by a discontinuous and fenestrated endothelium, a disrupted or absent basal membrane and a lower count of adjacent perycites (**Figure 3**, right panel).[113-115] The sizes of interendothelial fenestrations of the tumour microvasculature typically vary between 100–800 nm, depending on the solid tumour, its stage and localization.[116] Consequently, the tumour vascular walls are significantly more leaky and permeable to active macromolecules and nanotherapeutics with appropriate size, allowing their efficient extravasation from the blood vessels' lumen to the tumour interstitium.[117,118] Although the particle size is the physical parameter driving the passive tumour extravasation and accumulation, the surface properties of nanoparticles also play determinant roles in these phenomena, as they greatly impact the hydrodynamic radii, stealthiness, blood half-life and clearance of nanomedicines.[119]

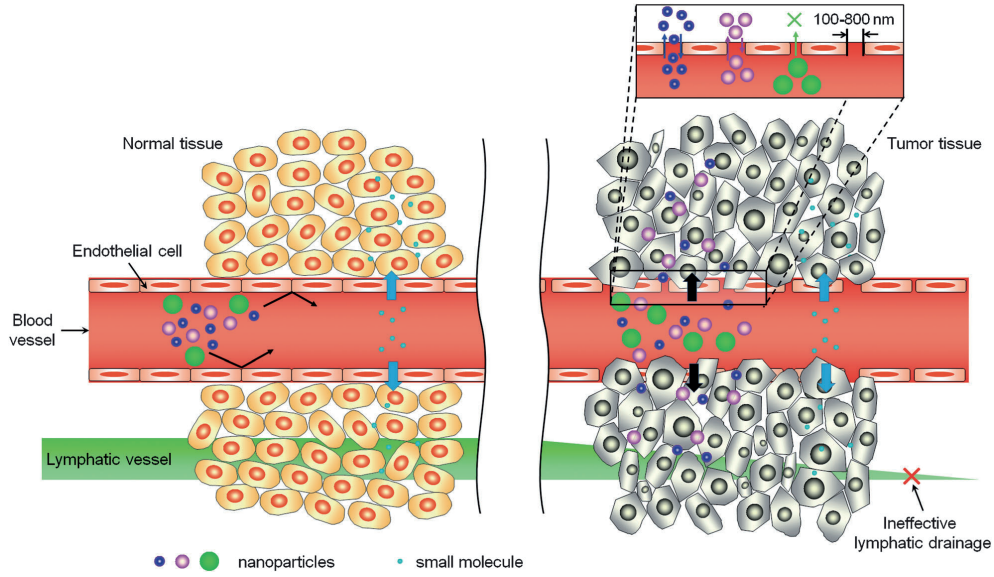

Figure 3. *The extravasation of nanoparticles with different sizes and small molecules in normal (left) and tumour (right) tissues. The enhanced permeation and retention effect is a unique feature of most tumours, allowing nanoparticles of appropriate sizes to preferably extravasate and accumulate in cancerous tissues than in normal tissues. Copyright © (2014) Wiley-VCH Verlag GmbH & Co. KGaA. Reprinted with permission from ref.[13].*

In addition to the enhanced permeation of the tumour microvasculature, tumours generally exhibit a defective lymphatic drainage, resulting from the rapid proliferation of cancerous and stromal cells, and a condensed ECM (**Figure 3**, right panel).[120] This suppressed lymphatic flow reduces significantly the clearance of nanomedicines that

extravasate to the tumour perivascular space, thus favouring their accumulation and penetration into the tumour tissue.[61,112] However, this phenomenon also contributes to an increased interstitial fluid pressure (IFP) in the tumour parenchyma, which competes with the extravasation pressure for the diffusion of nanotherapeutics through the permeable tumour vasculature, and may eventually efflux the extravasated nanoparticles back into the systemic circulation.[121] The aforementioned pathophysiologic features of the TME are the mechanistic fundaments of the enhanced permeation and retention (EPR) effect, originally demonstrated by Matsumura and Maeda in 1986,[61] and represent the foundation of the passive targeting and delivery of nanomedicines to tumours (**Figure 4**, left panel).

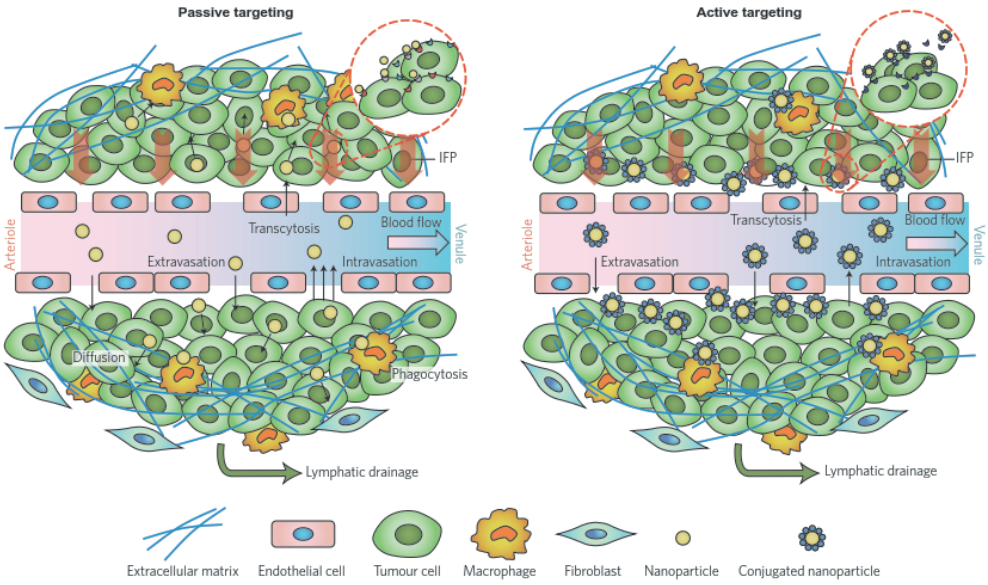

Figure 4. *The mechanisms of passive (left) and active (right) targeting of nanoparticles into tumours. Abbreviations: IFP, interstitial fluid pressure. Copyright © (2017) Nature Publishing Group. Adapted and reprinted with permission from ref.*[122].

The majority of clinically approved cancer nanomedicines (*Section 2.1*) rely on the EPR effect as a mechanism for their tumour passive targeting and accumulation. However, recent investigations have revealed that the interpretations of the EPR effect over the past years are oversimplified and that the passive tumour targeting of nanomedicines is in fact a more complex and heterogeneous phenomenon than initially presumed.[14] Currently, it is clear that the physiology of the tumour microvasculature and microenvironment, and associated EPR effect, not only vary considerably between tumour types and patients, but are also spatiotemporally heterogeneous throughout the same tumour.[13,122] In addition, the ubiquitous release of the loaded therapeutic molecules in the tumour tissue can result in uptake by unintended cellular targets or in efflux from the tumour interstitium back into the bloodstream owing to the increased IFP. These undesired outcomes prevent the therapeutic agents from efficiently diffusing within the tumour mass and successfully reaching their

pharmacological targets.[123,124] All these hurdles contribute to ineffective, non-uniform and unpredictable therapeutic responses to passively targeted nanomedicines and can be attempted to be circumvented by actively targeting nanomedicines to tumours.

2.2.3.2 Active tumour targeting

The active tumour targeting of nanomedicines, also named as ligand-mediated tumour targeting, involves the surface functionalization of nanoparticulate systems with biologically active ligands that specifically recognize and bind to tumour-associated receptors, which are (over)expressed on the surface of tumour cells or components of the TME. This strategy can not only drive the nanoparticles to selectively accumulate at the targeted tumour tissue, but also contribute for an enhanced anchoring and internalization by the targeted cells through receptor-mediated endocytosis (**Figure 2F**), ultimately improving the therapeutic index of nanomedicines and their therapeutic payload.[12,63,101,125-127]

In order to fully exploit the benefits of active targeting, it is imperative to carefully and rationally engineer the actively targeted nanomedicines. The selection of the right targeting ligand used to functionalize the surface of the nanoplatforms is of utmost importance to efficiently deliver the nanomedicines to the intended cellular target and, consequently, to attain the desired therapeutic outcome. For this purpose, a wide repertoire of targeting moieties are currently available, including monoclonal antibodies and antibody fragments, proteins and peptides (*e.g.*, peptides containing the arginine-glycine-aspartic acid (RGD) sequence), nucleic acid ligands (*e.g.*, aptamers), small molecules (*e.g.*, folic acid and transferrin) and polysaccharides (*e.g.*, HA).[128-130] In addition, different parameters related to the nanoparticle design should be considered and optimized, including the intrinsic physicochemical properties of the nanocarrier (*i.e.*, the particle size, shape, surface charge and hydrophobicity), as well as the avidity of the targeting ligand to the targeted receptor, the ligand density and the coupling chemistry used.[130,131] Moreover, it is important to consider that the specific molecular recognition and ligand-receptor binding of active targeting nanovehicles require their availability at the vicinity of the cognate receptors present at the targeted cells' surface. Therefore, nanomedicines that actively target the receptors expressed in solid tumours still need to rely on the EPR effect and passive targeting to extravasate from the tumour microvasculature and accumulate at the tumour tissue (**Figure 4**, right panel).[127,132] Accordingly, the targeting and therapeutic efficiencies of actively tumour targeted nanomedicines are significantly impacted by the inherent properties of the nanoplatforms and the density of the targeting ligand, as these factors play a determinant role on the biological processes of opsonization, MPS-associated clearance, systemic half-life and, consequently, the passive accumulation of nanoparticles at the tumour site (*Sections 2.2.2* and *2.2.3.1*).[127,130-133]

In an alternative approach to the tumour cell targeting, nanomedicines can be designed to actively target non-tumoural cells of the TME.[134] Owing to its active involvement in the tumorigenic process, the tumour vasculature has been early identified as a potential target for cancer nanomedicines.[135,136] The active vascular targeting strategy fundamentally foresees to promote the tumour extravasation and accumulation of the targeted nanosystems, with minimal dependency on the EPR effect.[137] In this context, various vascular targeting

ligands have been screened for targeting biomarkers that are specific or overexpressed in the tumour vascular endothelium and exhibit low or no expression in the normal vasculature.[137,138] For example, internalizing RGD (iRGD; CRGDK/RGPD/ED), a cyclic tumour homing peptide containing the RGD sequence, has been recognized to specifically bind the transmembrane $\alpha v\beta_3$ and $\alpha v\beta_5$ integrins, which are highly overexpressed on the surfaces of tumour endothelial cells.[139] Upon binding to the tumour angiogenic endothelium, the iRGD peptide undergoes proteolytic cleavage, unrevealing a C-terminal motif with affinity to neuropilin-1, which mediates the tumour penetration and internalization into cancerous cells.[136,140] Therefore, the surface modification of nanovectors with iRGD peptide has been shown *in vivo* to efficiently promote the extravasation from the tumour vasculature and penetration into the tumour parenchyma, overall resulting in an enhanced intratumoural delivery and therapeutic efficiency of the active payload.[136,141] In addition to the active vascular targeting, a variety of nanoformulations have been designed to target stromal cells in the TME,[134] such as tumour-associated fibroblasts and macrophages,[142,143] as well as components of the ECM, including heparan sulphate, chondroitin sulphate and HA.[12,144]

In turn, HA, an anionic linear glycosaminoglycan consisting of alternating units of D-glucuronic acid and *N*-acetyl-D-glucosamine, has recently been recognized as a potential tumour targeting moiety itself, owing to its high binding affinity to the CD44 receptor and resultant CD44-mediated endocytosis.[145-148] The CD44 biomarker is a type-1 transmembrane glycoprotein endogenously expressed at low levels in healthy tissues and is known to be a major component of the ECM, playing a key role in diverse physiological events, including cell proliferation, differentiation, and migration.[149-151] However, this receptor has also shown be upregulated in a large number of solid tumours, and a correlation between its overexpression and the pathological processes of tumorigenesis and tumour progression, invasion, metastasis and drug resistance has already been established.[152-157] In addition to CD44-binding affinity, biological functions and inherent biocompatibility, biodegradability and non-immunogenicity, HA exhibits advantageous physicochemical characteristics, such as high aqueous solubility, hydrophilicity and stabilizing properties, and a chemical structure that allows further modification in aqueous conditions. All these attractive features render this biomaterial with great promise for applications in cancer nanomedicine.[145-148] Accordingly, HA has been extensively used in the design and development of various nanoparticulate systems for targeted cancer therapy and diagnostics, including HA-drug conjugates, HA-based nanocomplexes and nanogels, HA-decorated inorganic nanoparticles, HA-modified lipid-based nanocarriers, and HA-based self-assembling nanoparticles.[145-148]

2.2.4 Cellular internalization and intracellular trafficking

Upon extravasation from the tumour microvasculature and accumulation at the tumour site, nanomedicines need to efficiently surpass the cell membrane barrier and be internalized by the tumour cells, in order to deliver the therapeutic payload to the intracellular pharmacological targets and exert an efficacious therapeutic effect. When in close proximity to the cells, nanoparticles can interact with the cell membrane through the selective binding to membrane-embedded receptors or the non-specific association to the membrane surface based on hydrophobic and electrostatic interactions.[13,31]

The initial interaction of the nanoparticulate systems with the surface of the cell membrane subsequently triggers their cellular internalization, a process generally known as endocytosis.[158] There are four major endocytic pathways involved in the cellular uptake of nanoparticles, namely clathrin-mediated and claveolin-mediated endocytosis, pinocytosis and phagocytosis (**Figure 5**), which generally differ on the nanoparticle–cell interactions established, the properties of the internalized cargo, the size of the resulting endocytic vesicles and the intracellular machinery involved in the process at the molecular level.[158-160] The first two endocytic mechanisms predominantly rely on the specific recognition and binding of the nanoplatforms to receptors (over)expressed on the cell surface, resulting in their receptor-mediated endocytosis.[161,162] In this regard, the functionalization of the nanomedicines' surface with targeting ligands not only can significantly contribute to their preferential accumulation at the tumour site, as described in the previous section, but also play a paramount role on enhancing their cellular internalization *via* clathrin- and claveolin-mediated endocytosis.[63,125,162] Alternatively, the non-specific adsorption of untargeted nanoparticles to the cell membrane through electrostatic and hydrophobic interactions can lead to the cellular uptake by pinocytosis. This actin-driven endocytic pathway consists on the invagination and pinching off fractions of the cell membrane, creating large endocytic vesicles that non-specifically engulf the surrounding extracellular fluid and particles.[158-160] In this case, the nanoparticle–cell interactions and consequent cellular internalization process are significantly determined by the physicochemical characteristics of the nanomaterials, including size, geometry, aspect ratio, surface charge and surface chemistry.[98,163-165] Therefore, the design and optimization of the nanomedicines is absolutely crucial for maximizing their cellular interactions and internalization and, consequently, for the intracellular delivery and efficacy of nanotherapeutics.[131,133,166] In addition, specialized cells, such as macrophages, monocytes and neutrophils, present the capability to detect and engulf large particles through phagocytosis.[158,167] As previously described in *Section 2.2.2*, this endocytic process represents the main mechanism responsible the clearance of nanoparticles by phagocytic cells of the MPS and, therefore, one of the major biological barriers limiting the efficient delivery of nanomedicines to tumours.[90]

After cellular internalization, nanomedicines are generally confined within endocytic vesicles and successively trafficked along the endolysosomal pathway, involving molecular motor proteins and cytoskeletal components. During the dynamic and complex process of intracellular trafficking, the endocytic vesicles initially transport their nanoparticulate contents into early or sorting endosomes, after which they can be either exocytosed from the cells, transported to other subcellular organelles or follow the endolysosomal pathway, ultimately leading to degradation in the lysosomes (**Figure 5**).[31,162] The maturation of early endosomes into later endosomes and lysosomes is accompanied by a rapid acidification of the endosomal lumen to pH values of approximately pH 5, thus creating a conductive environment for the function of the recruited degradative enzymes responsible for the degradation of the lysosomal content.[31,162] Therefore, the development of strategies that render nanomedicines with the capacity to escape the endolysosomal network is crucial for the efficient delivery of the therapeutic payload to the cytoplasmic pharmacological targets, with particular relevance for biologic cargos, and represents an active focus of cancer nanomedicine research. Some of these strategies are described in the following subsection.

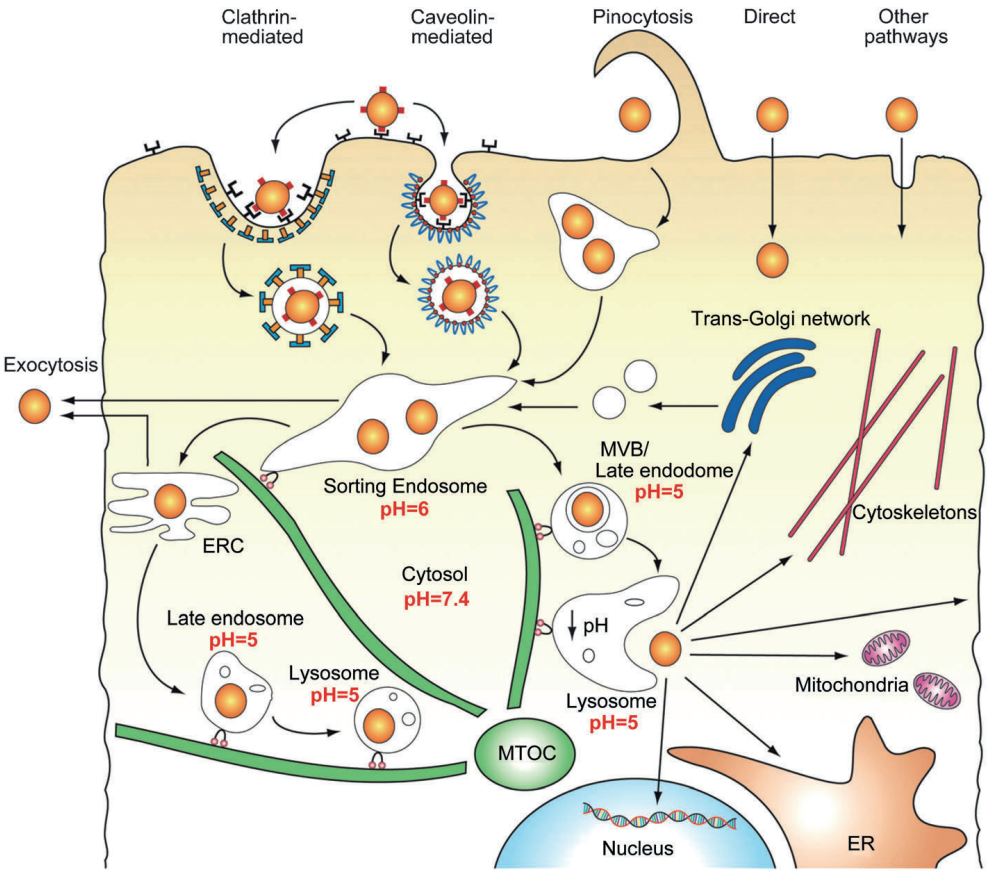

Figure 5. *The cellular internalization and intracellular trafficking of nanoparticles. Note the variation in pH values between the different intracellular compartments. Abbreviations: ER, endoplastic reticulum; ERC, endocytic recycling compartment; MTOC, microtubule-organizing centre; MVB, multivesicular bodies. Copyright © (2014) Wiley-VCH Verlag GmbH & Co. KGaA. Reprinted with permission from ref.*[13].

2.2.4.1 Endolysosomal escape strategies

In order to successfully deliver therapeutic molecules to the cytoplasmic and other intracellular compartments and avoid the degradative environment of the lysosomes, nanomedicines need to be designed and engineered with the capacity to efficiently evade the endolysosomal pathway. Accordingly, different biochemical strategies have been exploited to attain this goal, which underlie distinct mechanisms of endolysosomal escape, including the pH buffering of the endosomal acidic lumen and the disruption of the endosomal membrane by pore formation, fusion or photochemical destabilization.[159,168]

One approach to induce the endolysosomal escape of nanomedicines consists on the inclusion of polyamine cationic polymers in the nanoformulations, such as the widely

investigated poly(ethylenimine) (PEI),[169-171] poly(amidoamine) (PAA),[172-175] and poly (L-histidine)-containing polymers[176,159,168,177] These polymeric molecules are typically characterized by a high density of secondary and tertiary amines and a buffering capacity between pH 5.0–7.4, enabling the nanoparticles to escape the acidic endolysosomal compartments *via* the "proton-sponge" effect. [169,178] This mechanism postulates that, during the endolysosomal trafficking, the continuous protonation of the polyamine polymers and prevention of the endosomal acidification triggers an increased transport of protons mediated by the membranal ATPase pump, in order to re-establish the acidic intraendosomal pH. The augmented influx of protons and balancing counter-ions subsequently leads to an increased osmotic pressure inside the endosomal compartments and, eventually, to the swelling and osmolysis of the endosomal membrane (**Figure 6**).[169,178] However, while PAA and polyhistidine-based polymers are normally designed to be biocompatible and biodegradable, major concerns arise from PEI's well-known cytotoxicity, non-biodegradability and instability in biological buffers, which considerably limit its applicability in nanobiomedicine.[179,180]

In addition, the endosolysosomal escape of nanovectors can be facilitated through the surface functionalization with viral-derived (*e.g.*, human immunodeficiency virus (HIV) gp41-derived peptide (HGP),[181,182] influenza virus hemagglutinin (HA2) *N*-terminal peptide,[183-185] HIV transactivator of transcription (TAT)-derived peptide[186-188] and papilloma virus L2 minor capsid protein-derived peptide (L240)[189,190]) or synthetic pH-responsive (*e.g.*, glutamic acid-alanine-leucine-alanine (GALA)[191-193] and KALA[194-196]) fusogenic peptides.[159,168,197] Generally, these membrane-disruptive fusogenic peptides are amphipathic molecules that undergo a structure conformational change in response to the acidic endosomal pH, acquiring the capability to penetrate or induce the formation of pores in the endosomal membrane, causing its destabilization and disruption, and ultimately resulting in the cytoplasmic release of the entrapped nanoparticulate systems.[159,168,197]

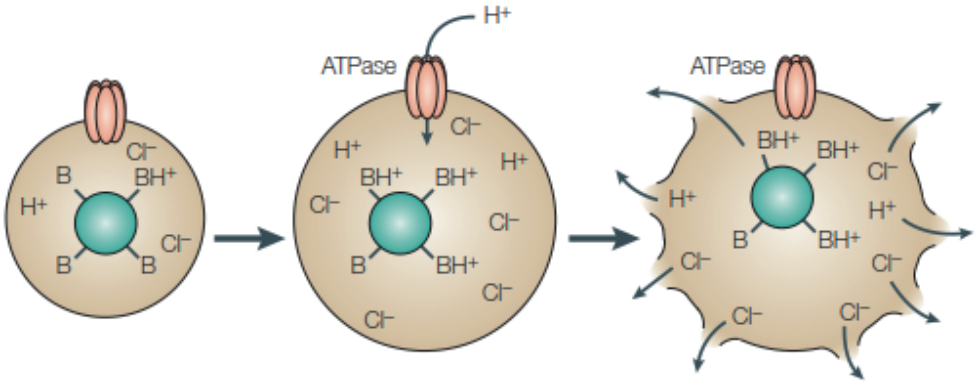

Figure 6. *Schematic representation of the "proton-sponge" mechanism. The protonation of proto-sponge moieties results in an increased influx of protons and counter-ions into the endocytic vesicles. The increasing osmotic pressure causes the vesicle to swell and rupture. Copyright © (2005) Nature Publishing Group. Reprinted with permission from ref.*[178].

2.3 Porous silicon particles

PSi was first reported by Arthur Uhlir Jr. and Ingeborg Uhlir in 1956, at the Bell Laboratories,[198] but it was only 15 years after that the porous crystalline silicon (Si) structure of this material was described.[199] Thereafter, considerably growing attention has been drawn to PSi, particularly due to the remarkable work of Prof. Leigh Canham, who discovered the photoluminescence of highly porous Si wires, owing to the two-dimensional quantum size effect[200] and, later on, demonstrated the *in vitro* biocompatibility and bioactive properties of PSi.[201] These findings are considered the milestones for the following application of PSi materials in biomedicine, particularly in the field of drug delivery.[16-21]

Over the last decade, PSi nanoparticles have been extensively explored as a nanotool for biomedical applications, due to significant advances in their fabrication and surface modification methods, the manipulation and fine-tuning of their physicochemical properties, as well as the increasing comprehension of their interactions with biological systems.[19] In this regard, PSi nanoparticles present advantageous physicochemical and biological features, including a high surface-to-volume ratio, large surface area (300–1000 $m^2.g^{-1}$) and pore volume (0.9 $cm^3.g^{-1}$), high chemical, mechanical and thermal stability, as well as superior biocompatibility and biodegradability.[16] Additionally, the top-down fabrication method of these nanoparticles enables their scaled-up production and an easy control over their particle and pore sizes, depending on the fabrication parameters applied.[18,202,203] Moreover, the surface of PSi nanoparticles can be straightforwardly modified with different functional groups, and further functionalized with numerous polymers and biomolecules, in order to attain control over the release of therapeutic cargos, target specific organs, tissues and cells, or improve the biological performance.[27,204,205]

In this section, the methods for fabrication and surface modification of PSi nanoparticles will be described, along with aspects related with their biocompatibility and biodegradability. Furthermore, some of the latest advances of the biomedical application of these nanoplatforms will be reviewed, highlighting their use as targeting and drug delivery systems for cancer nanomedicine.

2.3.1 Fabrication and surface modification of PSi

PSi is commonly fabricated by an electrochemical anodization method, in which monocrystalline Si wafers are electrochemically etched, forming a uniform PSi layer on the surface of the bulk Si.[16,19,206,207] For this purpose, a Si wafer is introduced between two electrolyte cells, with platinum (Pt) electrodes on both sides of the Si wafer. The upper side of the Si substrate, acting as the anode, is immersed in a hydrofluoric acid (HF) based aqueous or ethanolic electrolyte solution, while the lower side of the Si wafer, working as the cathode, is in close contact with a conductive metal anode. When applying an etching current between the Pt electrodes, the oxidation and electrochemical etching, occurring at the anode, results in the Si dissolution and formation of a PSi layer, exclusively on this side of the Si wafer. Oppositely, at the cathode, the proton reduction leads to hydrogen (H_2) formation and elimination, contributing for the electrolyte penetration into the pores and, consequently, the formation of a homogenous PSi layer.[16,206]

The properties of the PSi layer obtained, including the thickness, degree of porosity and the pore size and shape, are dependent on the conditions applied in its fabrication. Therefore, these parameters, such as the HF concentration and composition of the electrolyte solution, the density and voltage of the electrical current, the type, resistivity, doping and crystallographic orientation of the Si wafer, temperature, time, and illumination intensity, can be finely tuned to reproducibly obtain PSi layers with well-defined structures.[19,203,206]

The freshly etched PSi presents an unstable and reactive surface consisting of hydrophobic Si hydride terminals (Si-H_x), which are very susceptible to hydrolysis and oxidation under open atmospheric conditions, resulting in a more hydrophilic surface and affecting its porous structure and optoelectronic properties. The rate and extension of surface oxidation is highly influenced by the temperature, relative humidity and composition of the atmosphere.[16,206] This high reactivity of the surface Si hydride terminals compromises the application of native PSi in drug delivery, since it can reduce and, consequently, degrade the active payloads adsorbed to the PSi surface.[16,207] Therefore, different methodologies, including oxidation, hydrosilylation, thermal carbonization, and thermal hydrocarbonization are generally applied to stabilize the native PSi surface, before using this material in drug delivery and other biomedical applications.[206]

Controlled oxidation is one of the most common approaches used for stabilizing the native PSi surface, and it can be attained by different methods, such as chemical,[208] anodic[209] and thermal oxidation.[207] In the last method, the increased temperatures induce the oxidation of both the Si-Si backbone and the Si-H_x terminals, forming Si-O-Si, -O_ySiH_x and Si-OH bonds,[210,211] and rendering thermally oxidized PSi (TOPSi), which is characterised by a stable, hydrophilic and biocompatible oxidized surface.[212] Although these features can be generally considered attractive for the application of TOPSi in drug delivery, its oxidized surface may react with certain loaded compounds. Moreover, the insertion of oxygen atoms within the Si-Si backbone can results in the expansion of the PSi structure and consequent reduction of the pore diameter and volume, as well as on an accelerated dissolution of the PSi matrix in aqueous physiological media.[28]

Hydrosilylation is another method for stabilizing the surface of PSi, which involves the reaction of the surface Si-H_x species with unsaturated compounds containing alkene (C=C), alkyne (C≡C), or aldehyde (C=O) bonds, resulting in the formation of Si-C-C, Si-C=C and Si-C-O bonds, respectively.[213-216] These modifications can be achieved by using different methods, including Lewis acid catalysed reactions, white light promotion, cathodic electrografting or thermal hydrosilylation.[16,203] In addition to increasing the stability of the PSi surface, the hydrosilylation enables its further functionalization with different molecules at the opposite end of the aliphatic chains.

Thermal carbonization and thermal hydrocarbonization are two alternative surface stabilization methods that commonly consist on treating the native PSi surface with acetylene at high temperatures. The thermal carbonization involves the flushing of acetylene at temperatures above 700 ºC and results on the substitution of the Si-H_x surface ends for hydrogen-free Si-C bonds, rendering thermally carbonized PSi (TCPSi), which is characterized by a more stable hydrophilic surface.[217] In the case of thermal hydrocarbonization, the acetylene treatment is carried out at temperatures below 650 ºC, forming both Si-C and Si-CH bonds at the PSi surface (**Figure 7**).[218] Similarly to the PSi

obtained by thermal hydrosilylation, the surface of thermally hydrocarbonized PSi (THCPSi) can be subsequently modified with carboxylic acid functional groups (-COOH), by performing a thermal treatment with undecylenic acid (**Figure 7**).[219,220] The resulting undecylenic acid modified THCPSi (UnTHCPSi) can be further covalently conjugated with a wide variety of polymers, biomacromolecules, fluorescent dyes and other compounds, which represents a key feature for the application of these materials in biomedicine.[221,222]

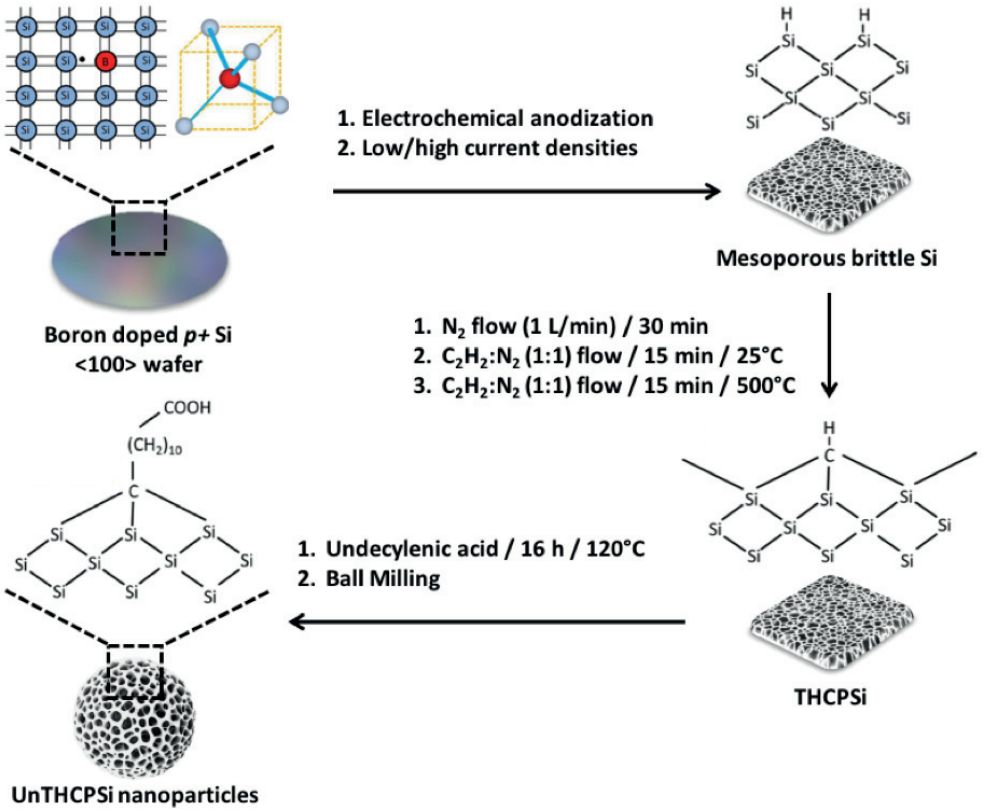

Figure 7. *Schematic illustration of the fabrication method of UnTHCPSi nanoparticles. Abbreviations: Si, silicon; THCPSi, thermally hydrocarbonized Psi; UnTHCPSi, undecylenic acid thermally hydrocarbonized PSi.*

2.3.2 Biocompatibility and biodegradability of PSi

The biocompatibility and biodegradability of any material are highly relevant and decisive features for its application in biomedicine. In the case of PSi, the *in vitro* biocompatibility was first reported by Canham in 1995, who correlated the pore morphology of this material with its bioactivity.[201] Accompanying the increasing interest on the application of PSi for biomedical purposes, the biocompatibility of PSi has been extensively investigated, both *in vitro* and *in vivo*,[22,24,212,223-226] along with its inflammatory and immune responses,[24,227] and

its biofate.[224,228-230] Overall, the biocompatibility of PSi materials was revealed to be highly dependent on their physicochemical properties, including the size,[225] pore size[226] and surface chemistry.[24,227]

The biocompatibility of PSi particles has been extensively evaluated in gastrointestinal (GI) tract associated *in vitro* and *in vivo* models.[22,226,231,232] For example, THCPSi and TOPSi nanoparticles were shown not to induce any significant *in vitro* toxic effect, oxidative stress, nor inflammatory response in Caco-2 colon cancer cells or RAW 264.7 mouse leukemic monocyte macrophages. Moreover, after *in vivo* oral administration, ^{18}F-labelled THCPSi particles showed not to be absorbed from a subcutaneous deposit and to pass intact through the GI tract. When administered intravenously, the same nanoparticles were mainly distributed in the liver and spleen, thus indicating a rapid clearance from the blood circulation.[22] In a more recent study, the *in vitro* toxicity of TOPSi nanoparticles, with pore sizes varying between 17 and 58 nm, and amine functionalized PSi nanoparticles, was investigated in a Caco-2/HT-29 cell co-culture. The amine functionalized PSi nanoparticles exhibited higher cytotoxicity than the TOPSi counterparts with similar pore size. Additionally, an increment in the pore size demonstrated to augment the cytotoxicity of TOPSi nanoparticles, as a consequence of the larger pore size itself or the variations in the production method applied to increase the pore size of the nanoparticles. For that purpose, an annealing step was performed prior to the thermal oxidation of TOPSi nanoparticles, which revealed to decrease the density of surface –OH groups, thus also showing a correlation between the surface chemistry of PSi nanoparticles and their cytotoxic effect.[226]

In addition, the effect of the surface chemistry on the cytotoxicity of PSi nanoparticles was assessed *in vitro* and *in vivo* in immune and red blood cells (RBCs) based on histopathological analysis and biochemical parameters. In general, the *in vitro* studies demonstrated a correlation between the surface chemistry and charge of the PSi nanoparticles and their cytotoxic effect, with a higher dependency on the surface charge, than on the hydrophilicity/hydrophobicity. In this regard, positively charged and hydrophilic 3-aminopropyltrietoxysilane modified TCPSi (APSTCPSi) nanoparticles exhibited higher levels of ATP depletion, genotoxicity and impact on the RBCs morphology, compared to their negatively charged counterparts, among which, the more hydrophobic UnTHCPSi showed higher cytotoxicity than TOPSi, TCPSi and THCPSi. After *in vivo* intravenous administration of the different PSi nanoparticles, the histopathological and biochemical analyses showed generally biosafe profiles of these nanoparticulate systems. In this respect, despite mild histological changes in kidney, liver and spleen, particularly for APSTCPSi and UnTHCPSi nanoparticles, no notable changes were observed in the serum levels of biochemical and haematological parameters.[24]

In a complementary study, the impact of the surface chemistry on the immunological response of PSi nanoparticles was investigated by evaluating the immunostimulatory responses, namely the dendritic cells (DCs) maturation, T cells proliferation and cytokine secretion, induced by a non-toxic concentration of the PSi nanoparticles. The results showed that TOPSi and THCPSi nanoparticles induced immunoactivation responses, by enhancing the expression of surface co-stimulatory markers of DCs (*i.e.*, CD80, CD83, CD86 and MHC-II), and increasing the cytokines mediating T cell differentiation. Contrarily, TCPSi

and APSTCPSi nanoparticles did not show any immunostimulatory signs, thus suggesting their potential for delivering immunosuppressive molecules.[227]

The biocompatibility of PSi micro and nanoparticles was also assessed when studying their application in the treatment of myocardial infarction. In this study, 7 and 19 μm sized THCPSi microparticles induced a significantly higher activation of inflammatory cytokines and fibrosis promoting genes, in comparison to similarly sized TOPSi microparticles and 110 nm sized nanoparticles. However, none of the tested nanoplatforms affected the cardiac function or haematological parameters, therefore demonstrating the high *in vivo* biocompatibility of these nanomaterials in the heart tissue.[225]

In addition to the biocompatibility, the biodegradability of materials is of utmost importance when envisioning their biomedical application. In this regard, PSi is known to degrade in aqueous solutions by oxidative hydrolysis, into orthosilicic acid,[23] which has been naturally found in numerous tissues[16,233] and shown to be biocompatible[229,230] and excreted by renal clearance.[233] The degradation rate of PSi depends on different factors, such as the degree of crystallinity,[234] the pore size, pore volume, and surface area,[235] the surface chemistry,[236,237] and the pH of the medium.[238] An increase in the porosity and surface area of PSi and, consequently, the extension of the hydrolysable surface, results in a faster degradation.[235] Furthermore, the surface chemistry of PSi has an effect on its degradation rate, by influencing the hydrophilicity and, consequently, the surface wettability, as well as by determining the chemical reactivity to hydrolysis and oxidation.[23,236,239] For instance, as previously discussed, the surface stabilization of freshly etched PSi by controlled oxidation, hydrosilylaytion or hydrocarbonzation, reduces the reactivity towards oxidation and hydrolysis, thus enabling a control over PSi's degradability. Therefore, all these parameters should be taken into consideration and fine-tuned, when designing PSi materials with desired biodegradability for a specific biomedical application.

2.3.3 Non-specific cellular uptake and intracellular trafficking of PSi particles

In order to understand the interactions established at the nano-bio interface, it is of utmost importance to comprehend the cellular and intracellular compartments and inherent biologic mechanisms, as well as the way these interact and are influenced by the physicochemical properties of the interacting nanomaterials.[31] Considering the negative surface charge of the cell surface rendered by the lipids, proteins, and receptors composing the cell membrane, the surface charge of PSi and other nanoparticles is a key feature determining their cellular interaction and intracellular trafficking.[240] In addition, the extension and mechanisms of cellular internalization of nanoparticles are dependent on other parameters, such as the concentration, particles size, morphology, surface chemistry, and the exposure time to the cells.[241,242]

The cellular internalization of PSi nanoparticles occurs predominantly *via* endocytosis, leading to the formation of endocytic vesicles that subsequently fuse with endosomes. These primary endosomal compartments can either expel the PSi nanoparticles back to the extracellular environment or mature into secondary endosomes, which in turn fuse with lysosomes responsible for the degradation of the internalized PSi nanomaterial (*Section 2.2.4*).[243] Therefore, the therapeutic efficiency of PSi based nanoformulations crucially

depends on the capacity of the nanocarriers to evade the endocytic pathway and release the therapeutic cargo in the cytoplasm of the cells, especially when considering the delivery of biomolecules. In general, the electrostatic interaction of positively charged nanoparticles with the negatively charged moieties in the cell membranes favours their cellular association and internalization. In addition, cationic nanoparticulate systems can more efficiently escape the endolysosomal compartments, when compared to their anionic counterparts.[244,245] A strategy to circumvent this limitation involves the functionalization of negatively charged nanoparticles with positively charged polymers featuring a high density of protonable amine groups, which buffers the pH, generates a proton influx and, consequently, increases the osmotic pressure inside the endosomes, leading to the disruption of the endosomal membrane and escape of the nanoparticles from these compartments (*Section 2.2.4.1*).[168] For example, PSi nanoparticles were modified with PEI for complexing and delivering siRNA into the cytoplasm of human breast cancer cells, after escaping the endolysosomal compartments by exploring the aforementioned mechanism.[246]

Although less attention has been drawn to improve the intracellular trafficking and endosomolytic properties of the PSi nanoparticles, significant efforts have been done for enhancing the cellular interaction and uptake of these nanoplatforms, particularly by developing targeted PSi nanoparticles that exhibit cell/tissue specificity and induce the cellular internalization by receptor-mediated endocytosis.[18] Some of these strategies will be further outlined in the following section of this dissertation (*Section 2.3.4.2*).

2.3.4 Biomedical applications of PSi particles

Since the bioactivity of PSi was first reported *in vivo* by Canham, significant strides have established this material as a promising platform for biomedical purposes, including the development of biosensors,[247] implants,[248] biomimetic organelles or nanoreactors,[249] *in vivo* imaging probes[228,230,250,251] and drug delivery systems,[16,18] with application in cancer therapy[252,253] and cancer immunotherapy,[254-256] diabetes[231,232,257,258] and cardiovascular diseases.[221,259] This section of the dissertation highlights some of the most recent progresses on the application of PSi as a drug delivery and cancer targeting platform, as well as its integration in advanced and multifunctional drug delivery systems. In this regard, **Table 3** provides examples of the application of PSi nanoparticles in the cancer biomedical field.

Table 3. *Examples of PSi nanoparticles for cancer biomedical applications.*

PSi	Surface modification	Drug(s)	*In vitro*/*In vivo* model(s)	Main conclusions	Refs
Cancer drug delivery					
UnTHCPSi	PSi-PEI-PMVEMA@ ASHF	5-fluorouracil Celecoxib	Caco-2 HT-29	pH-responsive combined drug delivery Enhanced drug permeability *In vitro* antiproliferation effect	260

UnTHCPSi	HABCD	Sorafenib	MCF-7 MDA-MB-231	Improved colloidal and plasmatic stabilities Sustained drug release Enhanced *in vitro* cellular interactions and antiproliferation effect	222
	PEI MTX AS1411	Methotrexate Sorafenib	MDA-MB-231 NIH-3T3	Enhanced *in vitro* cellular uptake and combined antiproliferation effect in nucleolin-positive cells	261
	PEG VD11-4-2	Doxorubicin	MCF-7	pH-dependent drug release Drug release monitoring *In vitro* hypoxia-induced cancer cell targeting and antiproliferation effect	262
	AmQu	Doxorubicin	MCF-7 DOX/MCF-7^{R}	pH-responsive drug release Drug release monitoring Multidrug resistance reversing Enhanced *in vitro* cellular interactions and antiproliferaion effect	263
THCPSi	PSi@MF/H/ MFHF	Atorvastatin Celecoxib	HT-29	Multistage pH-controlled combined drug delivery *In vitro* antiproliferation effect	264
	PEG-*b*-PLA/ PEG-*b*-PHIS micelles	Sorafenib	RAW 264.7 PC3MM2	pH-triggered drug release *In vitro* reduced macrophage interactions pH-dependent antiproliferation effect	265

TOPSi	PAE Pluronic F127	Doxorubicin Paclitaxel	HeLa RAW 264.7	Sequential pH-responsive combined drug delivery Enhanced *in vitro* cellular interactions and antiproliferation effect	204
APSTOPSi	NIPAm-DMA-AEM	Doxorubicin	HeLa Hep2 3LL tumour bearing mice	Thermal-responsive drug release upon IR or RF irradiation Enhanced *in vitro* and *in vivo anticancer* therapeutic effects	266
APSTCPSi	NA	Methotrexate Sorafenib	U87 MG EA.hy926	Dual drug delivery *In vitro* antiproliferation effect	267
TCPSi	PSi@AcDex CPP	Methotrexate Sorafenib Paclitaxel	MCF-7 MDA-MB-231	pH-responsive multidrug delivery Enhanced cellular internalization and *in vitro* antiproliferation effect	268
Cancer active targeting					
PSi	MLR2 Ab mAb528 Ab Rituximab	Camptothecin	SH-SY5Y U87MG U87MG.Δ2–7 HR1K DOHH-2	Enhanced cellular uptake and antiproliferative effect in antigen-overexpressing cells	269
	Anti-CD20 Ab	Camptothecin AuNCs	HR1K Jurkat	Enhanced *in vitro* cellular association in CD20-expressing cells *In vitro* combined chemo and hyperthermal therapeutic effects when exposed to EM field	270
THCPSi	CooP peptide	NA	MDA-MB-231 MDA-MB-231 tumour bearing mice	Enhanced *in vitro* cellular association Enhanced *in vivo* tumour targeting and accumulation in MDGI-expressing tumours	271

APSTCPSi	RGD iRGD	Sorafenib	EA.hy926	Enhanced *in vitro* cellular internalization and antiproliferation effect	205
Cancer immunotherapy					
LPSi	Agonistic CD40 mAb (FGK45)	NA	BMDC C57BL/6	Enhanced CD40-mediated cellular uptake and B cell activation	272
UnTHCPSi	Anti-CD326 Ab	Sorafenib	MCF-7 MDA-MB-231	Enhanced *in vitro* cellular uptake, ADCC activity, cytokine release and antiproliferation effect in CD326-expressing cells Combined cancer chemo-immunotherapy	273
TOPSi	PSi@ SpAcDex@ CCM Trp2	NA	KG1 BDCM PBMC	Cytocompatibility Co-stimulatory signal induction Multistage nanovaccines with adjuvant properties	254
Cancer photodynamic therapy					
PSi	NA	NA	HeLa NIH-3T3	Photosensitizers for singlet oxygen generation *In vitro* phototoxicity	274
	Porphirin	NA	MCF-7	Enhanced *in vitro* cellular uptake and phototoxicity	275
	Porphirin Mannose	NA	MCF-7	Enhanced *in vitro* cellular uptake and two-photon-induced phototoxicity	276
Cancer photothermal therapy					
PSi	NA	NA	CT-26 CT-26 tumour bearing mice	*In vitro* and *in vivo* photothermal ablation in combination with 808 nm NIR laser	277
	DMSO stabilization	NA	BXPC-3	*In vitro* photothermal ablation in combination with 808 nm NIR laser	278

PSi	Polyaniline	Doxorubicin	4T1 HUVEC 4T1 tumour bearing mice	Dual pH/NIR light-triggered drug release *In vitro* and *in vivo* synergistic chemo-photothermal therapeutic effects	279
UnTHCPSi	PSi-AuNRs @Calcium alginate nano hydrogel	Afatinib Docetaxel Erlotinib Doxorubicin	MCF-7 MCF-7/DOX SKBR-3 SKBR-3/AR MDA-MB-231 NCl-H2087	Inhibition of multidrug resistance *In vitro* synergistic multidrug-photothermal antiproliferation effects	280
APSTCPSi	IR820 Doxorubicin	Doxorubicin	MCF-7 MCF-7/ADR	Dual pH/NIR light-triggered drug release *In vitro* synergistic chemo-photothermal antiproliferation effects in drug resistant cells	281
Cancer gene or RNAi therapy					
PSi	APS	MRP1 siRNA	T98G	Effective downregulation of MRP1 mRNA and protein expression *In vitro* cellular apoptotic and necrotic effects	282
Cancer imaging					
LPSi	PEG	NA	2008-mCherry and SKOV3 tumour bearing mice	*In vivo* late time-gated tumour imaging	283
	SiO_2 shell PEG iRGD	NA	4T1 tumour bearing mice	*In vivo* time-gated tumour imaging	251
		NA	HeLa tumour bearing mice	*In vivo* tumour targeting and two-photon imaging	284
THCPSi	^{18}F-labeling SLNC	NA	MDA-MB-231 tumour bearing mice	Improved dispersibility *In vivo* tumour imaging	285
UnTHCPSi	L1-Gd Cetuximab Rituximab	NA	NIH-3T3 U87 HR1K	*In vitro* cellular targeting to antigen-expressing cells MRI contrast agents	286

Cancer theranostics					
LPSi	Dextran	Doxorubicin	MDA-MB-435 HeLa MDA-MB-435 tumour bearing mice	Biocompatibility Biodegradability *In vitro* antiproliferative effect and imaging *In vivo* tumour imaging	230
		NA	3T3-L1 CF2Th Hep2	*In vitro* bioimaging and antiproliferation effect upon ultrasonic irradiation	287
UnTHCPSi	AF488 ^{111}In-labeling iRGD	Sorafenib	PC3MM2 PC3MM2 tumour bearing mice	Enhanced *in vivo targeted* tumour accumulation and suppression *In vivo* tumour imaging	250

Abbreviations: Ab, antibody; AcDex, acetalated dextran; ADCC, antibody-dependent cell-mediated Cytotoxicity; AEM, 2-aminoethyl methacrylate hydrochloride; AF488, Alexa Fluor® 488; AmQu, 3-aminopropoxy-linked quercetin; APCs, antigen presenting cells; APS, 3-aminopropyltrietoxysilane APSTCPSi, APS modified TCPSi; APSTOPSi, APS modified TOPSi; ASHF, hydroxypropyl-methylcellulose acetate succinate; AuNCs, gold nanoclusters; AuNRs, gold nanorods; BMDC, bone marrow-derived dendritic cells; CCM, cancer cell membrane; CPP, cell-penetrating peptide; DMA, N,N'-dimethylacrylamide; DMSO, dimethyl sulfoxide; DOX, doxorubicin; EM, electromagnetic; HABCD, heptakis(6-amino-6-deoxy)-β-cyclodextrin; IR, infrared; iRGD, internalizing RGD; LPSi, luminescent PSi; mAb, monoclonal antibody; MDGI, mammary-derived growth inhibitor; MF/HF/MFHF, hypromellose acetate succinate; MRI, magnetic resonance imaging; mRNA, messenger RNA; MTX, methotrexate; NA, not applicable; NIPAm, N-isopropylacrylamide; NIR, near infrared; PAE, poly(beta-amino ester); PBMC, peripheral blood monocytes; PEG, polyethylene glycol; PEG-b-PHIS, PEG-block-poly(L-hystidine); PEG-b-PLA, PEG-block-polylactide methyl ether; PEI, poly(ethylenimine); PMVEMA, poly(methyl vinyl ether-alt-maleic acid); PSi, porous silicon; RF, radiofrequency; RGD, arginine-glycine-aspartic acid sequence; siRNA, small interfering RNA; SLNC, solid lipid nanocomposite; SpAcDex, spermine-modified AcDex; TCPSi, thermally carbonized PSi; THCPSi, thermally hydrocarbonized PSi; TOPSi, thermally oxidized PSi; UnTHCPSi, undecylenic acid modified THCPSi.

2.3.4.1 PSi particles for drug delivery

In addition to the superior biocompatibility and suitable biodegradability of PSi particles, the unique nanoporous structure, large pore volume and high surface area-to-volume ratio of these platforms render them an ideal candidate for drug delivery purposes. Different types of therapeutic cargos, including small drug molecules, proteins,[231,257,288] peptides[232,258,289-292] and nucleic acids[246,293-298] can be efficiently loaded into the porous network of PSi carriers, and released in a controlled mode by pore diffusion or upon the dissolution of the PSi matrix.[19,28,299] The drug loading and release profiles of molecules incorporated into the pores of PSi

are governed by the physicochemical properties of the PSi material, such as the pore size and volume, surface charge, chemistry, and modification, hydrophobicity/hydrophilicity and its degradation rate. In addition, the physicochemical properties of the payload, as well as the solvent, method and technical parameters used for drug loading are determinant for the efficiency and reproducibility of the loading process and for attaining the intended release behaviour.[28,203,300,301]

Different methods can be applied for loading active molecules into the pores of PSi materials, including immersion, covalent grafting, impregnation and drug entrapment by oxidation.[28,203] Among these techniques, the immersion method is the most frequently used, owing to its straightforwardness, the feasibility to load a wide range of molecules with distinct physicochemical properties, and the possibility to be carried out in mild chemical conditions and at room temperature, thus being suitable for loading labile compounds, such as biomolecules.[301] This method consists of the simple immersion of the PSi particles in a drug solution and relies on the diffusion of this solution into the porous structure of PSi and subsequent physical adsorption of the drug molecules to the pore surface. The phenomenon of physical adsorption is driven by the spatial confinement and chemical interactions established between the loaded molecules and the PSi pore surface. Therefore, it is highly dependent on the physicochemical characteristics of the PSi particles, namely the pore size,[226,302] surface chemistry and hydrophilicity/hydrophobicity,[302] the intrinsic properties of the loaded molecules, the surface tension, viscosity and concentration of the drug loading solution, the loading time, and the temperature.[16,17] Consequently, all these parameters have a significant impact on both the drug loading efficiency and reproducibility, and the release kinetics of the loaded molecules from the PSi matrix.[28]

An alternative and more robust approach for drug loading into PSi carriers involves the covalent grafting of the drug molecules to the inner and/or outer surface of the PSi materials.[267,275,301,303,304] In this case, the release of the active payload from the PSi particles only occurs after cleavage of the covalent bonds of the PSi-drug conjugates or degradation of the PSi matrix. Therefore, this methodology enables a precise control over the drug loading and release kinetics by tuning the type and conditions of the coupling chemistry applied and/or the degradation rate of the PSi framework. Although this approach grants more reproducible loading and release profiles in comparison to the physical adsorption method, the attainable drug loading degree is generally inferior, since it depends on the number of functional groups available for drug conjugation at the PSi surface.[301] This method was applied, for example, for conjugating methotrexate (MTX) to the pore surfaces of PSi nanoparticles, resulting in a prolonged release of this anticancer agent for up to 96 h and enhanced *in vitro* antiproliferative effect.[267]

In addition, an increased retention of the drug molecules inside the PSi materials and, consequently, a sustained drug release can be achieved by oxidizing the surface of the PSi pores after drug loading. During the oxidation process, additional oxygen atoms are inserted in the PSi matrix, leading to a reduction of the pore volume and an efficient entrapment of the active payload inside the PSi pores.[25,305] Following this approach, two compounds, cobinamide and rhodamine B, were co-loaded with an oxidizing agent, sodium nitrite, inside freshly etched PSi films, which were subsequently fractured into PSi microparticles. The oxidation-mediated trapping of the model compounds into the PSi material showed, not only

to improve the drug loading degree, but also and most importantly, to remarkably sustain the drug release by 20-fold, compared to the pre-loading oxidized counterparts.[305]

One of the main challenges and focuses in the field of drug delivery, particularly for cancer therapy, is associated with the poor aqueous solubility of drugs and consequent limited bioavailability. The formulation of poorly water-soluble drugs into PSi particulate systems has been demonstrated to significantly increase their dissolution in aqueous media.[16,299] When loaded in the nanosized pores of PSi particles, the drug molecules are spatially confined and restricted from rearranging into three-dimensional crystal lattices, thus remaining stable in an amorphous state or forming nanocrystals, which ultimately results in a higher dissolution rate, compared to the bulk counterparts.[299] This strategy has been applied for enhancing the aqueous solubility of a plethora of active compounds, including furosemide,[299,306,307] griseofluvin,[16,308] ibuprofen,[302,309] indomethacin,[310] celecoxib,[226] itraconazole,[311,312] ethionamide,[312] saliphenylhalamide,[313] sorafenib (SFB)[205,222] and cisplatin.[314]

Despite the above mentioned advantageous features of PSi particles for loading and delivering the therapeutic agents, the degradation and off-target uncontrolled release of the loaded cargo, owing to the unrestrained access of the release media and biological fluids to the open pores of the PSi matrix, are major drawbacks limiting the application of these biomaterials for drug delivery. Therefore, different strategies have been explored for circumventing this problem and attaining control over the drug release kinetics from the PSi particles, including the loading of the drug molecules by covalent grafting or oxidation-induced trapping previously described in this section, the physical capping of the pore apertures,[238,307] the chemical grafting of pore gating and stimuli-responsive systems,[204,315-318] or the encapsulation of the PSi particles within other carriers.[260,264,268,319-322]

The drug diffusion process from PSi-based drug delivery systems can be modified by physically adsorpting or covalently conjugating biocompatible and biodegradable non-responsive polymers or lipids to the surface of PSi particles. This strategy has been applied, for example, by coating the surface of PSi particles with chitosan for prolonging the release of insulin and enhancing insulin permeation across an *in vitro* intestinal monolayer model.[231] In another study, a solid-lipid nanocomposite combining glycerol monostearate and phosphatidylcholine was deposited onto the surface of PSi nanoparticles, improving their cytocompatibility, colloidal dispersity and *in vitro* stability in human plasma, and sustaining the release of the encapsulated furosemide.[307]

Furthermore, the surface of PSi particles can be functionalized with different stimuli-responsive gate-keeping systems, in order to attain a spatiotemporal control over the drug release kinetics. In this regard, a smart PSi-based nanocomposite, envisioned for sequential combination cancer therapy, was engineered by combining PSi nanoparticles and a pH-responsive nanovalve system. This dual-drug delivery nanoplatform was designed by covalently conjugating a pH-responsive cationic polymer, poly(β-amino ester), to the surface of DOX-loaded PSi nanoparticles, followed by stabilization with PTX-encapsulating micelles composed by a PEG and poly(propylene glycol) triblock copolymer. As a result, a remarkable synergistic chemotherapeutic effect was achieved *in vitro*, through an immediate release of PTX from the polymeric micelles, followed by a pH-triggered release of DOX from the PSi nanoparticles.[204]

2.3.4.2 PSi particles for active cancer targeting

Although PSi-based particulate systems have been demonstrating a high promise for drug delivery purposes, the biosafety and therapeutic efficiency of PSi-based nanomedicines, particularly when considering cancer therapy, is highly dependent on their capacity to accumulate in the malignant tissue, specifically attach to the targeted cells and deliver the therapeutic cargo in a sufficient concentration at the site of action. Therefore, one of the major focuses with respect to the application of PSi nanoparticles in cancer nanomedicine has been to develop active targeting strategies to selectively guide these nanovehicles to the surface of the cancer cells and trigger the receptor-mediated endocytosis locally. In this context, the surface chemical versatility of the PSi nanoparticles represents one of the most attractive features, for enabling the surface functionalization with a variety of targeting ligands, such as tumour homing peptides,[205,271] targeting antibodies,[26,30,256,269] and DNA aptamers,[261] thus tremendously expanding the potential of this nanoplatform for cancer drug delivery and therapeutic purposes.

In this regard, the surface of THCPSi nanoparticles was decorated with a tumour homing peptide targeting the mammary-derived growth inhibitor (MDGI) receptor. After intravenously administered into nude mice bearing subcutaneous MDGI-expressing tumours, the targeted nanoparticles showed an approximate 9-fold higher accumulation at the tumour site, in comparison to the non-functionalized particles.[271] In another approach, a straightforward and efficient method based on copper-free click chemistry was applied to covalently conjugate RGD and iRGD tumour penetrating peptides on the surface of APSTCPSi nanoparticles for targeting the tumour neovasculature. Both RGD and iRGD modified PSi nanocarriers exhibited a significantly enhanced cellular uptake in EA.hy926 endothelial cells *in vitro*, when compared to the unmodified APSTCPSi nanoparticles.[205]

In addition to tumour homing peptides, the surface of PSi nanocarriers can be functionalized with targeting antibodies that are specific to different tumours. For example, MLR2, mAb528 and Rituximab antibodies have been successfully conjugated onto the surface of PSi nanoparticles to specifically target neuroblastoma, glioblastoma and B lymphoma cells, respectively.[269] Furthermore, size- and shape-controlled PSi nanodiscs were recently fabricated by a new method combining colloidal lithography and metal-assisted chemical etching, loaded with an anticancer agent, camptothecin, and further modified with a MLR2 anti-p75 antibody for targeting the p75NTR neurotrophin receptor expressed on the surface of neuroblastoma cells (SH-SY5Y). After antibody functionalization, the drug loaded nanodiscs were found to be selectively attached and killed the cancer cells.[26] Alternatively, the tumour homing of PSi nanovectors can be attained by exploring biological targets overexpressed in stroma cells. Accordingly, a Ly6C antibody was conjugated on the surface of PSi nanoparticles as a dual targeting to pancreatic tumour associated endothelial cells and macrophages. Contrarily to the control nanocarriers, the Ly6C antibody decorated PSi nanoparticles exhibited high affinity to the cells expressing Ly6C *in vitro*. Moreover, the targeted nanocarriers were shown to accumulate in the tumour associated endothelial cells within 15 minutes, after their intravenous injection in orthotopic human pancreatic cancer bearing nude mice. Interestingly, after extravasation through the endothelial cell monolayer, the targeted PSi nanoparticles were engulfed by the Ly6C expressing tumour associated macrophages. It was demonstrated that, at 4 h after

administration, 9.8 ± 2.3% of the Ly6C targeted nanocarriers were accumulated in the pancreatic tumours as opposed to 0.5 ± 1.8% of the non-targeted nanoparticles.[30]

2.3.4.3 Progress in PSi-based multifunctional drug delivery systems

Taking advantage of the aforementioned attractive properties for drug delivery and tumour targeting, PSi-based materials can be used to design and engineer advanced drug delivery systems, as well as theranostic tools for the simultaneous therapy and diagnostics of cancer.

Along with the functionalization by targeting moieties, the surface chemical versatility of PSi nanoparticles provides the possibility for radio and fluorescent-labelling, therefore enabling to track the *in vivo* biofate of these targeted nanoparticulate systems.[29,221,250,259,271] For example, UnTHCPSi nanoparticles were dual-labelled with ^{111}In radiolabel for monitoring their biofate using live single photon emission computed tomography (SPECT/CT) imaging, and Alexa Fluor® 488 (AF488) fluorescent dye for long-term biodistribution studies. The dual-labelled PSi nanoparticles were subsequently functionalized with an iRGD targeting peptide, generating a targeted and dual-labelled multifunctional nanovector for directed cancer theranostics. In this study, the *in vivo* biodistribution of both targeted and non-targeted multifunctional nanovectors was investigated, following both intravenous and intratumoural injection in a prostate cancer xenograft mice model. While the intravenously administered nanovectors were mainly distributed to the liver and spleen of the mice, the intratumourally administered counterparts were revealed to accumulate and be retained at the tumour site, even at 26 h post-injection.[250]

The PSi nanoparticles have also been applied as a nanoplatform encapsulated within various micro- and nano-carriers to form advanced multifunctional drug delivery composites.[260,264,268,319-322] In this regard, an advanced nanocomposite comprising PSi nanoparticles encapsulated into a pH-responsive acetalated dextran (AcDex) polymeric matrix was efficiently fabricated by a one-step nanoprecipitation microfluidic technique, for combined cancer therapy. A multiplicity of chemotherapeutics possessing distinct physicochemical properties, namely SFB, MTX and PTX, were simultaneously and efficiently loaded into the PSi@AcDex nanocomposites with precise ratiometric control. In order to enhance the intracellular delivery of the active payloads, the formulated nanocomposites were surface functionalized with a nona-arginine cell penetrating peptide. As a consequence of the enhanced cell penetrating properties and subsequent pH-triggered decomposition of the nanoplatforms in the endolysosomal compartments, an efficient intracellular release of the combined chemotherapeutic drugs was achieved, resulting in a potent concentration-dependent antiproliferative effect on breast cancer cells.[268] Similarly, a multifunctional nano-in-micro composite, incorporating PSi nanoparticles, gold nanorods and magnetic nanoparticles into giant liposomes, was engineered by microfluidics. This advanced composite was contemplated for the controlled co-delivery of hydrophilic and hydrophobic drugs, as well as DNA nanostructures, while presenting both photothermal and magnetic responsiveness.[322]

PSi particles have also been successfully used as a vehicle for other nanoparticulate drug delivery systems. For instance, nano-in-micro multistage vectors were assembled by encapsulating drug-loaded nanocarriers into hemispherical PSi microparticles, which size,

shape and surface chemical properties were optimized for attaining a desired *in vivo* biodistribution and enhancing the accumulation at the tumour vasculature.[323,324] In a similar approach, quasi-hemispherical PSi microparticles modified with a E-selectin thioaptamer ligand were explored for delivering PTX-loaded liposomes to the bone marrow endothelium.[325] Moreover, the same drug was formulated into PEG-block-poly(ε-caprolactone) micelles subsequently loaded into the pores of PSi particles, delaying the drug release and efficiently supressing the tumour growth in mice bearing MDA-MB-468 breast cancer cells.[326]

In addition to drug nanocarriers, PSi was reported as a suitable platform for accommodating a wide range of smaller nanoparticles within its porous structure, including carbon nanotubes,[327] quantum dots,[328] hollow gold nanoshells,[329] and SPIONs.[330,331] In the last example, the incorporation of SPIONs nanoparticles within the PSi carriers considerably potentiates its applicability in biomedicine, not only for enabling the magnetically driven delivery of therapeutic agents,[330] but also for providing the opportunity to integrate both therapeutic and magnetic resonance imaging modalities in advanced multifunctional theranostic systems.[331]

Despite the great promise of PSi nanoparticles for formulating different types of small drug molecules and biomolecules, and the remarkable progresses on the development of advanced and multifunctional PSi-based drug delivery systems, the successful application of these nanocarriers for cancer drug delivery and therapy is still defied by their ineffectiveness to deliver the active cargo at sufficient therapeutic concentrations to their site of action, mostly owing to their limited non-specific cellular interaction and internalization, intracellular trafficking, and lack of specificity for the targeted cancer cells or tissues. Therefore, there is still the need for designing innovative PSi-based nanoplatforms that not only circumvent these bottlenecks, but also integrate both therapeutic and diagnostic modalities, moving towards the development of a new generation of multifunctional PSi-based nanoformulations with potential application in cancer nanomedicine.

3 Aims of the study

Despite the recent exciting breakthroughs in the field of cancer nanomedicine, the complexity and heterogeneity of both cancer pathophysiology and therapeutic nanotechnology still challenge the application and clinical translation of nanoparticulate systems, demanding the emergence and optimization of novel and more advanced nanoformulations. Over the past decades, PSi nanoparticles have demonstrated great potential for drug delivery applications, owing to advantageous physicochemical and biological properties, with particular emphasis in cancer nanomedicine. However, major deadlocks associated with colloidal and plasmatic instabilities, poor cell-targeting efficiency and *in vivo* PK, limited cellular association, internalization and intracellular trafficking, as well as premature and uncontrolled release of the therapeutic cargos, still defy the implementation of these nanoparticles as effective anticancer drug delivery systems.

In this regard, this dissertation outlines several strategies, including the surface modification of PSi nanoparticles with biofunctional polymers and the engineering of advanced multifunctional PSi-based nanocomposites, with the main aim of circumventing some of the aforementioned bottlenecks for the more successful application of this nanoplatform in cancer nanomedicine.

The specific objectives of this dissertation are the following:

1. To investigate the potential of the surface biofunctionalization of PSi nanoparticles with an amine-modified hyaluronic acid derivative in order to increase the specific cellular interactions and uptake by targeted CD44-overexpressing breast cancer cells, as well as to improve the colloidal and plasmatic stabilities **(I)**.

2. To evaluate the impact of the surface polymeric modification of PSi nanoparticles on the cytocompatibility, non-specific cellular internalization, endosomal escape, methotrexate release profile, and *in vitro* antiproliferative effect of the nanocarrier **(II)**.

3. To fabricate a multifunctional PSi-based nanocomposite encapsulating both sorafenib-loaded PSi and Au nanoparticles into a polymeric nanocomplex, aiming at improving the cytocompatibility, cellular association and internalization, intracellular trafficking, cytoplasmic delivery and chemotherapeutic effect of the drug-loaded PSi nanoplatform **(III)**.

4. To design and develop a multifunctional nano-in-nano composite, consisting of DNA-gated PSi nanoparticles encapsulated within polymeric nanocomplexes for combined cancer therapeutics or theranostics, and for further evaluation towards intracellular bioresponsive dual-drug delivery **(IV)**.

4 Experimental

This section summarizes the experimental methods used in this dissertation. The detailed description of all the materials, instrumentation and methods used in this work can be found in the respective original publications (**I**–**IV**).

4.1 Fabrication of nanocomposites (I–IV)

4.1.1 Fabrication of UnTHCPSi nanoparticles (I–IV)

The UnTHCPSi nanoparticles were fabricated by electrochemically anodizing monocrystalline boron-doped *p*+-type Si ⟨100⟩ wafers, with resistivity values of 0.01–0.02 Ω.cm, in a 1:1 (*v/v*) aqueous HF(38%)-ethanol electrolyte. The multilayer structure was formed by applying an etching profile consisting of repeating low/high current density pulses, designed to form fracture planes at desired intervals. Hydrogen-terminated free-standing multilayer PSi films were subsequently lifted off from the substrate by abruptly increasing the etching current density to the electropolishing region. The PSi films were then dried at 65 ºC for several hours to evaporate the electrolyte.[228] In order to improve the PSi surface stability and to remove the adsorbed moisture and residual oxygen, the PSi films were inserted into a quartz tube under continuous N_2 flow (1 $L.min^{-1}$) for at least 30 min at room temperature. In order to render the PSi films a hydrocarbon termination and, consequently, improved surface stability towards oxidation, a thermal hydrocarbonization treatment was performed by exposing the PSi films to a 1:1 (*v/v*) N_2:acetylene (C_2H_2) flow (1 $L.min^{-1}$), for 15 min at room temperature, followed by heat treatment at 500 ºC for 15 min, and cooling back to room temperature under N_2 flush.[22] For functionalizing the THCPSi's surface with carboxylic groups, the films were immersed into 10-undecylenic acid for 16 h at 120 ºC. The resulting UnTHCPSi films were finally wet-milled in a high energy ball mill, using 1-decene as milling medium for minimizing surface oxidation, in order to obtain the UnTHCPSi nanoparticles.[219]

4.1.2 Surface functionalization of UnTHCPSi nanoparticles (I–IV)

4.1.2.1 Preparation of UnTHCPSi-amine modified hyaluronic acid nanoparticles (I)

An amine modified hyaluronic acid (HA^+) was synthesized, prior to conjugation to the surface of UnTHCPSi nanoparticles. For this purpose, an aqueous solution of HA sodium salt (200 mg, 30 mmol) was sequentially dialyzed for 20 h against 4 L of 0.01 N hydrochloric acid (HCl) and Milli-Q water. The acidic form of HA (172 mg, 0.045 mmol of acidic groups) was recovered by lyophilisation, and subsequently dissolved in 14 mL of anhydrous dimethylsulfoxide (DMSO). The carboxylic groups of HA were activated by adding 80 mg (0.70 mmol) of sulfo-*N*-hydroxysulfosuccinimide (Sulfo-NHS) and 124 µL (109 mg, 0.70 mmol) of 1-ethyl-3-[3-dimethylaminopropyl]carbodiimide (EDC), allowing the reaction to occur for 60 min at room temperature. Following step, the substitution of the carboxylic

groups of HA, was done by addition of NH_2-PEG_2-NHBoc (223 mg, 0.90 mmol, 2 eq.) and *N*-ethyldiisopropylamine (DIPA) (70 mg, 0.54 mmol, 1.2 eq.) under stirring, after which the reaction was set to proceed for 4 days. The resulting HA-PEG_2-NHBoc was then precipitated in acetone (140 mL), washed three times with the same solvent, filtered, and dried under vacuum to remove the residual DMSO. The terminal amine groups of HA-PEG_2-NHBoc were deprotected by dissolving the polymer (50 mg) in 5 mL of trifluoroacetic acid (TFA) at 0°C. After stirring for 20 h at 4 °C, 20 mL of Milli-Q water was added, and the solution was neutralized with sodium hydroxide (NaOH). Finally, the sodium salt of HA^+ was obtained by dialyzing the solution for 20 h against 2 L of 0.1 M NaCL and Milli-Q water, followed by lyophilisation.[332]

For preparing the UnTHCPSi-amine modified hyaluronic acid ($UnHA^+$) nanoparticles, the synthesized HA^+ was covalently conjugated to the carboxylic groups of UnTHCPSi nanoparticles *via* EDC/NHS coupling chemistry. In this regard, 1.5 mg of UnTHCPSi nanoparticles were dispersed in 4 mL of 10 mM 2-(*N*-morpholino)ethanesulfonic acid (MES) saline buffer (pH 5.2). The precursor carboxylic groups of the UnTHCPSi nanoparticles were activated by reacting with 6 mg (0.05 mmol) of *N*-hydroxysuccinimide (NHS) and 8 µL (0.05 mmol) of EDC, under stirring at room temperature and at 800 rpm for 90 min. After activation, the HA^+ was added to the reaction vial at a UnTHCPSi:HA^+ ratio (*w/w*) of 1:2, and the nucleophilic substitution was left to occur overnight under the same stirring conditions. The excess of reagents was removed by rinsing the modified nanoparticles three times with Milli-Q water. Finally, the $UnHA^+$ nanoparticles were re-dispersed in Hank's balanced salt solution-4(-2-hydroxyethyl)-1-piperazineethanesulfonic acid (HBSS−HEPES) buffer (pH 7.4) and stored at 4 ºC until further use.

4.1.2.2 Preparation of UnTHCPSi-poly(ethylenimine)-poly(methyl vinyl ether-alt-maleic acid) nanoparticles (II)

The UnTHCPSi-poly(ethylenimine)-poly(methyl vinyl ether-*alt*-maleic acid) (UnPP) nanoparticles were prepared by successive covalent conjugation of hyperbranched PEI (Mw ~25,000) and poly(methyl vinyl ether-*alt*-maleic acid) (PMVE-MA) onto the surface of the UnTHCPSi nanoparticles.

In the first step of UnPP production, the carboxylic groups of UnTHCPSi nanoparticles were activated by dispersing 1.5 mg of these nanoparticles in 4 mL of MES saline buffer (pH 5.2), followed by the addition of 6 and 7 mg of NHS and EDC, respectively. After reacting for 2 h under stirring at room temperature and at 800 rpm, the activated surface of UnTHCPSi nanoparticles was exposed to an excess of PEI at an UnTHCPSi:PEI ratio (*w/w*) of 1:10 and left to react overnight, under stirring in the aforementioned conditions. The resulting UnP nanoparticles were extensively rinsed with Milli-Q water to remove the unreacted reagents and re-suspended in HBSS−HEPES buffer (pH 7.4).

In the subsequent step, EDC/NHS coupling chemistry was used to conjugate PMVE-MA to the surface of the previously obtained UnP nanoparticles. For this purpose, poly(methyl vinyl ether-*alt*-maleic anhydrate) (PMVE-MAh; Mw ~216,000) was first dissolved in HBSS−HEPES buffer (pH 5.2) and heated for 3 h at 70 ºC, in order to obtain the PMVE-MA copolymer. Next, PMVE-MA was activated by EDC/NHS for 2 h, and

subsequently added to the UnP nanoparticles dispersed in the same buffer, at a UnP:PMVE-MA ratio (*w/w*) of 1:1. The resulting UnPP nanoparticles were washed twice with Milli-Q water, by repeated centrifugation for 5 min at 15,000 rpm and re-dispersion for obtaining a reagent-free final product. Finally, the nanoparticles were re-suspended in HBSS−HEPES buffer (pH 7.4) and stored at 4 ºC until further use.

4.1.2.3 Preparation of UnTHCPSi-cystine-acridine-DNA nanoparticles (IV)

The bioresponsive UnTHCPSi-cystine-acridine-DNA (UnCAD) nanocomposites were engineered by biofuntionalizing the surface of UnTHCPSi nanoparticles with cysteine and 9-aminoacridine as redox responsive inducer and DNA intercalator, respectively, using EDC/NHS coupling chemistry. Briefly, 20 µL of EDC and 15 mg of NHS were separately dissolved in 4 mL of 10 mM MES saline buffer (pH 5.2). After that, 3 mg of UnTHCPSi nanoparticles were dispersed in the EDC solution and tip-sonicated for 20 sec, followed by addition of the NHS solution. The reaction vial was left under stirring at room temperature for 2 h, for activating the carboxylic groups of the UnTHCPSi nanoparticles, which were then purified from the unreacted coupling reagents by centrifugation at 13,000 rpm for 6 min. Next, 25 mg of cystine was dissolved in 1 mL of HCL, mixed with 7 mL of 0.1 M phosphate buffer solution (PBS; pH 9.0), followed by pH adjustment of the final solution to 9.0. The activated UnTHCPSi nanoparticles were re-suspended in 2 mL of cystine solution and left to react for 18 h under stirring at room temperature and at 800 rpm. Due to pH-dependent cystine solubility, the reaction was performed at a higher pH than the optimal range suggested by the manufacture for the nucleophilic substitution of NHS-esters (pH 7−8). Therefore, an excess of cystine and a longer reaction time were used for compensating the slower conjugation kinetics. The resulting UnTHCPSi-cystine (UnC) nanoparticles were centrifuged at 13,000 rpm for 6 min, washed twice with 0.1 M PBS (pH 9.0) and once with Milli-Q water, and again activated *via* EDC/NHS chemistry in 10 mM of MES saline buffer (pH 5.2), as mentioned above. The activated UnC nanoparticles were purified by centrifugation and re-suspended in a 9-aminoacridine solution prepared by dissolving 30 mg of this compound in 7 mL of ethanol-PBS (0.1 M, pH 5.2) (3:4 *v/v*) mixture. The reaction was left to occur for an additional 18 h period and the resulting UnTHCPSi-cystine-acridine (UnCA) nanoparticles were again centrifuged, washed once with ethanol and twice with Milli-Q water. Finally, DNA was anchored at the surface UnCA nanoparticles through intercalation with the acridine moieties. For accomplishing the DNA coating, 6 mg of DNA was dissolved in 1.5 mL of PBS (pH 7.4), and mixed with the UnCA nanoparticles suspended in 3 mL of the same buffer solution. After stirring for 24 h, the UnCAD nanoparticles were isolated by centrifugation and washed three times with PBS (pH 7.4). DNase free buffers and materials were used in all the steps of DNA intercalation.

4.1.2.4 Fluorescent labelling of nanoparticles (I−III)

Fluorescently labelled UnTHCPSi, UnHA^{+}, and UnPP nanoparticles were obtained by physically adsorbing fluorescein isothiocyanate (FITC) onto their surface (**I** and **II**). For that purpose, FITC was first dissolved in a 1:5 (*v/v*) mixture of 0.1 M of HEPES (pH 7.5) and

ethanol, and subsequently added to the nanoparticles at a nanoparticles:FITC ratio of 10:1 (*m/m*).

Alternatively, the AF488 fluorescent dye was covalently conjugated to the carboxylic groups of UnTHCPSi nanoparticles by EDC/NHS coupling chemistry (**III**). In this case, 1.5 mg of UnTHCPSi were dispersed in 4 mL of MES buffer (pH 5.2). After that, 8 µL EDC and 6 mg of NHS were added to the nanoparticles suspension, and the activation of the precursor carboxylic groups of the UnTHCPSi nanoparticles was allowed to occur for 2 h at room temperature, under stirring at 800 rpm. Next, 20 µg of AF488 hydrazine was added to the reaction vial at 1:75 (*w/w*) ratio (AF488:UnTHCPSi nanoparticles), and the conjugation was proceeded for additional 2 h at the same stirring conditions. The AF488-labelled UnTHCPSi nanoparticles were purified from the excess of coupling reagents and excess of AF488 by washing once with 10 mM of HCl and twice with Milli-Q water.

4.1.3 Fabrication of L-cysteine-poly(ethylenimine)-poly(methyl vinyl ether-alt-maleic acid) nanocomplexes (III–IV)

The L-cysteine-poly(ethylenimine)-poly(methyl vinyl ether-*alt*-maleic acid) (CPP) nanocomplexes composed of three different polyelectrolytes, namely L-cysteine, PEI and PMVE-MA, were produced by an ionotropic gelation technique.[333-335] In a first step, PMVE-MAh was dissolved in 0.2× HBSS buffer (pH 5.2) at a concentration of 1.67 mg.mL^{-1} for, at least, 3 h at 70 ºC, to obtain the PMVE-MA copolymer. Additionally, a L-cysteine solution (5.0 mg.mL^{-1}) was prepared in acetate buffer (pH 4.0), containing a 1:1 (*v/v*) ratio mixture of 1.7 M of acetic acid and 0.1 M of sodium acetate. PEI was dissolved in Milli-Q water at a concentration of 10.0 mg.mL^{-1}. For preparing the CPP nanocomplexes, 500 and 300 µL of the L-cysteine and PEI solutions, respectively, were mixed and constantly stirred. Next, 3.4 mL of the PMVE-MA solution was slowly added to the mixture, under stirring at 800 rpm and ultrasonication using a Vibra-cell VCX 750 ultrasonic processor (Sonics, Sonics and Materials, Inc., CT, USA) at 30% amplitude, and post stirring for 1 min in the same conditions.

4.1.4 Fabrication of UnCPP, UnAuCPP, and UnCAD@CPP nanocomposites (III–IV)

The UnCPP (**III**), UnAuCPP (**III**), and UnCAD@CPP (**IV**) nanocomposites were engineered by nanoencapsulating UnTHCPSi nanoparticles, UnTHCPSi and Au nanoparticles, and UnCAD nanoparticles, respectively, into the CPP nanocomplexes. The nanoencapsulation was accomplished by resuspending the encapsulates, more precisely 500 µg of UnTHCPSi and UnCAD nanoparticles, and 20 µg of Au nanoparticles in the PMVE-MA solution, followed by ultrasonication for 30 sec, prior to addition in the L-cysteine:PEI mixture. After that, the fabrication protocol continued, as previously described for the bare CPP nanocomplexes (*Section 4.1.3*).

4.2 Physicochemical characterization of nanocomposites (I−IV)

The physical properties of UnTHCPSi nanoparticles were characterized with N_2-sorption at −196 ºC, using a TriStar 3000 gas sorption apparatus (Micromeritics Inc., GA, USA). The specific surface area was calculated from the isotherm using the Brunauer-Emmett-Teller (BET) theory,[336] and the total pore volume was considered to be the total amount adsorbed at a relative pressure p/p0 = 0.97. The average pore diameter was estimated from the values of specific surface area and total pore volume obtained, assuming that the pores of the UnTHCPSi were cylindrical.

The average hydrodynamic diameter (Z-average), polydispersity index (PdI) and surface zeta (ζ)-potential of the different nanoparticulate systems developed in this thesis were analysed by dynamic light scattering (DLS) and electrophoretic light scattering (ELS), respectively, using a Zetasizer Nano ZS equipment (Malvern Instruments Ltd., Malvern, UK). Prior to the measurements, the nanoparticles were diluted in Milli-Q water to a final concentration varying from 25−55 $\mu g.mL^{-1}$, and subsequently loaded into disposable polystyrene (Sarstedt AG & Co., Nümbrecht, Germany) or disposable folded capillary cells (DTS1070; Malvern Instruments Ltd., Malvern, UK) for the size or ζ-potential analyses, respectively. All the sample measurements were performed in triplicate.

The morphology of the nanocarriers was evaluated by transmission electron microscopy (TEM), using a Jeol JEM-1400 microscope (Jeol Ltd., Akishima, Tokyo, Japan), operating at an acceleration voltage of 80 kV. In this regard, the bare and polymer-conjugated UnTHCPSi nanoparticles (**I−II**) were centrifuged, re-dispersed in ethanol at a concentration of 10 $\mu g.mL^{-1}$, ultrasonicated for 30 sec, dropped onto carbon-coated copper TEM grids (150 mesh; Ted PELLA Inc., CA, USA), and allowed to dry overnight at room temperature. In the last two works of this thesis (**III−IV**), the specimens were prepared by diluting the nanocomposites suspensions to a final concentration of approximately 5.5×10^2 $\mu g.mL^{-1}$, in which the aforementioned carbon-coated cooper TEM grids were immersed for 1 min, followed by drying using filter paper and air-drying overnight at room temperature.

The surface chemical compositions of the bare and polymer-functionalized UnTHCPSi nanoparticles (**I−II**) were investigated by attenuated total reflectance Fourier transform infrared (ATR−FTIR) spectroscopy, using a Bruker VERTEX 70 FTIR spectrophotometer (Bruker Optics Inc., MA, USA) fitted with a horizontal MIRacle™ single reflection ATR accessory (Pike Technologies, WI, USA). All the samples were dried at room temperature for 48 h, prior to recording of the ATR-FTIR spectra in the wavenumber region between 4000−650 cm^{-1} with a 4 cm^{-1} resolution, using OPUS 5.5 software.

For confirming successful nanoencapsulation of the UnTHCPSi and Au nanoparticles into the CPP nanocomplexes, the chemical elements composing these nanoencapsulates, *i.e.*, Si and Au, respectively, were identified by energy dispersive X-ray (EDX) microanalysis. For this purpose, TEM specimens were prepared following the protocol described above and the EDX spectra were recorded using an Oxford INCA 350 EDX microanalysis system (Oxford Instruments plc, Oxfordshire, UK) connected to a Hitachi S-4800 field emission scanning electron microscope (SEM, Hitachi High-Technologies Corp., Minato-ku, Tokyo, Japan), operating at a 30 kV accelerating voltage.

4.3 Drug loading and release (II−IV)

4.3.1 Loading of model drug molecules (II−IV)

The bare UnTHCPSi and surface-modified UnTHCPSi nanoparticles (**II−IV**) were loaded with different model drug molecules, by an immersion method using highly concentrated drug solutions.[16]

The anticancer drug MTX was loaded into UnTHCPSi, UnP and UnPP nanoparticles by immersing the nanoparticles into a 10 $mg.mL^{-1}$ concentrated solution of the drug in PBS (pH 8.0), at a 20:1 (*w/w*) ratio (MTX:UnTHCPSi) and under stirring for 2 h at 400 rpm and room temperature (**II**). The MTX-loaded nanoparticles were purified from the unloaded drug by centrifugation at 15,000 rpm for 7 min, followed by two washing steps with Milli-Q water.

SFB was loaded within the porous structure of UnTHCPSi nanoparticles, prior to the fabrication of UnCPP and UnAuCPP nanocomplexes (*Section 4.1.4*) (**III**). In this regard, the SFB-loaded UnTHCPSi nanoparticles (SFB@UnTHCPSi) were prepared by redispersing the UnTHCPSi nanoparticles in a 5 $mg.mL^{-1}$ concentrated SFB solution in methanol (MeOH) at a 50:1 (*w/w*) ratio (SFB:UnTHCPSi), followed by ultrasonication for 5 sec and stirring for 2 h at 800 rpm and at room temperature. After drug loading, the excess of drug solution was removed by centrifugation at 15,000 rpm for 10 min, and the drug molecules adsorbed to the nanoparticles surface were removed by washing the drug-loaded nanoparticles twice with Milli-Q water.

The loading of both hydrophilic and hydrophobic molecules within the pores of UnCA nanoparticles was performed before DNA capping and nanoencapsulation into the CPP nanocomplexes, as described in the *Sections 4.1.2.3* and *4.1.4*, respectively (**IV**). For loading the hydrophobic chemotherapeutic agent SFB, 3 mg of the UnCA nanoparticles were resuspended in 30 mL of a drug solution in acetone (4 $mg.mL^{-1}$) and left under stirring for 3 h at room temperature. After drug loading, the nanocarriers were centrifuged and washed twice with Milli-Q water. Moreover, for verifying the potential of the developed nanosystems to responsively deliver hydrophilic molecules, calcein was loaded into the UnCA nanoparticles by immersing 3 mg of the nanoparticles in 30 mL of 10 mM of PBS (pH 7.4), containing 0.8 mM of calcein, followed by stirring for 24 h at room temperature to allow the calcein molecules to diffuse into the pores of the nanocarriers. In this particular case, the DNA capping process was performed in a PBS solution supplemented with 0.8 mM of calcein, in order to avoid the release of the cargo during the process. The excess of calcein and DNA was then removed from the calcein-loaded UnCAD nanoparticles by centrifugation and three washing steps with Milli-Q water.

The drug loading degree (LD) of the different nanocarriers, calculated as the weight percentage of the drug in the nanocarrier, was determined by immersing the drug-loaded nanoparticles into a suitable solvent, enabling the complete release of the payloads, followed by the quantification with high pressure liquid chromatography (HPLC). The detailed description of the protocols used for drug loading measurements and the HPLC experimental setups can be found individually in the respective original publications (**II−IV**).

4.3.2 Encapsulation of model compounds via click-chemistry (IV)

In addition to SFN loading into the UnTHCPSi nanoparticles, also FITC was encapsulated as a model molecule within the CPP matrix of UnCAD@CPP *via* thiol-isocyanate click chemistry,[337] for fluorescent labelling of the nanocomposites and as a proof-of-concept for co-drug delivery and potential theranostic applications. The highest encapsulation efficiency of FITC was optimized by testing different concentration of the fluorescent dye. After optimization, 30 μg of FITC was dissolved in 70% ethanol, and subsequently added to 3.4 mL of PMVE-MA solution containing 500 μg of UnCAD nanoparticles. Next, the fluorescent UnCAD@CPP nanocomplexes were prepared, as previously described in the *Section 4.1.4*.

The encapsulation efficiency of FITC into UnCAD@CPP nanocomposites was quantified by an indirect method. For this purpose, the FITC-loaded UnCAD@CPP nanocomposites were centrifuged for 5 min at 13,000 rpm, and 200 μL of the supernatant was collected into 96-well plates, after which the FITC amount in the supernatant was determined using a Varioskan™ Flash Multimode Reader (Thermo Scientific, Thermo Fisher Scientific, MA, USA), according to a pre-plotted calibration curve. Furthermore, the total amount of FITC (encapsulated and non-encapsulated) was quantified from the nanocomposites suspension, using the nanocomposite formulation without FITC as a blank. All the experiments were performed in triplicate.

4.3.3 *In vitro* drug release studies (II−IV)

4.3.3.1 In vitro release of model drugs (II−III)

For investigating the *in vitro* drug release of MTX from UnTHCPSi, UnP and UnPP nanoparticles, 250 μg of MTX-loaded nanocarriers were re-dispersed in 20 mL of PBS (pH 7.4), and stirred for 12 h at 100 rpm and at 37 ºC (**II**).

Similarly, the drug release profiles of SFB-loaded UnTHCPSi, UnCPP and UnAuCPP nanocomposites were evaluated. For this purpose, the amount of the different nanocomposites corresponding to 200 μg of SFB@UnTHCPSi nanoparticles were dispersed in 20 mL of 10 mM of HBSS−HEPES (pH 7.4) and 10 mM of HBSS−MES (pH 5.5), and left under stirring for 6 h, at 300 rpm and at 37 ºC (**III**). Owing to the very poor water solubility of SFB, the drug release media were supplemented with fetal bovine serum (FBS) at the final concentration of 10% (*v/v*), in order to aid the dissolution of SFB.[205] In the case of pure SFB dissolution testing, approximately 200 μg of the drug was dispersed in 200 mL of the aforementioned drug release media.

In both studies (**II** and **III**), 200 μL aliquots of each sample were withdrawn at predetermined timepoints and replaced with equal volume of the corresponding pre-warmed media, for maintaining a constant volume of the release media. The sampling aliquots were centrifuged for 3 min at 15,000 rpm, and the concentration of the drug release from the nanoparticles was quantified in the supernatant by HPLC. In the case of SFB drug release testings (**III**), the sample supernatants were diluted with an equal volume of MeOH, vortexed for 30 sec, and again centrifuged in the same conditions prior to the HPLC analysis, in order

to precipitate the serum protein constituents of the FBS included in the release media. The experimental HPLC setups used in each study can be found individually in the respective original publications (**II−III**). All the experiments described in this section were performed, at least, in triplicate.

4.3.3.2 Multi-responsive release of model drugs (IV)

The *in vitro* drug release profiles of SFN-loaded UnTHCPSi, UnCAD and UnCAD@CPP nanocomposites were determined by re-dispersing 400 µg of the drug-loaded nanocarriers in 40 mL of PBS supplemented with 10% FBS (pH 7.4) for the aforementioned purpose. The samples were stirred for 6 h at 150 rpm and at 37 ºC. For evaluating the redox and DNase responsiveness of the nanocomposites, *in vitro* drug release studies were also conducted in media containing 10 mM of glutathione (GSH) and 25 $U.mL^{-1}$ of DNase, respectively. The aliquots collected were then centrifuged for 5 min at 13,000 rpm, and the SFB concentration in the supernatant was analysed by HPLC, according to the experimental setup described in the original publication (**IV**).

In addition, for investigating the calcein release from the developed nanocomposites, 1 mg of calcein-loaded nanoparticles were dispersed in 10 mL of PBS containing 10% FBS (pH 7.4), and stirred for 6 h at 150 rpm and at 37 ºC. The amount of calcein released over time was monitored by fluorescence spectroscopy (λ_{ex} = 458 nm and λ_{em} = 510 nm). All the measurements were performed in triplicate.

4.4 Human plasma stability of nanocomposites (I−II)

The impact of the human plasma proteins on the stability of bare and polymer-functionalized UnTHCPSi nanoparticles was investigated. For performing these experiments, 300 µg of bare and polymer-conjugated UnTHCPSi nanoparticles were dispersed in 200 µL of PBS (pH 7.4) and incubated with 1500 µL of human plasma, under stirring at 800 rpm and at 37 ºC for 2 h. Sample aliquots (200 µL) were withdrawn after 1, 5, 10, 15, 30, 60, 90, and 120 min, for measuring the nanoparticles size, PdI and ζ-potential by DLS and ELS, respectively, as previously described (*Section 4.2*), using a Zetasizer Nano ZS equipment (Malvern Instruments Ltd., Malvern, UK). At least three independent measurements were performed for each experimental setup. Anonymous human plasma samples were obtained from the Finnish Red Cross Blood Service, with the permission from the respective institutional ethical committee.

4.5 *In vitro* cell based studies (I−IV)

4.5.1 Cell lines and cell culturing (I−IV)

Human breast adenocarcinoma cells, namely MDA-MB-231 (**I−IV**) and MCF-7 (**I−II**) cell lines, were selected for the *in vitro* cell based studies and obtained from the American Type Culture Collection (ATCC, VA, USA). Briefly, the MDA-MB-231 and MCF-7 breast

adenocarcinoma cells were cultured in standard Roswell Park Memorial Institute (RPMI) 1640 medium and Dulbecco's Modified Eagle's Medium (DMEM), respectively, both supplemented with 10% (*v/v*) FBS, 1% non-essential amino acids (NEAA), 1% L-glutamine, and 1% streptomycin-penicillin (100 IU.mL^{-1}) (all from HyClone, GE Healthcare Life Sciences GmbH, UT, USA). The cell cultures were maintained in 75 cm^2 culture flasks (Corning Inc. Life Sciences, NY, USA) at 37 ºC and at an atmosphere of 95% humidity and 5% CO_2 (BB 16 gas incubator, Heraeus Instruments GmbH, Hanau, Germany). The cell culture medium was replaced every other day and subculturing was performed when the cells were at 80% of confluency, until the time of the experiments. For subculturing and prior to each *in vitro* study, the cells were harvested with a 0.25% (*v/v*) trypsin-PBS-ethylenediaminetetraacetic acid (EDTA) solution.

4.5.2 Cellular toxicity studies (I−IV)

4.5.2.1 Cytotoxicity (I−IV)

The *in vitro* cytotoxicity values of all the developed nanoparticulate systems were assessed towards MDA-MB-231 (**I−IV**) and MCF-7 (**I−II**) breast cancer cells by measuring the ATP activity of the cells after incubation with the different nanoparticles, which was correlated to the number of alive cells present in culture. For this purpose, an ATP-based cell viability assay was carried out, according to the manufacturer's specifications and as previously described elsewhere.[212] Briefly, the cells were harvested, resuspended in their correspondent cell culturing medium at the concentration of 1.5–2.0 × 10^5 cells.mL^{-1}, seeded in 96-well plates (Corning Inc. Life Sciences, NY, USA) at a cell density of ~1.5–2.0 × 10^4 cells per well, and allowed to attach overnight at 37 ºC. Thereafter, the cell culture medium was removed and the cells were washed twice with pre-warmed 1× HBSS (pH 7.4) (**I−II**) or HBSS−HEPES (pH 7.4) (**III−IV**) buffers, prior to addition of 100 µL of the various nanoparticles resuspended in the same buffer solutions, at concentrations ranging from 12.5 to 200 µg.mL^{-1}, and incubated for 6 and 24 h at 37 ºC. After incubation, 100 µL of CellTiter-Glo® reagent assay (Promega Corporation, WI, USA) was added to each well and the luminescence was measured using a Varioskan™ Flash Multimode Reader (Thermo Scientific, Thermo Fisher Scientific, MA, USA). Positive (1% Triton X-100 solution) and negative (1× HBSS (pH 7.4) or HBSS−HEPES (pH 7.4) buffer solutions) controls were included in each 96-well plate and treated similarly as described above. All the data sets were compared to the negative control, considered as 100% cell viability, and corresponded to the average of at least three independent measurements.

4.5.2.2 Hemotoxicity (III−IV)

Heparin-stabilized fresh human blood was obtained from anonymous donors from the Finnish Red Cross Blood Service and used within 2 h. For isolating the RBCs from the serum, 2.5 mL aliquot of blood was gently mixed with 5 mL of Dulbecco's phosphate buffered saline (D-PBS) and centrifuged for 6 min at 2,500 rpm. After that, the RBCs were

washed five times with 5 mL of sterile D-PBS solution, and a 5% haematocrit suspension was obtained by diluting 1 mL of the RBCs pellet with D-PBS to the final volume of 20 mL.[338] The haemolytic effect of the various nanoparticulate systems was evaluated by adding 100 µL of the 5% haematocrit to 400 µL of the different nanoparticle suspensions in D-PBS, until reaching the final concentrations of 25, 50, 100 and 200 $\mu g.mL^{-1}$. The samples were vortexed for 5 sec and subsequently incubated at room temperature and static conditions for 1, 4, 8, 12 and 24 h. After each incubation period, the samples were gently vortexed for 5 sec and centrifuged for 3 min at 13,000 rpm. Next, 100 µL aliquots of the sample supernatants were transferred to a 96-well plate (Corning Inc. Life Sciences, NY, USA), for quantifying the haemoglobin absorbance values at 577 nm, with a reference wavelength of 655 nm, using a Varioskan™ Flash Multimode Reader (Thermo Scientific, Thermo Fisher Scientific, MA, USA). D-PBS and Milli-Q water were used as negative and positive controls, respectively. The results denote the average of, at least, three independent experiments.

4.5.3 Cellular targeting, association and internalization (I−IV)

4.5.3.1 Transmission electron microscopy imaging (I−IV)

The cellular association, internalization and intracellular localization of the developed nanoparticulate systems was investigated by TEM imaging analysis. Generally, MDA-MB-231 (**I**−**IV**) and MCF-7 (**I**−**II**) breast cancer cells were harvested as previously described (*Section 4.5.1*), resuspended in RPMI 1640 and DMEM media, respectively, seeded onto 13-mm round-shaped coverslips placed at the bottom of 24-well plates (Corning Inc. Life Sciences, NY, USA), and allowed to attach overnight at 37 ºC prior to exposure to the different nanoparticles.

In the studies **I** and **II** of this thesis, MDA-MB-231 and MCF-7 cells were seeded in the 24-well plates at a cell density of 10^5 cells per well. After attachment and removal of the cell culture media, the cells were exposed to 500 µL of bare and polymer-modified UnTHCPSi nanoparticles suspensions in HBSS−HEPES buffer (pH 7.4), at the concentration of 50 $\mu g.mL^{-1}$, for a period of 6 h at 37 ºC.

In the case of the study **III**, MDA-MB-231 cells were seeded in the 24-well plates at the cell density of 2×10^5 cells per well. Following the overnight attachment, the cell culture medium was removed, the cells were washed once with pre-warmed HBSS-HEPES buffer (pH 7.4), and exposed to 700 µL of the UnTHCPSi, UnCPP and UnAuCPP nanocomposites suspensions in HBSS−HEPES buffer + 10% FBS (pH 7.4), at the concentration equivalent to 10 $\mu g.mL^{-1}$ of UnTHCPSi, for 3h at 37 ºC.

In the study **IV**, MDA-MB-231 cells were seeded in the 24-well plates at a cell density of 10^5 cells per well, followed by incubation for two nights at 37 ºC for allowing the cell attachment. After removing the cell culture media, the cells were exposed to 500 µL of the UnCAD and UnCAD@CPP nanocomposites suspensions in HBSS−HEPES buffer + 10% FBS (pH 7.4), at the concentration equivalent to 20 $\mu g.mL^{-1}$ of UnTHCPSi, for 4h at 37 ºC.

Thereafter, the nanoparticles suspensions were carefully aspirated and the cover slips were gently washed twice with HBSS-HEPES buffer (pH 7.4) prior to cell fixation with 2.5% glutaraldehyde in 0.1 M of PBS buffer (pH 7.4), for 1 h at room temperature. After

fixation, the samples were washed twice with HBSS−HEPES buffer (pH 7.4) and sodium cacodylate buffer (NaCac) for 3 min, followed by post-fixation with 1% osmium tetroxide in 0.1 M NaCac buffer (pH 7.4). The cells were then dehydrated with 30−100% ethanol for 10 min and embedded in epoxy resin. Ultrathin sections with approximately 60 nm thickness were sliced parallel to the coverslips, post-stained with uranyl acetate and lead citrate, and finally analysed by TEM.

4.5.3.2 Flow cytometry analysis (I−IV)

Before investigating the capability of the HA conjugation on the surface of UnTHCPSi nanoparticles to help in targeting to CD44-overexpressing cells, the expression of the CD44 receptor was evaluated by flow cytometry in MDA-MB-231 and MCF-7 breast cancer cell lines, according to a protocol adapted from the manufacturer's specifications. Briefly, the cells were harvested, as described above (*Section 4.5.1*), and suspended in 1× PBS (pH 7.4), at a concentration of 1.5×10^7 cell.mL^{-1}. Next, 50 µL of the cell suspensions were incubated with equal volumes of BD Horizon™ PE-CF594 mouse anti-human CD44 antibody (BD Biosciences, NJ, USA) stock solutions, with increasing concentrations of 5.0, 10.0, and 20.0 µg.mL^{-1}, for 45 min at 4 ºC in the dark. After the reaction, the unbound portion of anti-human CD44 antibody was removed by centrifugation at 1,000 rpm for 5 min and three washing steps with 1× PBS (pH 7.4) buffer. The cells were then resuspended in 800 µL of 1× PBS (pH 7.4), filtered using a 70 µm nylon cell strainer (BD Biosciences, NJ, USA), and collected into test tubes. The flow cytometry analysis was then performed using a LSR II flow cytometer (BD Biosciences, NJ, USA), with a laser excitation wavelength of 488 nm, and a 610/620 nm detector filter.

In addition, flow cytometry analysis was also performed to quantitatively measure the cellular association and internalization of the various nanoplatforms in MDA-MB-231 (**I**−**IV**) and MCF-7 (**I**−**II**) breast adenocarcinoma cells. For all the experiments, the cells were harvested, as previously described (*Section 4.5.1*), resuspended in the corresponding cell culture media, seeded in 6-well plates (Corning Inc. Life Sciences, NY, USA) and incubated overnight at 37 ºC to allow cells attachment to the wells. The attached cells were then washed twice with HBSS−HEPES buffer (pH 7.4), before exposing them to the different fluorescently labelled nanoparticles.

In the studies **I** and **II** of this thesis, MDA-MB-231 and MCF-7 cells were seeded in the 6-well plates at a cell density of 7×10^5 cell per well exposed to FITC-labelled UnTHCPSi and UnHA$^+$ nanoparticles (50 and 100 µg.mL^{-1}) (**I**), as well as FITC-labelled UnTHCPSi, UnP and UnPP nanoparticles (50 µg.mL^{-1}) (**II**), for 6 h at 37 ºC. The cells were then detached using 300 µL of 0.25% trypsin–PBS–EDTA solution, centrifuged for 3 min at 500 rpm and washed three times with HBSS−HEPES buffer (pH 7.4) in order to remove the non-associated nanoparticles. Prior to the flow cytometry analysis, the cells were fixed with 2.5% glutaraldehyde in 0.1 M of PBS (pH 7.4) for 30 min and resuspended in 700 µL of HBSS-HEPES buffer (pH 7.4). In addition, in the study **II**, the fluorescence of the nanoparticles associated to the surface of the cell membrane was quenched by exposing the cells to a 0.005% (*v*/v) trypan blue (TB) solution before cell fixation, followed by three times washing.

The same experiments were conducted in the studies **III** and **IV**. In this case, 6×10^5 MDA-MB-231 cells were seeded in the same 6-well plates. After the aforementioned attachment and washing, the cells were incubated with 3.5 mL of AF488-labelled UnTHCPSi, UnCPP and UnAuCPP nanosuspensions at the concentration equivalent to 10 $\mu g.mL^{-1}$ of UnTHCPSi for 1 and 3 h at 37 ºC (**III**), as well as with the same volume of FITC-labelled UnCAD and UnCAD@CPP suspensions at the UnTHCPSi concentration of 20 $\mu g.mL^{-1}$, for 1, 3 and 6 h at 37 ºC (**IV**). With the aim of removing the unassociated nanoparticles, the cells were washed three times with HBSS−HEPES buffer (pH 7.4), detached with 3.5 mL of 0.25% trypsin–PBS–EDTA solution and washed again twice with the same buffer. Contrarily to the studies **I** and **II**, the flow cytometry analyses were carried out in alive cells, which were resuspended in 700 µL of HBSS−HEPES (pH 7.4) and kept in ice until the time of measurement. All the flow cytometry analyses were performed using a LSR II flow cytometer (BD Biosciences, NJ, USA), with a laser excitation wavelength of 488 nm. A minimum of 10,000 events per sample were recorded using a FACSDiva software. The data presented are representative of three independent experiments, and were analysed and plotted using Flowjo 7.6 software (Tree Star, OR, USA).

4.5.4 Endosomolytic effect and intracellular trafficking (II−IV)

The intracellular trafficking and endosomolytic properties of the engineered nanoplatforms were studied by confocal fluorescence microscopy with MDA-MB-231 (**II−IV**) and MCF-7 (**II**) cells. In all the experiments performed, the cells were harvested, resuspended in the suitable cell culture media, seeded in Lab-Tek® 8-chamber slides (Thermo Scientific, Thermo Fisher Scientific, MA, USA) and allowed to attach at 37 ºC. Thereafter, the cells were exposed to the various fluorescently labelled nanoparticulate systems, and subsequently stained for their cellular organelles, as described in detail in this section.

For the study **II** of this thesis, MDA-MB-231 and MCF-7 cells were seeded at a density of 5×10^4 cells per chamber. After 24 h incubation, the cell medium was removed and replaced with 200 µL of FITC-labelled UnTHCPSi, UnP and UnPP nanoparticle suspensions in HBSS−HEPES (pH 7.4) at the concentration of 50 $\mu g.mL^{-1}$, whereupon the cells were incubated for 6 h at 37 ºC. Next, the nanoparticle suspensions were removed and the cells were washed three times with HBSS−HEPES buffer (pH 7.4). The acidic organelles of the cells were stained with 200 µL of LysoTracker® Blue DND-22 (50 nM; Invitrogen, CA, USA) for 30 min at 37 ºC. The cells were washed twice with HBSS−HEPES buffer (pH 7.4) and, subsequently, the cell membranes were stained by adding 200 µL of Cell Mask™ Deep Red® (3 $\mu g.mL^{-1}$; Invitrogen, CA, USA) for 3 min at 37 ºC. Finally, the cells were washed twice with HBSS−HEPES buffer (pH 7.4) and fixed using a 2.5% glutaraldehyde solution for 20 min.

In the studies **III** and **IV**, 5×10^4 (**III**) or 4×10^4 (**IV**) MDA-MB-231 cells were seeded in each chamber of the 8-chamber slides and incubated for 48 h at 37 ºC to allow the cell adhesion. After removal of the cell culture medium, the cells were carefully rinsed with HBSS−HEPES buffer (pH 7.4) and treated with 250 µL of AF488-labeled UnTHCPSi, UnCPP and UnAuCPP nanoparticles (**III**), as well as FITC-labelled UnCAD, UnCAD@CPP and CPP nanoparticles (**IV**) suspensions in HBSS−HEPES (pH 7.4) + 10%

FBS, at a concentration corresponding to 20 μg.mL^{-1} of UnTHCPSi nanoparticles, for 1, 3 and 6 h (only in study **III**) at 37 ºC. The nanoparticle suspensions were then removed and the unassociated nanoparticles were washed out three times with HBSS−HEPES buffer (pH 7.4). Thereafter, the staining of the acidic cellular compartments was performed by incubation of the cells with 300 μL of 500 nM LysoTracker® Red DND-99 (Invitrogen, CA, USA) for 30 min at 37 ºC. In the samples corresponding to the cells exposed to bare CPP nanocomplexes (**IV**), the cell membrane was stained by adding 300 μL of a CellMask™ Deep Red® staining solution (5 μg.mL^{-1}; Invitrogen, CA, USA) for 3 min at 37 ºC. The excess of tracking agents was removed by washing the cells twice with HBSS−HEPES buffer (pH 7.4). The cells were then fixed with 4% paraformaldehyde (PFA), for 15 min, and washed again twice with HBSS−HEPES buffer (pH 7.4). Afterwards, the nucleus of the cells was stained with 300 μL of 4',6-diamidino-2-phenylindole (DAPI) for 6 min, followed by a final five-time washing step with HBSS−HEPES buffer (pH 7.4).

Finally, the samples were analysed under an inverted confocal fluorescence microscope (Leica SP5 II HCS A, Wetzlar, Germany). The images obtained in the study (**III**) were processed using the ImageJ 1.50i software (National Institutes of Health, MD, USA).

4.5.5 *In vitro* chemotherapeutic effect (II−III)

The *in vitro* chemotherapeutic effect of MTX and MTX-loaded UnTHCPSi, UnP and UnPP nanoparticles was evaluated by measuring the antiproliferative effect on MDA-MB-231 and MCF-7 breast cancer cells (**II**), using the ATP-based cell viability assay described in the *Section 4.5.2.1*. Typically, MDA-MB-231 and MCF-7 cells were harvested, resuspended in RPMI 1640 and DMEM media, respectively, seeded in 96-well plates (Corning Inc. Life Sciences, NY, USA) at a cell density of 1.5×10^5 cells per well, and allowed to adhere overnight at 37 ºC. After that, the cell media was replaced with 100 μL of MTX-loaded UnTHCPSi, UnP and UnPP nanoparticle suspensions with different concentrations, and the cells were incubated for 6 h at 37 ºC. In addition, cells were similarly treated with pure MTX solutions, at concentrations corresponding to the drug-loaded nanoparticles. Moreover, HBSS−HEPES buffer (pH 7.4) and 1% Triton X-100 were used as negative and positive controls, respectively. After incubation, 100 μL of CellTiter-Glo® reagent assay (Promega Corporation, WI, USA) was added to each well and the luminescence was measured using a Varioskan™ Flash Multimode Reader (Thermo Scientific, Thermo Fisher Scientific, MA, USA).

The antiproliferative effect of SFB-loaded UnTHCPSi, UnCPP and UnAuCPP nanocomposites was also evaluated on MDA-MB-231 breast cancer cells (**III**), after 6 and 24 h of cell exposure to the different SFB-loaded nanoparticle suspensions, at the concentrations equivalent to 6.25, 12.5, 25, 50 and 100 μg.mL^{-1} of UnTHCPSi, and following the same protocol as described above (*Section 4.5.2.1*). All the data sets were compared to the negative control, considered as 100% cell proliferation, and were performed at least in triplicate.

5 Results and discussion

5.1 Hyaluronic acid functionalization of porous silicon nanoparticles for active cancer targeting (I)

The successful application of nanoparticulate drug delivery systems in cancer therapy is highly dependent on their physicochemical and biofunctional characteristics.[66] The surface properties of nanoparticles, such as surface charge, hydrophobicity, surface chemistry and presence of functional groups, can significantly influence their cellular interactions, as well as the adsorption of plasma proteins and the protein corona formation, which may ultimately impact the biofate and biological performance.[67,70,339,340] In addition, the surface functionalization of nanoparticles with targeting moieties can significantly improve the blood circulation longevity and accumulation at the targeted tumour site, increasing the affinity and specificity in tumour cells, enhancing the cellular interactions and intracellular penetration.[341,342]

In this context, a PSi-based targeting nanosystem was developed by biofunctionalizing the surface of UnTHCPSi nanoparticles with an amine-modified HA derivative, aiming at increasing the specific cellular interactions and uptake of this nanoplatform by targeting CD44-overexpressing cancer cells, and improving the colloidal and plasma stabilities. Both bare and HA^+-modified UnTHCPSi nanoparticles were characterized, and subsequently compared in terms of stability in aqueous medium and human plasma. Furthermore, the HA^+-mediated targeting of the developed nanosystem was evaluated towards CD44-overexpressing cells, after assessing the expression levels of the targeted receptor in two different breast cancer cell lines.

5.1.1 Physicochemical characterization and stability in human plasma

The UnTHCPSi nanoparticles used in this study were initially characterized for their physical properties, presenting a specific surface area of 218 ± 3 $m^2.g^{-1}$, a total pore volume of 0.63 ± 0.01 $cm^3.g^{-1}$, and an average pore diameter of 12.2 ± 0.4 nm. Additionally, the hydrodynamic size, PdI and ζ-potential of both bare and HA^+-conjugated UnTHCPSi nanoparticles were determined by DLS and ELS, respectively (**Figure 8**), and their morphology was investigated by TEM (**Figure 8**). After functionalization, the size of the nanoparticles was increased from 208.1 ± 1.6 nm to 228.3 ± 2.6 nm, and the ζ-potential altered from −41.6 ± 1.5 mV to −17.7 ± 0.4 mV, possibly owing to the presence of free amine groups from the HA^+ conjugated on the nanoparticles' surface. The UnTHCPSi and $UnHA^+$ nanosparticles presented PdI values of 0.07 ± 0.01 and 0.09 ± 0.02, respectively, therefore indicating high monodispersities of both the nanoparticles suspensions. The results obtained suggest a successful conjugation of HA^+ onto the UnTHCPSi nanoparticles' surface.

In addition, the HA^+-modified UnTHCPSi nanoparticles showed significantly improved colloidal stability, relative to bare counterparts, as evidenced by the similar macroscopic appearance of both the nanoparticles suspensions, after re-dispersion in

HBSS−HEPES buffer (pH 7.4) and storage at room temperature for 4 h (**Figure 8**). The intrinsic instability of the UnTHCPSi nanoparticles in aqueous environment results from their hydrophobic surface and consequent tendency for reducing the interfacial area, leading to a reduced dispersibility and aggregation phenomena over time. Contrarily, the conjugation of HA^+ at the nanoparticles surface contributes for the stabilization in aqueous solutions by steric hindrance, due to the solvation of the polymer chains.[343-345]

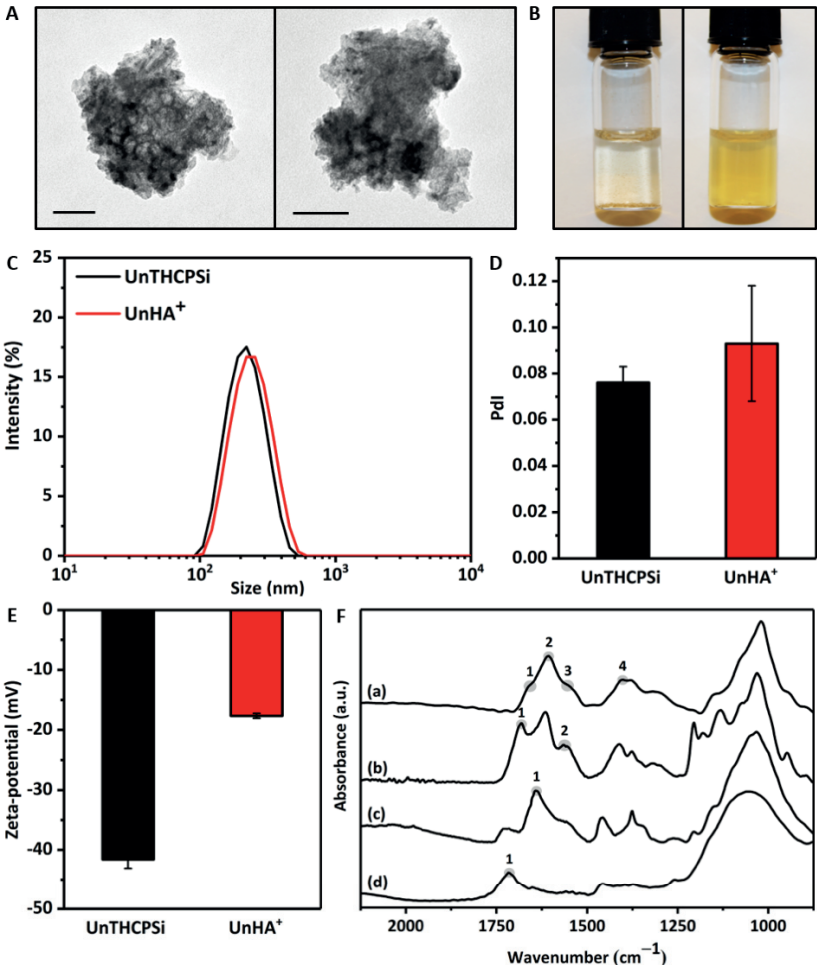

Figure 8. *(A) TEM images of the UnTHCPSi and $UnHA^+$ nanoparticles with the scale bars representing 100 nm. (B) Colloidal stability of UnTHCPSi and $UnHA^+$ nanoparticles, after incubation in HEPES buffer (pH 7.4), for 4 h at room temperature. (C−E) Characterization of the particle size distribution (C), PdI (D) and ζ-potential (E) of the UnTHCPSi and $UnHA^+$ nanoparticles. Bars represent the mean ± s.d. of at least three independent experiments ($n \geq 3$). (F) FTIR absorbance spectra of HA (a), HA^+ (b), $UnHA^+$ (c) and UnTHCPSi (d) with relevant features of each spectrum highlighted and numbered for clarification. Copyright © (2014) The Royal Society of Chemistry. Adapted and reprinted with permission from ref.*[346].

The FTIR spectra of HA, HA^+, UnTHCPSi and $UnHA^+$ nanoparticles were obtained to first confirm the amine modification of HA and further corroborate the conjugation of the resulting HA^+ onto the nanoparticles' surface (**Figure 8F**). The prominent C–O band at the 900–1200 cm^{-1} identifies the carbohydrate chain of HA, which is characteristic of polysaccharides. Moreover, the chemical structure of HA features two bands related to the amides I and II at *ca*. 1670 cm^{-1} (**Figure 8F**-a1) and 1540 cm^{-1} (**Figure 8F**-a3), as well as the stretching bands at 1607 cm^{-1} (**Figure 8F**-a2) and 1400 cm^{-1} (**Figure 8F**-a4), corresponding to the carboxylate C=O and C–O stretching vibrations, respectively.[347,348] Next, the HA was modified with NH_2-PEG_2-NHBoc on the carboxylic acid groups by a carbodiimide-mediated reaction. According to the spectrum of the resulting HA^+ (**Figure 8F**-b), the basic chemical structure of HA was preserved, and the success of the amine-modification through amide bonding could be confirmed by the emergence of a broad band at *ca*. 1680 cm^{-1} (**Figure 8F**-b1) and a band at 1550 cm^{-1} (**Figure 8F**-b2). Regarding the UnTHCPSi nanoparticles, a broad band between 900 and 1200 cm^{-1} and a C=O stretching at 1715 cm^{-1} are visible in the corresponding spectra (**Figure 8F**-d), related to the Si–C structure and carboxylic acid groups, respectively. After surface functionalization of the UnTHCPSi nanoparticles with HA^+, the spectrum of $UnHA^+$ (**Figure 8F**-c) exhibited the formation of an amide I bond, resulting from the covalent conjugation of HA^+, recognisable by the broad absorption band at 1640 cm^{-1} (**Figure 8F**-c1). In addition, the amide II bond structure of HA^+ corroborates the accomplishment of the chemical conjugation. The FTIR results herein confirm the successful synthesis of the HA^+ and its subsequent conjugation onto the surface of UnTHCPSi nanoparticles, both attained *via* EDC/NHS coupling chemistry.

Ideally, the nanoparticulate systems that are envisioned to be administered intravenously should minimally interact with the plasma proteins, in order to avoid the formation of protein corona, which may lead to aggregation, rapid opsonisation by the MPS and clearance from the body.[271,349] For circumventing this problem, nanoparticles can be, for example, functionalized with different polymeric moieties, thus modifying their surface properties and minimizing the interaction with plasma proteins.[230,350] In this regard, the effect of the HA^+ functionalization of UnTHCPSi nanoparticles on the protein corona formation was evaluated by monitoring and comparing changes in the physicochemical properties of both UnTHCPSi and $UnHA^+$, namely their size, PdI and ζ-potential, after incubation with human plasma at 37 ºC for 2 h (**Figure 9**). Immediately after contact with human plasma, the size of the bare UnTHCPSi nanoparticles increased from *ca*. 200 nm to *ca*. 600 nm, suggesting a rapid adsorption of the plasma proteins onto the surface of these nanocarriers. Contrarily, no significant variation in the particle size was observed for the $UnHA^+$ nanoparticles throughout the incubation period tested (**Figure 9A**). Additionally, the $UnHA^+$ nanosuspension showed to remain relatively monodisperse in human plasma, presenting PdI values of *ca.* 0.2, in contrast with the bare counterparts, the polydispersity values of which were increased above 0.5, presumably owing to protein corona formation and aggregation of the nanoparticles (data not shown). Moreover, the adsorption of the plasma proteins onto the UnTHCPSi nanoparticles surface resulted in an attenuation of the ζ-potential values from *ca.* –42 mV to –15 mV, while the surface charge of the $UnHA^+$ remained constant during the experimental period (**Figure 9B**).

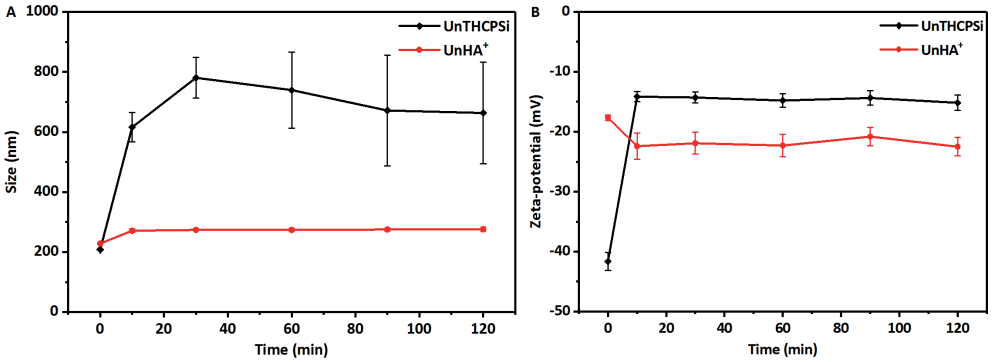

Figure 9. *Effect of the human plasma protein adsorption on the size (A) and ζ-potential (B) of the UnTHCPSi and UnHA$^+$ nanoparticles after incubation with human plasma for 120 min at 37 ºC. Values are represented as mean ± s.d. (n ≥ 3). Copyright © (2014) The Royal Society of Chemistry. Adapted and reprinted with permission from ref.*[346].

As evidenced by the minimal variations in the nanoparticles size, PdI and ζ-potential of the UnHA$^+$ nanoparticles over time, the HA$^+$ conjugation was revealed to effectively minimize the plasma protein adsorption, protein corona formation and particle aggregation, as a result of the highly hydrophilic properties, thus significantly improving the stability of UnTHCPSi nanoparticles in human plasma. When foreseeing intravenous administration, this effect might have a significant contribution for minimizing the opsonisation by the MPS and increasing the blood half-life and tumour accumulation of the developed nanoformulation.[351-353]

5.1.2 CD44 expression and hyaluronic acid-mediated cell targeting

Before investigating the impact of the HA$^+$-functionalization of UnTHCPSi nanoparticles on the targeting of CD44-overexpressing cells, the CD44 expression was assessed in both MDA-MB-231 and MCF-7 breast cancer cells (**Figure 10**). For this purpose, the cells were primarily stained with three different concentrations of PE-CF594-labeled anti-human CD44 antibody, and subsequently analysed by flow cytometry. The increase in the mean fluorescence intensity (MFI) of the stained cells, compared with the respective negative controls, showed that both the cell lines studied expressed the CD44 receptor. Furthermore, the data presented suggested significantly higher levels of CD44 expression in MDA-MBA-231 than in MCF-7 cells. As shown in **Figure 10**, the MFI of MCF-7 cells was increased *ca.* 9-fold, independent of the anti-human CD44 antibody concentration used, when compared with the negative control, thus suggesting a saturation of the complementary antibody binding sites. Contrarily, the fluorescence signal of the MDA-MB-231 cancer cells was successively increased up to *ca.* 670-fold, with increasing anti-human CD44 concentration.[354]

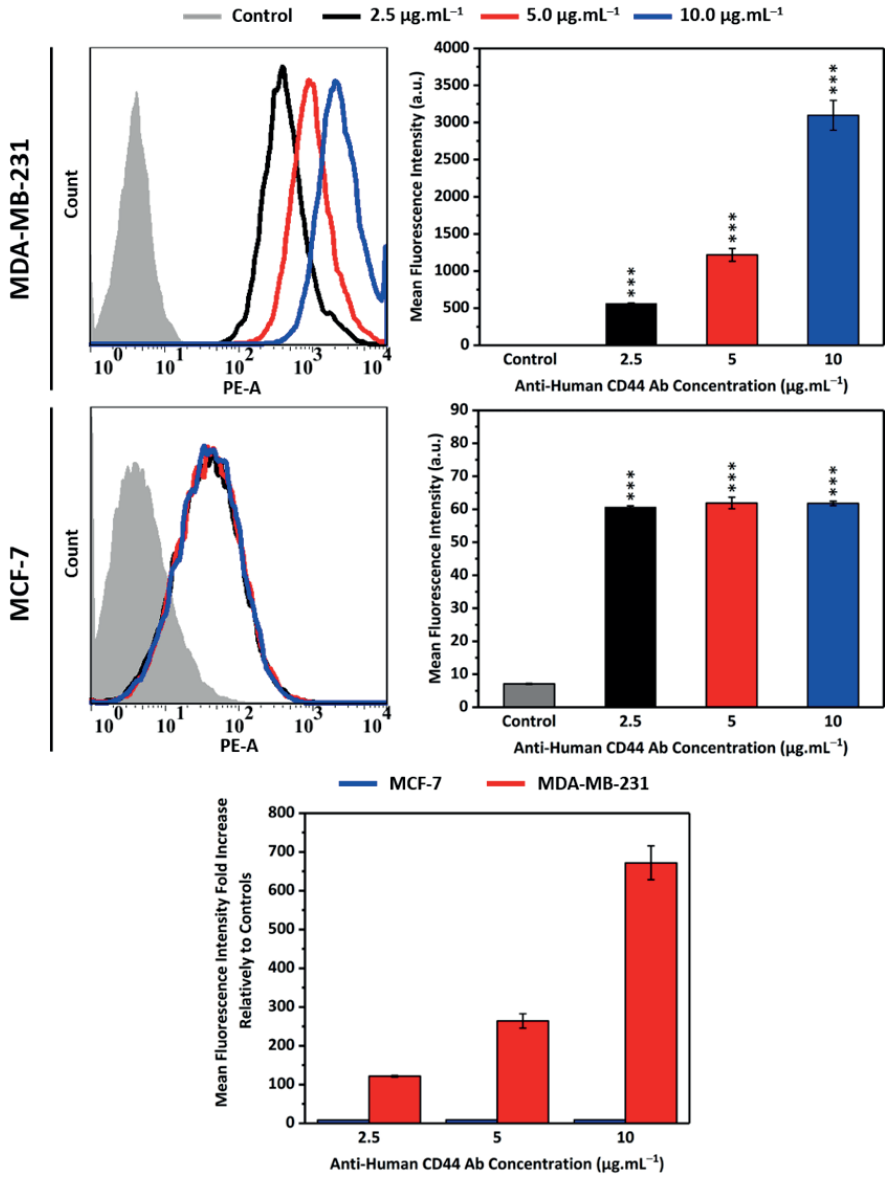

Figure 10. *Flow cytometry analysis of the CD44 expression in MDA-MB-231 and MCF-7 breast cancer cells. The cells were incubated with PE-CF594-labeled anti-human CD44 antibody at the concentrations of 2.5, 5.0 and 10.0 µg.mL^{-1}, for 45 min at 4 ºC. The flow cytometry histograms of the stained and unstained (control) cells were obtained, and the correspondent mean fluorescence intensity was quantified and subsequently compared for evaluating the CD44 expression in both the cell lines. Error bars represent mean ± s.d. (n ≥ 3). Statistical analysis was performed by means of Student's t-test, with the level of significance set at probabilities of *p < 0.05, **p < 0.01 and ***p < 0.001. Copyright © (2014) The Royal Society of Chemistry. Adapted and reprinted with permission from ref.*[346].

In order to evaluate the effect of HA^+ on the cellular association of the nanoplatforms with MDA-MB-231 and MCF-7 breast cancer cells through a CD44-mediated targeting mechanism, both the cell cultures were incubated with FITC-labelled UnTHCPSi and $UnHA^+$ nanosuspensions at the concentrations of 50 and 100 $\mu g.mL^{-1}$, for 6 h at 37 ºC, and subsequently analysed by flow cytometry (**Figure 11**).

Incubation of both the cell lines with bare UnTHCPSi nanosuspension at the lower concentration did not result in significant variations of the fluorescence intensity, when compared to the respective control samples. In addition, when the nanoparticle concentration was increased to 100 $\mu g.mL^{-1}$, an increment of the cellular association was observed in a similar extension for both the cell lines, meaning that the interaction with the cells was unspecific. Contrarily, in the case of $UnHA^+$ nanoparticles, a considerable enhancement of the fluorescence intensity was observed, particularly in the CD44-overexpressing MDA-MB-231 cells, also at the lower nanoparticle concentrations. Moreover, the treatment with the highest concentration of the HA^+ modified-nanoparticles resulted in a significant intensification of the fluorescence signals, in the order of 29.5 and 8.3-fold for MDA-MB-231, as well as 4.9 and 1.8-fold for MCF-7 cells, relatively to the corresponding negative controls and bare counterparts, respectively.

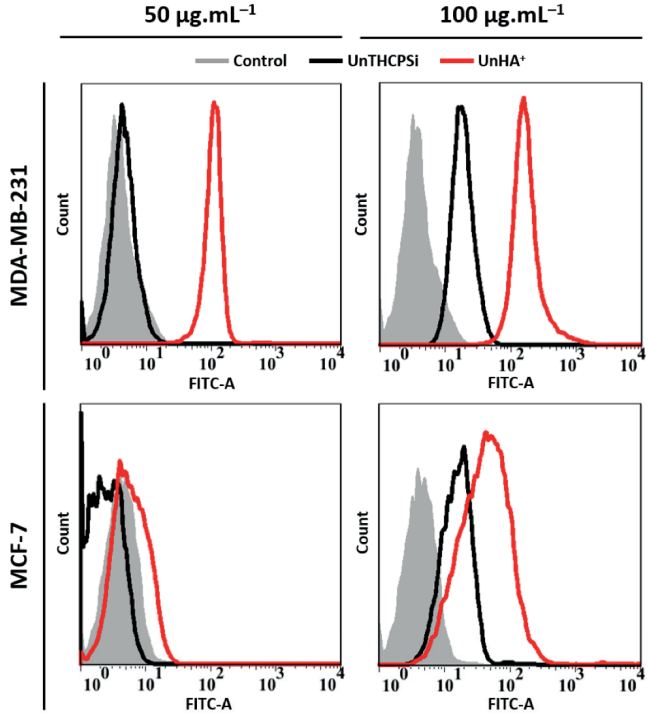

Figure 11. *Flow cytometric analysis of the cellular association of UnTHCPSi and $UnHA^+$ nanoparticles with MDA-MB-231 and MCF-7 breast cancer cells. The cells were incubated with the nanoparticles suspensions at the concentrations of 50 and 100 $\mu g.mL^{-1}$, for 6 h at 37 ºC. Copyright © (2014) The Royal Society of Chemistry. Adapted and reprinted with permission from ref.*[346].

Overall, the HA^+-functionalization of bare UnTHCPSi nanoparticles considerably augmented the cellular interactions of these nanosystems, particularly and more significantly with the CD44-overexpressing MDA-MB-231 cells, contrarily to the bare counterparts, which evidenced a concentration-dependent and cell type-independent cellular association. Therefore, and in agreement with the data presented above for the CD44 expression in both the cell lines studied, these results suggested that the conjugated HA^+ mediated and enhanced cellular association and internalization through a CD44-targeting mechanism.

5.2 Polymeric surface modification of porous silicon nanoparticles for enhancing cellular internalization and endosomal escape (II)

In addition to the surface functionalization of nanoparticulate systems with targeting moieties for enhanced cellular specificity, association and internalization, several strategies have been exploited for improving the performance at cellular and intracellular levels.[355,356] An example of such approach consists of the surface conjugation of cell-penetrating peptides to enhance the cellular interactions and uptake of nanoparticles, despite several drawbacks, including low metabolic stability, possible immunogenicity, and dependency of an effective membrane translocation on the amino acid arrangement and orientation upon conjugation to the nanoparticles surface.[357,358] As an attractive alternative approach, the nanoparticles surface can be modified with functional polymers, both for manipulating the intrinsic physicochemical properties, such as smoothness, size, shape, surface charge, hydrophilicity, polydispersity, and stability, and for improving the non-specific cellular interactions, uptake, intracellular trafficking, and drug release profiles, with the ultimate aim of attaining a desired therapeutic effect.[238,359,360]

Despite the remarkable physicochemical and biological properties of PSi nanoparticles, the limited cellular association and internalization, and subsequent incapacity to breach out from the endosomal compartments, still stand as major deadlocks defying the successful implementation of these nanocarriers as effective anticancer drug delivery systems. In this regard, a bilayered zwitterionic nanocomposite was developed by successively conjugating PEI and PMVE-MA polymers onto the surface of UnTHCPSi nanoparticles. This approach aimed at improving the limited cellular association and internalization of the UnTHCPSi nanoparticles, while complementing them with endosomolytic properties, through incorporation of free amine groups from the hyperbranched PEI disguised by the biocompatible and bioadhesive PMVE-MA polymer. The resulting nanoplatform, termed UnPP, was studied *in vitro* in terms of cytocompatibility, cellular interaction and uptake, and capability to induce endosomal escape in breast cancer cells. Additionally, the nanosystem was loaded with the chemotherapeutic drug MTX and further evaluated for drug release profile and antiproliferative effect in the same *in vitro* model.

5.2.1 Cytocompatibility

Despite the potential of cationic polymers, such as PEI, for enhancing the cellular internalization and inducing the early escape from endosomal compartments,[361,362] these materials have previously shown to create overt pores in the cellular membrane and, consequently, to disturb the homeostasis of ions and proteins that are essential for the normal cell function, eventually leading to an increased cytotoxicity.[363,364] Thus, the design and development of specific polymer-modified nanostructures with improved intracellular trafficking and cytoplasmatic release profiles of the active payloads, while simultaneously avoiding cytotoxicity, is essential for their application in cancer nanomedicine.

Therefore, in order to assess the *in* vitro cytotoxicity of both the bare and polymer-modified UnTHCPSi nanoparticles, as well as to understand the importance of the outer PMVE-MA polymer layer on the cytocompatibility of the developed nanosystems, the ATP activity of both MDA-MB-231 and MCF-7 breast cancer cells was evaluated after exposure to different concentrations of the nanoparticles for 6 and 24 h at 37 ºC (**Figure 12**).[24,212]

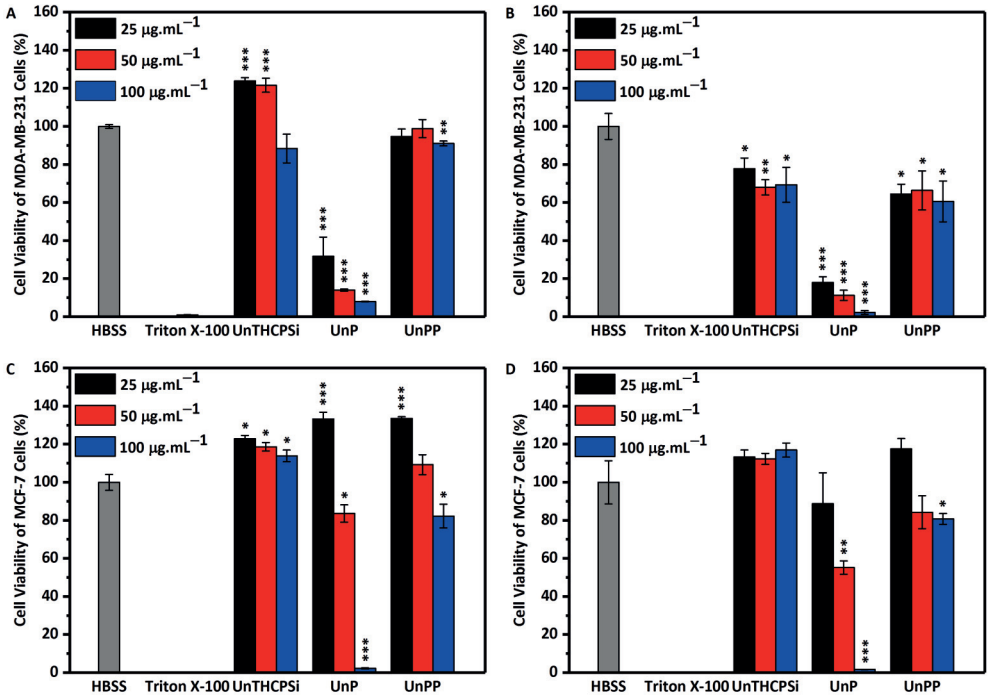

Figure 12. *Cell viability of MDA-MB-231 (A and B) and MCF-7 (C and D) breast cancer cells, after exposure to UnTHCPSi, UnP and UnPP nanoparticles suspensions at the concentrations of 25, 50 and 100 μg.mL^{-1} for 6 h (A and C) and 24 h (B and D) at 37 ºC. All data sets were compared to the negative control (HBSS buffer, pH 7.4). Error bars represent mean ± s.d. ($n \geq 3$). Statistical analysis was performed by means of one-way ANOVA with the level of significance set at probabilities of *$p < 0.05$, **$p < 0.01$, and ***$p < 0.001$. Copyright © (2014) Elsevier B.V. Adapted and reprinted with permission from ref.*[365].

According to **Figure 12**, the bare UnTHCPSi nanoparticles showed a satisfactory non-toxic effect in both the cell lines during the incubation period tested, which can be attributed to the negative surface charge, low aqueous stability and consequent low cellular interactions of these nanosystems. Contrarily, the PEI-modified nanocomposites showed high cytotoxicity values in both MDA-MB-231 and MCF-7 cells, in a time and concentration dependent manner, particularly for the highest concentration of 100 $\mu g.mL^{-1}$, owing to the free amine groups of the conjugated PEI polymer.[366] The subsequent conjugation of PMVE-MA onto the surface of UnP, masking the free positive charges of PEI, resulted in a significantly improved cytocompatibility of the bilayered UnPP nanocomposites. In comparison with the HBSS buffer control, no significant cytotoxic effect of UnPP nanoparticles was observed after 6 h of incubation with both the cell lines. However, the cell viability was considerably decreased after 24 h to *ca.* 64% for all the concentrations in MDA-MB-231 cells, and to *ca.* 83%, for the concentrations of 50 and 100 $\mu g.mL^{-1}$ in MCF-7 cells. The results obtained suggested that the UnPP nanocomposites can be considered safe for drug delivery applications during short incubation times and at concentrations lower than 100 $\mu g.mL^{-1}$.

5.2.2 Cellular interaction, uptake and endosomal escape

In order to understand the performance of UnTHCPSi nanoparticles and the developed polymer-modified nanocomposites at the cellular and intracellular levels, both MDA-MB-231 and MCF-7 breast cancer cells were exposed to different FITC-labelled nanocarriers at the concentration of 50 $\mu g.mL^{-1}$, for 6 h at 37 ºC, and subsequently analysed by flow cytometry and confocal fluorescence microscopy (**Figure 13**).

The flow cytometry experiments were conducted before and after quenching the fluorescence of the nanoparticles bound to the cell surface, using a TB solution. The overlap of the fluorescence corresponding to the control samples and bare UnTHCPSi nanoparticles evidenced a negligible cellular association and internalization of these nanocarriers by both MDA-MB-231 (**Figure 13A**) and MCF-7 (**Figure 13B**) cells, mainly due to their negative surface charge, lack of bioadhesivity and low aqueous stability.[344] In contrast, a considerable increment in the fluorescence intensity was observed for the cells incubated with UnP and UnPP nanocomposites, providing a clear evidence of the high cellular association of the polymer-conjugated nanoparticles with both the cell lines. Moreover, only the fluorescence values of the cells treated with the polymer-modified nanoparticles were partially quenched after the TB treatment, thus demonstrating the cellular internalization of these nanosystems after 6 h. The results observed for UnP nanoparticles were in agreement with previous reports in the literature demonstrating increased interaction of the positively charged nanoparticles with the negatively charged moieties of the cell membrane, followed by their internalization.[367] In the case of UnPP nanoparticles, the strong cellular association can be attributed to the high dispersibility of these nanocomposites and the bioadhesive properties of the PMVE-MA polymer conjugated on their surface.[368,369] Despite the unfavourable interaction between the negative surface charge of UnPP nanoparticles and the cell membranes, the results were in line with previous evidence of high cellular uptake of anionic nanoparticles by different types of cells.[370-373] This can be explained by the non-specific

binding of the nanoparticles to the scarce cationic domains on the surface of the cell membrane, or other mechanisms attributed to the intrinsic properties of polymers, such as cell surface targeting or cell penetration functions.[374,375]

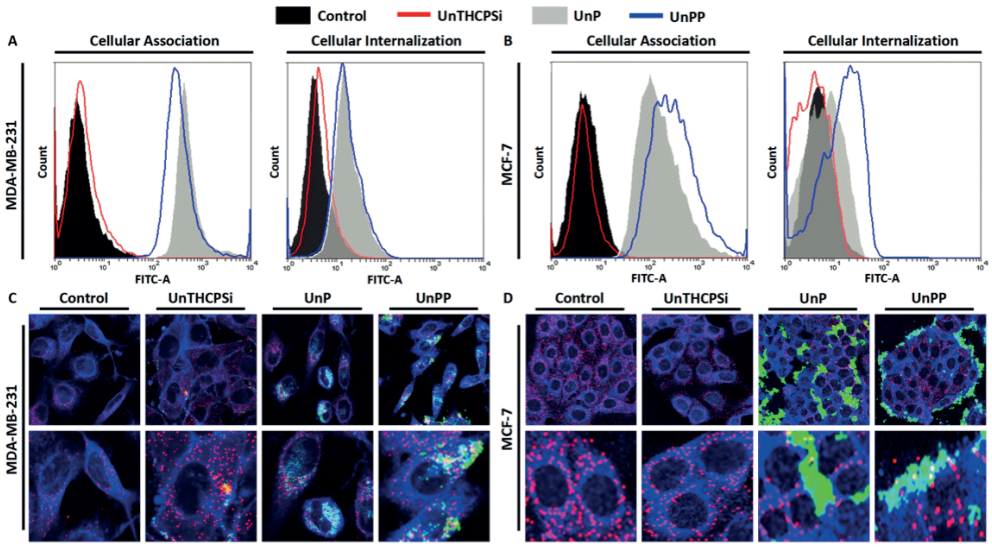

Figure 13. *(A−B) Flow cytometric analysis of MDA-MB-231 (A) and MCF-7 (B) breast cancer cells after incubation with FITC-labelled UnTHCPSi, UnP and UnPP nanoparticles at the concentration of 50 μg.mL^{-1} for 6h at 37 ºC. The MDA-MB-231 and MCF-7 cells were analysed before and after quenching the extracellular fluorescence using TB, for evaluating both the cellular association and internalization of the nanoparticles, respectively. The data presented is representative of at least two independent experiments. (C−D) Confocal fluorescence microscopy analysis of MDA-MB-231 (C) and MCF-7 (D) cells incubated with FITC-labelled UnTHCPSi, UnP and UnPP nanoparticles at the concentration of 50 μg.mL^{-1} for 6h at 37 ºC. Cells incubated with HBSS buffer (pH 7.4) were used as control. The images correspond to the merged and magnified panels of cells stained for their lysosomes and cell membranes, using Lysotracker® Blue DND-22 and Cell Mask™ Deep Red®, shown in red and blue pseudo-colours, respectively. The nanoparticles located at the outer surface of the cell membrane are presented in green colours. The nanoparticles internalized by the cells and co-localized with the acidic endosomal compartments are shown in yellow colour. The turquoise colour corresponds to the internalized nanoparticles that are located outside of the early endosomes and lysosomes. Copyright © (2014) Elsevier B.V. Adapted and reprinted with permission from ref.*[365].

Considering the fact that drug loaded nanoparticles entrapped in endosomes and lysosomes are subjected to degradation by specific enzymes, the endosomal escape of the developed polymer-conjugated nanocomposites is a critical requisite for an effective therapeutic outcome.[245] Therefore, the intracellular trafficking and endosomal escape of the UnTHCPSi, UnP and UnPP nanoparticles were investigated in the MDA-MB-231 and

MCF-7 breast cancer cell lines by confocal fluorescence microscopy and simultaneous imaging of the FITC-labelled nanoparticles, cell membranes, and the endolysosomal compartments of the cells. In accordance to the results previously obtained in the flow cytometry experiments, a negligible cellular uptake was observed for the bare UnTHCPSi nanoparticles in both the cell lines, while the remarkably enhanced cellular internalization of UnP and UnPP nanocomposites was confirmed in both MDA-MB-231 (**Figure 13C**) and MCF-7 (**Figure 13D**) cells, as elucidated by the turquoise colour in the merged and magnified confocal images. Furthermore, it was observed that only a minority of the polymer-modified nanoparticles were located inside the acidic endosomal compartments, as identified by the overlapped yellow colour, and also that some of the nanoparticles remained associated to the outer surface of the cell membrane, predominantly in the MCF-7 cells. These observations demonstrated that the polymer-modified nanocomposites were capable of efficiently interacting and internalized by the cells, breached out from the endosomal compartments and, consequently, localized in the cytoplasm. This phenomenon can be plausibly explained by the presence of free amine groups from the hyperbranched PEI layer, which were not further conjugated to the outer PMVE-MA layer in UnPP nanoparticles, thus inducing endosomal escape *via* a "proton-sponge" or "endosome buffering" mechanism.[376] Additionally, the endosomal escape of UnPP nanoparticles by the "proton-sponge" effect can possibly be amplified as a result of the rapid hydrolysis of the maleic acid amide (MAA) bonds, formed by conjugating the carboxyl groups of maleic acid to the amine groups of PEI and, consequently, to the dissociation of the PMVE-MA layer in the endosomal acidic pH.[377,378] Another explanation for the endosomolytic properties of the UnPP nanocomposites involves the fusion of the PMVE-MA layer into the lipid bilayer of the acidic compartments, leading to its disruption, as previously demonstrated for other specific anionic polymers.[366,379]

The flow cytometry and confocal fluorescence microscopy results also showed the capability of UnP nanocomposites to overpass the cell membranes of MDA-MB-231 cells after 6 h of incubation, confirming the fact that the functionalization of the UnTHCPSi nanoparticles with PEI efficiently enhanced the cellular association and internalization by these cancer cells. In contrast, the cellular uptake of UnP nanoparticles was significantly lower in the MCF-7 cells, possibly due to the higher resistance of these cells in comparison to MDA-MB-231 cells, as well as to their tendency to form condensed clusters, which minimized their interaction with the nanoparticles.

5.2.3 Methotrexate loading, release and antiproliferative effect

The bare UnTHCPSi nanoparticles and polymer-modified nanocomposites were loaded with the model anticancer agent MTX, a potent drug in breast cancer treatment,[380] and the different drug loading degrees, before and after polymer conjugation, were investigated. In this regard, the presence of both carboxyl and amine groups in the chemical structure of MTX increased the probability of interaction with the amine and carboxyl groups of the conjugated PEI and PMVE-MA polymers, respectively, thus possibly increasing the loading degree of MTX after the polymer-modification of the UnTHCPSi nanoparticles. While the bare UnTHCPSi nanoparticles presented a MTX loading degree of 6.4 ± 1.2%, the

successive PEI and PMVE-MA conjugations resulted in superior drug loading degrees of 12.6 ± 0.1% and 14.0 ± 0.5%, respectively. The low MTX loading in the bare UnTHCPSi nanoparticles could be attributed to the low affinity and interaction of this hydrophilic drug with the intrinsically hydrophobic pores of the nanoparticles. Contrarily, the augmented MTX loading degrees observed for the UnP and UnPP nanocomposites suggested that the polymeric modification of the UnTHCPSi nanoparticles significantly enhanced the interactions with the drug, through establishment of hydrogen and electrostatic bonding between the functional groups of the polymers and the active payload.

Next, the drug release profiles of MTX-loaded UnTHCPSi, UnP and UnPP nanoparticles were evaluated in PBS (pH 7.4) over a period of 12 h (**Figure 14A**). The UnTHCPSi nanoparticles showed a burst release of the loaded MTX, within a short period of 5 min, owing to the rapid diffusion of the drug from the nanoparticles pores. In contrast, the polymeric modification of the UnTHCPSi nanoparticles revealed to sustain the release of the active payload, as evidenced by the significantly lower release rates observed for the UnP and UnPP nanoparticles, corresponding to a constant drug release up to *ca.* 95 and 70% within the first 3 h, respectively. Thereafter, no significant changes were observed in the cumulative drug release throughout the time period tested. A plausible explanation for the slower drug release rate from the UnPP nanocomposites, in comparison to the UnP counterparts, was the presence of both amine and carboxyl groups from PEI and PMVE-MA, respectively, which increased the possibility of interactions with the same moieties in the MTX structure. These results suggested that the polymer modification of the UnTHCPSi nanoparticles surface represents an easy and efficient approach for tuning the release profile of active payloads, by capping the porous structure, and establishing hydrogen and electrostatic bonding with the loaded drug molecules.[238]

To demonstrate that the UnPP nanocomposites can efficiently deliver the anticancer payload inside the cells, the antiproliferative effect of MTX-loaded UnTHCPSi and UnPP nanoparticles was evaluated in both MDA-MB-231 (**Figure 14B**) and MCF-7 (**Figure 14C**) breast cancer cells, using an ATP-based activity assay after the exposure to different concentrations of drug-loaded nanocarriers for 6 h at 37 ºC. All the data sets were compared to the negative control, corresponding to cells incubated in HBSS buffer (pH 7.4) and considered as 100% of cell proliferation. The results showed that the free drug and the MTX-loaded UnTHCPSi nanoparticles presented similar antiproliferative profiles in both the cancer cell lines, reducing the cell viability from 90% to less than 35% for MDA-MB-231 cells, and from 95% to *ca.* 50% for MCF-7 cells. In turn, the MTX-loaded UnPP nanocomposites showed considerably higher cytotoxic effects in both the cell lines tested, compared to pure MTX and MTX-loaded UnTHCPSi counterparts. After exposure to the MTX-loaded UnPP nanoparticles, the ATP-activity of MDA-MB-231 and MCF-7 cells was decreased from 64% to less than 10%, and from 77% to *ca.* 27%, respectively. The lower antiproliferative effect of MTX-loaded UnTHCPSi nanoparticles could be attributed to the limited cellular association and uptake of these nanocarriers. In addition, the increased cellular internalization of UnPP nanocomposites by MDA-MB-231 cells, relative to MCF-7 cells, could explain the higher therapeutic efficiency of the MTX-loaded UnPP nanoparticles in the former cell line. Considering the intracellular mechanism of action of MTX on inhibiting folic acid reductase and DNA synthesis during cellular replication,[381,382] the potent

therapeutic effect of UnPP nanocomposites could be related with the capability of delivering the anticancer payload at higher amounts inside the cells. These results provided a clear evidence of the potent therapeutic efficiency of the developed nanoparticulate drug delivery systems in breast cancer cells.

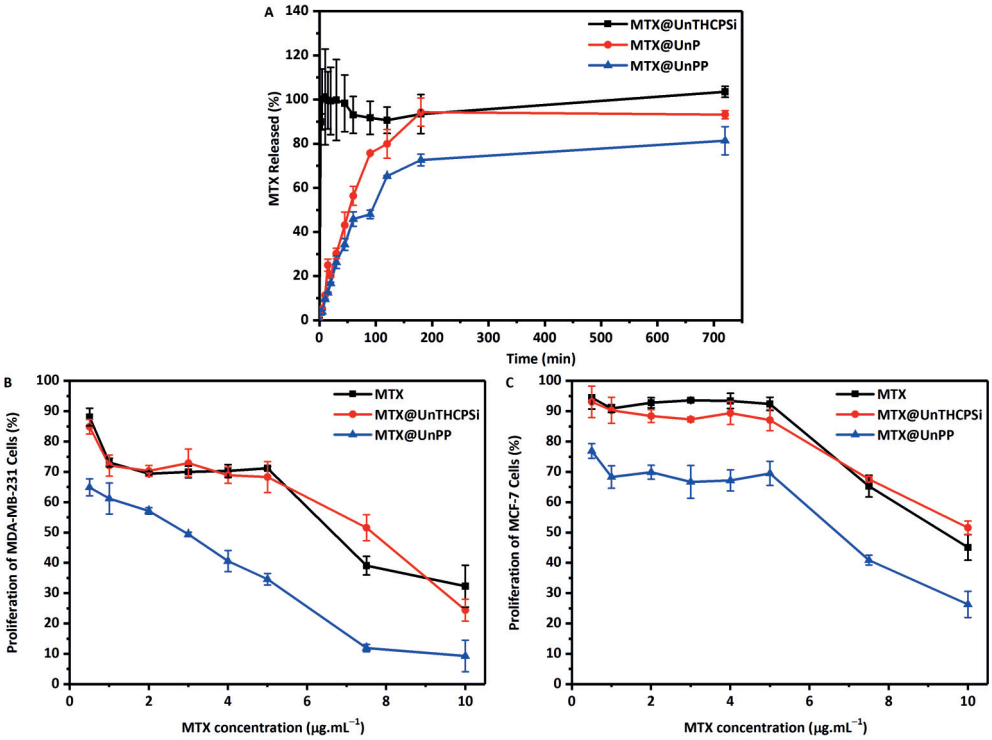

Figure 14. *(A) Drug release profiles of MTX-loaded UnTHCPSi, UnP and UnPP nanoparticles in PBS (pH 7.4) at 37 ºC. (B−C) Proliferation of MDA-MB-231 (B) and MCF-7 (C) breast cancer cells after exposure to free MTX, MTX@UnTHCPSi and MTX@UnPP nanoparticles for 6 h at 37 ºC. In MDA-MB-231 cells, free MTX and MTX@UNTHCPSi nanoparticles induced a mild concentration independent reduction on the cell proliferation, while the MTX@UnPP nanoparticles showed a potent concentration dependent antiproliferative effect. In MCF-7 cells, while the free drug and MTX@UnTHCPSi nanoparticles showed to not significantly affect the cell proliferation, the MTX@UnPP nanoparticles induced a moderate inhibition of the cell proliferation, independently of the concentration tested. Values denote the mean ± s.d. of three independent experiments (n = 3). Copyright © (2014) Elsevier B.V. Adapted and reprinted with permission from ref.*[365].

5.3 Multifunctional polymeric nanocomplexes encapsulating drug-loaded porous silicon and gold nanoparticles for intracellular drug delivery (III)

The surface modification of PSi nanoparticles with functional polymers has been proven to circumvent some of the major limitations that have been challenging the establishment of this nanoplatform as an effective anticancer drug delivery system. In the previous work, the functionalization of the UnTHCPSi nanoparticles with PEI and PMVE-MA showed to remarkably enhance the cellular association and endosomal escape and, consequently, improve the intracellular delivery and *in vitro* therapeutic efficacy of the loaded hydrophilic anticancer drug, MTX. However, a satisfactory therapeutic efficacy of nanomedicines does not only depend on the physicochemical features and biological performance of the nanocarrier, but is also affected by the inherent chemical properties of the active payloads, such as poor aqueous solubility and low chemical stability. In this regard, PSi nanoparticles assume particular relevance for enabling the confinement of hydrophobic drug molecules in an amorphous-like form within the porous structure, thus significantly enhancing the aqueous solubility of these therapeutics, while preventing their degradation.[28,202]

While an extensive research focus has been drawn to the surface functionalization of PSi nanoparticles for cancer targeting and therapeutic applications,[205,267,271] less attention has been paid to the design and engineering of multifunctional PSi@hydrophilic shell nanocomposites, mainly owing to methodological impediments and a greater formulation complexity. Despite the technical and formulation challenges, the successful development of these multifunctional nanosystems holds great promise, stemming from the opportunity to modulate the physicochemical and biological properties of the nanoencapsulate, as well as to integrate a combination of therapeutic and imaging agents into a nanotheranostic system. Therefore, the focus of this third study was to fabricate a multifunctional nano-in-nanocomplex platform, encapsulating both SFB-loaded UnTHCPSi and Au nanoparticles into an electrostatically assembled polymeric nanocomplex composed of a zwitterionic amino acid (L-cysteine), a bioadhesive polyanion (PMVE-MA), and an endosomolytic polycation (PEI). This innovative nanoformulation was aimed to enhance the cellular interactions and intracellular trafficking of the drug-loaded PSi nanocarriers, ultimately improving the cytoplasmic delivery and, consequently, the therapeutic efficacy of the loaded chemotherapeutic agent. For confirming the applicability of this strategy, the developed multifunctional nanosystem was physicochemically characterized and evaluated *in vitro* for cytocompatibility, cellular association and internalization, as well as for endosomolytic, cytoplasmic drug delivery and chemotherapeutic properties.

5.3.1 Physicochemical characterization

The UnTHCPSi nanoparticles used in this study were physically characterized by a specific surface area of 251 ± 16 $m^2.g^{-1}$, a total pore volume of 0.69 ± $cm^3.g^{-1}$ and an average pore diameter of 11.1 ± 0.4 nm. The size, PdI and ζ-potential values of the UnTHCPSi nanoparticles, CPP nanocomplexes, and UnCPP and UnAuCPP nanocomposites were

determined by DLS and ELS, respectively (**Table 4**). The bare UnTHCPSi nanoparticles and the CPP nanocomplexes presented a size of 173.7 ± 3.4 nm and 182.8 ± 0.1 nm, with PdI values of 0.10 and 0.14 nm, respectively. The nanoencapsulation of the UnTHCPSi nanoparticles into the CPP nanocomplexes resulted in the formation of the UnCPP nanocomposites, which exhibited a size of 241.0 ± 4.9 nm and a PdI of 0.18 ± 0.03, and the further incorporation of the Au nanoparticles in the formulation originated UnAuCPP nanocomposites with 346.2 ± 18.1 nm in diameter and a PdI of 0.24 ± 0.01. The PdI values lower than 0.3, for all the nanosuspensions, showed a relative monodispersity of the nanoparticles produced. Regarding the surface charge of the developed nanosystems, the UnTHCPSi nanoparticles exhibited a negative ζ-potential of −22.2 ± 0.4 mV, owing to their surface modification with carboxyl moieties. Oppositely, the CPP nanocomplexes featured a very strong positive surface charge of +40.3 ± 1.6 mV, resulting from the free amine groups of L-cysteine and hyperbranched PEI polymer. Equally to the CPP nanocomplexes, the UnCPP and UnAuCPP nanocomposites presented a positive ζ-potential of +40.1 ± 0.3 mV and +38.4 ± 0.3 mV, respectively, thus indicating the successful encapsulation of the negatively charged UnTHCPSi and Au nanoparticles into the nanocomplexes.

Table 4. *Physicochemical characterization of the UnTHCPSi, CPP, UnCPP and UnAuCPP nanoparticles in terms of size, PdI, ζ-potential, loading degree (LD) and encapsulation efficiency (EE) of SFB.*[a)]

Nanoparticle	Size (nm)	PdI	ζ-potential (mV)	LD (%)	EE (%)
UnTHCPSi	173.7 ± 3.4	0.10 ± 0.01	–22.2 ± 0.4	12.3 ± 3.0	—
CPP	182.8 ± 1.0	0.14 ± 0.00	40.3 ± 1.6	—	—
UnCPP	241.0 ± 4.9	0.18 ± 0.03	40.1 ± 0.3	—	99.3 ± 0.1
UnAuCPP	346.2 ± 18.1	0.24 ± 0.01	38.4 ± 0.3	—	99.9 ± 0.0

[a)] *Values denote the mean ± standard deviation ($n \geq 3$).*

For scrutinizing the nanoparticle size and morphology, as well as for verifying the nanoencapsulation of UnTHCPSi and Au nanoparticles into the structures of UnCPP and UnAuCPP nanocomposites, all the nanoparticulate systems were analysed by TEM (**Figure 15A**), where it was possible to visualize the characteristic irregular shape and porous structure of the UnTHCPSi nanoparticles. Contrarily, the CPP nanocomplexes showed regular spherical structures, and the general particle sizes corroborated the DLS results. Additionally, irregular dark contrasted areas, corresponding to UnTHCPSi nanoparticles, could be identified within the UnCPP and UnAuCPP nanostructures. Likewise, the TEM micrographs of UnAuCPP nanocomposites showed 10 nm spherical Au nanoparticles within the polymeric nanocomplexes, highlighted by the green arrows in **Figure 15A**.

In order to confirm the chemical composition of the nanostructures observed under TEM, particularly regarding the nanostructures identified within the UnCPP and UnAuCPP nanocomposites, each of the nanoparticles produced were examined by EDX microanalysis (**Figure 15B**). The spectra of the UnCPP and UnAuCPP nanocomposites clearly exhibited the prominent characteristic peak of the Si element at the energy value of 1.74 keV, corresponding to the encapsulated UnTHCPSi nanoparticles. In addition, both Au element-

related peaks could be identified at the energy levels of 2.12 and 9.7 keV in the spectrum of UnAuCPP nanocomposites, thus confirming the presence of Au nanoparticles within the structure. The described EDX microanalysis corroborated with the physicochemical characterization and, therefore, verified the success of the UnTHCPSi and Au nanoparticles encapsulation into the UnCPP and UnAuCPP nanocomposites.

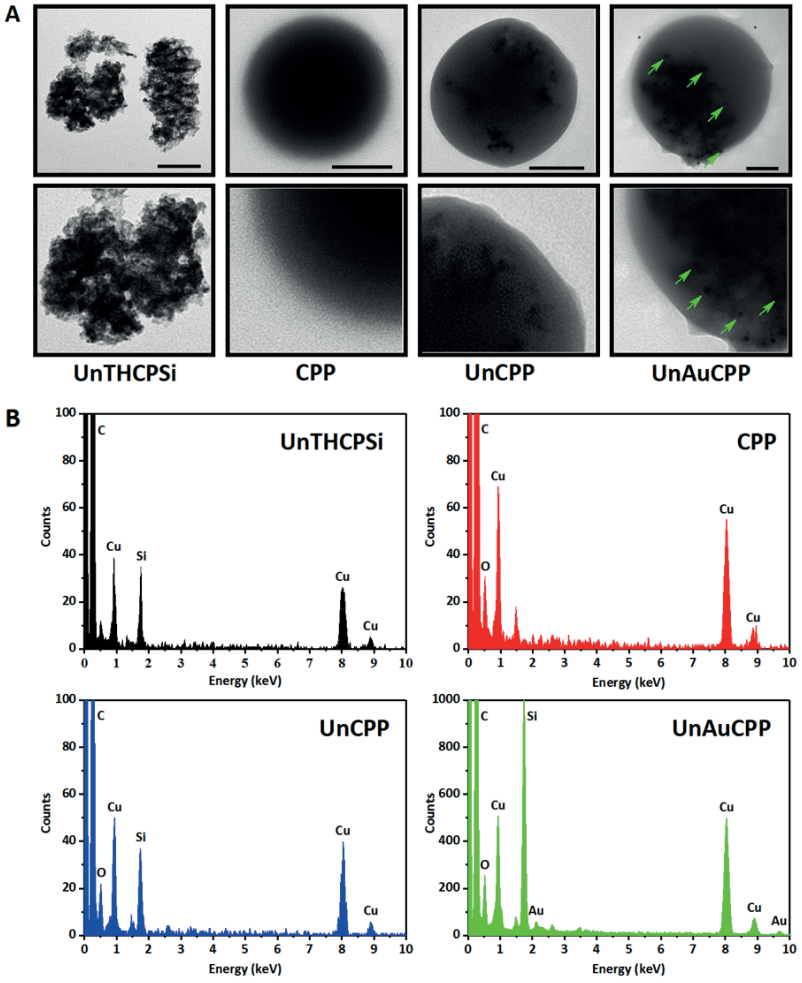

Figure 15. *Physicochemical characterization of UnTHCPSi, CPP, UnCPP and UnAuCPP nanoparticles. (A) TEM images of UnTHCPSi, CPP, UnCPP and UnAuCPP nanoparticles, showing the nanoencapsulation of UnTHCPSi and Au nanoparticles into the CPP nanocomplexes. Examples of the encapsulated Au nanoparticles are highlighted by the green arrows. Scale bars are 100 nm. (B) EDX spectra of UnTHCPSi, CPP, UnCPP and UnAuCPP nanoparticles, confirming the presence of Si and Au elements in the composition of the UnCPP and UnAuCPP nanocomposites. The peaks corresponding to Cu element drive from the TEM grids composition. Copyright © (2017) Future Medicine. Adapted and reprinted with permission from ref.*[383].

5.3.2 Cytocompatibility

As previously discussed, major concerns arise from the severe cytotoxicity of PEIs and their use in cancer nanomedicine.[179,180] Moreover, it is imperative to define a cytocompatible concentration range for the developed nanoparticulate systems, prior to their further evaluation. Therefore, the cell viability of MDA-MB-231 breast cancer cells was assessed by analysing the ATP activity after exposure to the UnTHCPSi, CPP, UnCPP and UnAuCPP nanosuspensions at concentrations between 12.5 and 200 $\mu g.mL^{-1}$, for 6 and 24 h at 37 ºC (**Figure 16**).

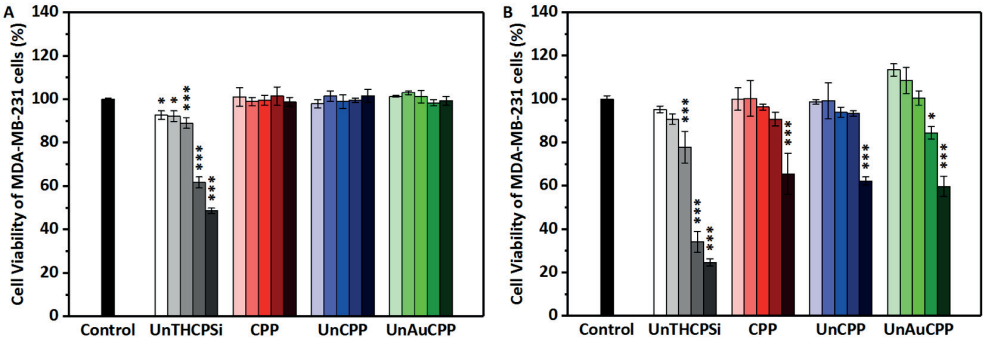

Figure 16. *(A–B) In vitro cytotoxicity of UnTHCPSi, CPP, UnCPP and UnAuCPP nanoparticles after incubation with MDA-MB-231 breast cancer cells, for 6 h (A) and 24 h (B) at 37 ºC. The cell viability was quantified by an ATP-based luminescence assay after exposing the cells to the nanoparticle concentrations of 12.5, 25, 50, 100 and 200 $\mu g.mL^{-1}$, corresponding to the successively darker colours. All the datasets were compared to the negative control, corresponding to cells incubated with 10 mM of HBSS–HEPES buffer (pH 7.4). Error bares denote mean ± s.d. ($n \geq 3$). Statistical analysis was performed by means of one-way ANOVA with the level of significance set at probabilities of $*p < 0.05$, $**p < 0.01$, and $***p < 0.001$. Copyright © (2017) Future Medicine. Adapted and reprinted with permission from ref.[383].*

After 6 h of incubation time, the bare UnTHCPSi nanoparticles induced an ATP depletion on MDA-MB-231 cells, particularly for the concentrations of 100 and 200 $\mu g.mL^{-1}$, which resulted in a statistically significant decrease in the cell viability to 61.7 ± 2.5 and 48.6 ± 1.3%, respectively, in comparison with the negative control cells. In contrast, for the same exposure period, the CPP, UnCPP and UnAuCPP nanocomplexes showed no cytotoxicity in the range of concentrations tested. The cytotoxic effect of UnTHCPSi nanoparticles was more clear after 24 h, therefore evidencing a time and concentration-dependency, while the CPP, UnCPP and UnAuCPP still showed high cytocompatibility values, with exception of the 200 $\mu g.mL^{-1}$ concentrated nanosuspensions, which decreased the cell viability values to *ca.* 65%. The superior cytocompatibility of the CPP, UnCPP and UnAuCPP nanocomposites represented a remarkable attainment, considering the highly positive charge of these nanocomplexes, and particularly the well-known cytotoxic

properties of the PEI polymer included in these nanoformulations.[170,179] The electrostatic interaction of the polycationic and cytotoxic PEI with the polyanionic and biocompatible PMVE-MA in the CPP nanocomplexes self-assembly process, could possibly reduce the cytotoxicity of the former polymer, ultimately resulting in superior cytocompatibility of the developed multifunctional nanocomposites.

5.3.3 Cellular association, internalization and endosomolytic effect

The therapeutic efficiency of the developed multifunctional nanomedicines is highly dependent on the capability for overcoming extra- and intracellular barriers, aiming at effectively delivering the UnTHCPSi nanoparticles and the therapeutic cargo to the cytoplasm of the tumour cells.[117] Thus, for investigating the cellular association and internalization of UnTHCPSi, UnCPP and UnAuCPP nanoparticulate systems, MDA-MB-231 breast cancer cells were exposed to the various nanosuspensions at a concentration equivalent to 10 $\mu g.mL^{-1}$ of UnTHCPSi, for 1 and 3 h at 37 ºC, and subsequent qualitative and quantitative analyses were performed by TEM (**Figure 17A**) and flow cytometry (**Figure 17B**), respectively. In this regard, the presented TEM micrographs were representative of MDA-MB-231 cells interacting with the different nanoplatforms, thus providing a better understanding on their extra- and intracellular distribution, while the flow cytometry analysis enabled the quantification of the cellular association and internalization. In agreement with the results presented in the previous study (*Section 5.2.2*), and according to the TEM images (**Figure 17A**) and corresponding flow cytometry histograms (**Figure 17B**), the bare UnTHCPSi nanoparticles showed negligible interactions and endocytosis by the cancer cells, which can be possibly explained by the negative surface charge, low colloidal stability in aqueous solutions and poor bioadhesiveness of these nanocarriers. In contrast, the UnCPP and UnAuCPP nanocomposites did significantly interact with the cellular membrane, and were subsequently endocytosed by the cancer cells, as shown in the corresponding TEM micrographs. After endocytosis, the nanocomposites exhibited the capacity to escape from the endosomal compartments of the cells within a period of 3 h, releasing the nanoencapsulated UnTHCPSi nanoparticles in the cytoplasm. These results demonstrated the remarkable potential of the CPP nanocomplexes for enhancing the cellular association, internalization and endosomolytic capacity of the encapsulated UnTHCPSi nanoparticles, releasing these encapsulates into the cytosolic compartment of the cells. The improved cellular association and uptake of the UnCPP and UnAuCPP nanocomposites may rely on both the positive surface charge of these nanosystems, which enhances and mediates the electrostatic interaction with the anionic moieties in the cellular membrane, as well as on the intrinsic bioadhesiveness of L-cysteine and PMVE-MA formulating the CPP nanocomplexes.[369,384] Furthermore, the cationic amine groups and consequent buffering properties of the hyperbranched PEI can explain the remarkable capability of the UnCPP and UnAuCPP nanocomposites for breaching out from the endosomal compartments, probably *via* the “proton-sponge” mechanism.[385]

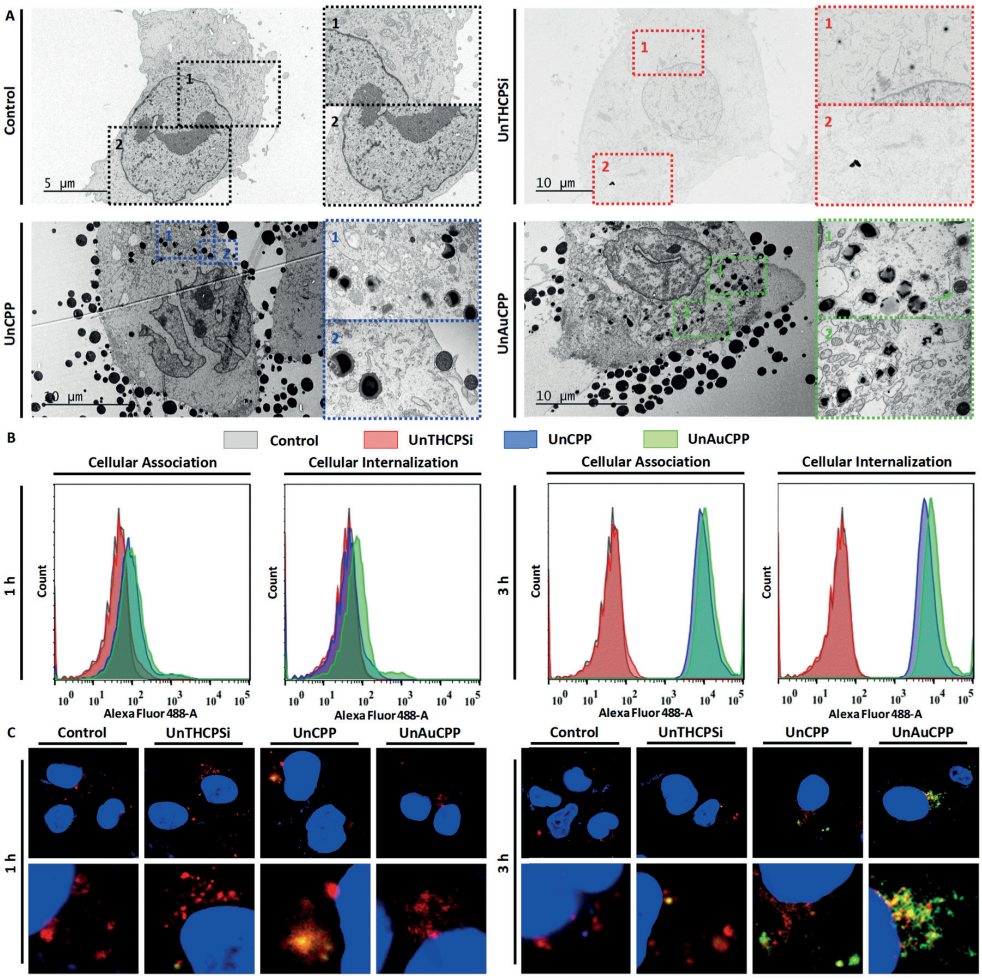

Figure 17. *Cellular association, internalization, and intracellular distribution of UnTHCPSi, UnCPP and UnAuCPP nanoparticles. (A) TEM images and corresponding numerically ordered magnifications of ultrathin sections of MDA-MB-231 breast cancer cells incubated with the different nanoparticles at the concentration equivalent to 10 µg.mL^{-1} of UnTHCPSi, for 3 h at 37 ºC. Cells incubated with 10 mM of HBSS−HEPES buffer (pH 7.4) + 10% FBS were used as control. (B) Flow cytometry analysis of the cellular association and internalization of UnTHCPSi, UnCPP and UnAuCPP nanoparticles. MDA-MB-231 cells were incubated with the various nanoparticles at the concentration equivalent to 10 µg.mL^{-1} of UnTHCPSi for 1 and 3 h at 37 ºC. Controls correspond to cells incubated with 10 mM of HBSS−HEPES buffer (pH 7.4) + 10% FBS. The UnTHCPSi nanoparticles were covalently labelled with Alexa Fluor® 488, prior to encapsulation into the CPP nanocomplexes. For evaluating both cellular association and internalization of the nanoparticles, the cells were analysed before and after extracellular fluorescence quenching with a TB solution, respectively. The results presented are representative of three independent experiments. (C) Confocal fluorescence microscopy analysis of MDA-MB-231*

breast cancer cells, after incubation with UnTHCPSi, UnCPP and UnAuCPP nanoparticles at the concentration equivalent to 20 μg.mL^{-1} of UnTHCPSi, for 1 and 3 h at 37 ºC. Cells incubated with 10 mM of HBSS−HEPES buffer (pH 7.4) + 10% FBS were used as controls. The UnTHCPSi nanoparticles were covalently labelled with Alexa Fluor® 488, prior to encapsulation into the CPP nanocomplexes. The cells were stained with Lysotracker® Red DND-99 and DAPI for their acidic endosomal compartments and nucleus, herein represented by the red and blue colours, respectively. The green colour denotes the nanoparticles interacting at the cells surface or internalized by the cells and evaded from the early endosomes and lysosomes, while the nanoparticles co-localized with those compartments are shown in yellow colour. Copyright © (2017) Future Medicine. Adapted and reprinted with permission from ref.[383].

The TEM analyses were corroborated by the flow cytometry results of the MDA-MB-231 breast cancer cells exposed to the UnCPP and UnAuCPP multifunctional nanocomposites (**Figure 17B**). In these experiments, a TB solution was used for quenching the fluorescence of extracellularly associated nanoparticles. As previously referred to in this section, no substantial differences were observed between the fluorescence signals of the cells exposed to bare UnTHCPSi nanoparticles and the corresponding negative control samples, demonstrating the low cellular interaction and uptake of these nanosystems. Contrarily, significantly higher fluorescence intensities were noticed for the cancer cells incubated with the UnCPP and UnAuCPP nanocomposites after a 3 h incubation time period, representing a solid evidence of the distinguished cellular association properties of these nanoplatforms. Interestingly, after the TB quenching, no variation of the fluorescence signal was detected, confirming the occurrence of endocytosis and the intracellular localization of the UnCPP and UnAuCPP nanocomplexes.

In order to investigate the capacity of UnCPP and UnAuCPP nanocomplexes to deliver the encapsulated UnTHCPSi nanoparticles in the cytoplasm of the cells, and to demonstrate the potential of these nanovehicles for cancer therapy, the UnTHCPSi nanoparticles were covalently labelled with AF488, and subsequently fabricated to UnCPP and UnAuCPP nanocomposites. Next, MDA-MB-231 breast cancer cells were exposed to the different nanosuspensions at a concentration equivalent to 20 μg.mL^{-1} of UnTHCPSi, for 1 and 3 h at 37 ºC. Afterwards, the nuclei and endosomal compartments of the cells were stained with DAPI and LysoTracker® Red DND-99, respectively, and the samples were analysed by confocal fluorescence microscopy (**Figure 17C**). As previously observed for the TEM and flow cytometry analyses, the bare UnTHCPSi nanoparticles were negligibly interacted and internalized by the cancer cells. Contrarily, as evidenced in the corresponding merged and magnified images presented in **Figure 17C**, the uptake of the fluorescently-labelled UnTHCPSi nanoparticles was significantly higher after the nanoencapsulation into UnCPP and UnAuCPP nanocomposites, predominantly after 3 h of incubation. Furthermore, it could be inferred that, following endocytosis, the nanocomposites were initially found entrapped into the acidic compartments of the cancer cells, as confirmed by the co-localization of the fluorescent signals from both the nanoparticles and the endosomes, represented by the yellow colour in the merged and magnified confocal panels. Additionally, after 3 h of exposure time, a significantly increased endocytosis of the UnCPP and UnAuCPP

nanocomposites was observed. The encapsulated UnTHCPSi nanoparticles were predominantly found in the cytoplasm of the cells, thus suggesting their endosomal escape, elucidated by the emergence of the green fluorescent signal in the overlapped pictures.

In summary, the results obtained demonstrated the capacity of the CPP nanocomplexes to remarkably enhance the cellular interaction and internalization of the UnTHCPSi nanoparticles, through the assembly of multifunctional nanocomposites possessing positive surface charge and bioadhesive properties. In addition, the CPP nanocomplexes significantly improved the intracellular trafficking of the encapsulated UnTHCPSi nanoparticles, facilitating their endosomal escape *via* the "proton-sponge" or "endosome buffering" mechanism, and efficiently delivering those to the cytoplasm of the cancer cells.

5.3.4 Sorafenib loading, release and chemotherapeutic efficacy

The therapeutic efficiency and safety profiles of an anticancer drug delivery system depends on both the physicochemical properties and biological performance at the extra- and intracellular levels, and the ability to effectively deliver the loaded therapeutic agent to the cytoplasm of the cancer cells. In this case, the premature drug release of the active cargo during circulation of the nanovehicles in the bloodstream, as well as the inefficient protection from degradation still remain as bottlenecks encountered in the formulation and application of nanomedicines for cancer therapy.[386]

SFB was selected as a hydrophobic anticancer drug model,[387] and loaded into the pores of UnTHCPSi nanoparticles prior to the preparation of the UnCPP and UnAuCPP nanocomposites, in order to evaluate the drug loading capacity of the developed nanosystems (**Table 4**). A loading degree of 12.3 ± 3.0% (*w/w*) was obtained for the SFB@UnTHCPSi nanoparticles, and no drug leakage was detected during the nanoencapsulation into the UnCPP and UnAuCPP nanocomposites, considering that nearly 100% of the drug amount initially loaded into the UnTHCPSi nanoparticles was efficiently encapsulated into the assembled nanocomposites.

After the drug loading, the release profiles of SFB from the different nanocarriers were evaluated in HBSS−HEPES (pH 7.4; **Figure 18A**) and HBSS−MES (pH 5.5; **Figure 18B**) buffer solutions supplemented with 10% FBS for assisting the SFB dissolution, as previously reported in the literature.[205,264] Approximately 1% of the pure bulk SFB was dissolved in both drug release media after 6 h, owing to the extremely low aqueous solubility of the drug. Notwithstanding the hydrophobicity, the loading of SFB into the porous matrix of the UnTHCPSi nanoparticles resulted in significant improvement of the drug's dissolution to *ca.* 68 and 43% at pH 7.4 and 5.5, respectively. The enhancement of the SFB's dissolution, and the burst release behaviour exhibited by the SFB@UnTHCPSi nanoparticles resulted from the confinement of the drug in amorphous-like form within the porous structure of the UnTHCPSi nanoparticles and the inhibition of drug crystallization.[311,366] When formulated into SFB@UnCPP and SFB@UnAuCPP nanocomposites, the cumulative SFB release was declined to a maximum of *ca.* 51 and 31% after 6 h, respectively, an effect that was attributed to the physical blockage of the UnTHCPSi pores as a consequence of the encapsulation into the CPP nanocomplexes, and/or to the electrostatic interactions occurring between the drug molecules and the polymeric nanocomplexes. The results presented confirmed the potential

of UnTHCPSi nanoparticles for formulating anticancer agents with unfavourable water solubility by improving the dissolution rate, and suggested that the developed multifunctional nanocomposites could effectively retain the SFB inside their nanostructure, avoiding the premature release and, consequently, sustain the release from the UnTHCPSi nanoparticles.

Finally, the *in vitro* chemotherapeutic effect of the engineered multifunctional nanocomposites was investigated by assessing the inhibition of MDA-MB-231 breast cancer cells proliferation after 6 h (**Figure 18C**) and 24 h (**Figure 18D**) exposure to successively increasing concentrations of pure bulk SFB and the various SFB-loaded nanoparticle suspensions, all represented in terms of SFB molar concentration.

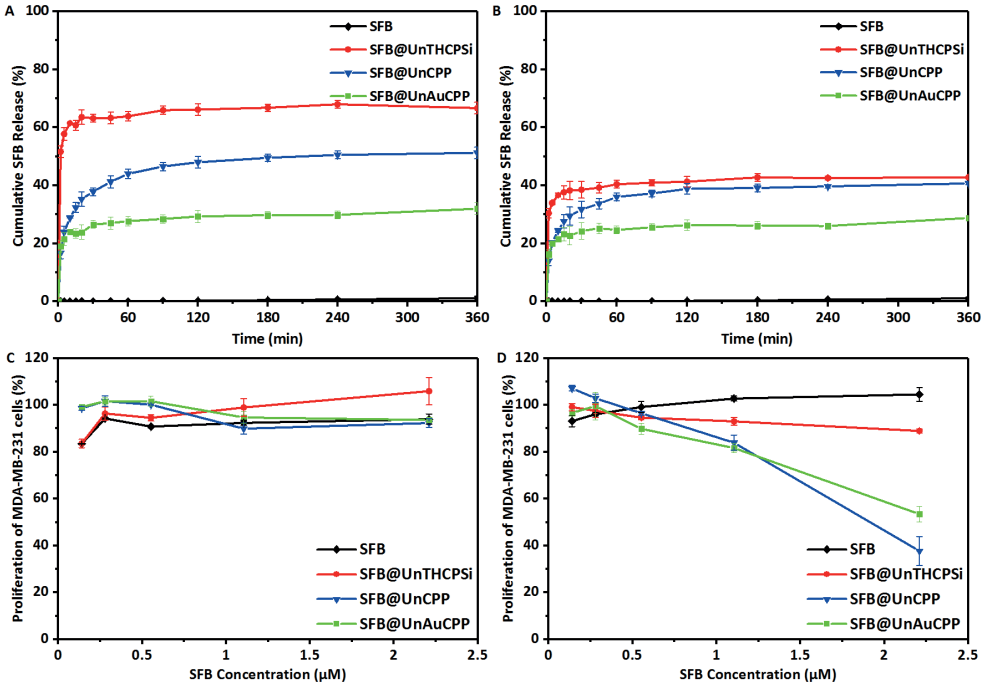

Figure 18. *(A−B) Drug release profiles of pure SFB, SFB@UnTHCPSi, SFB@UnCPP and SFB@UnAuCPP in 10 mM of HBSS−HEPES (pH 7.4) + 10% FBS (A) and 10 mM of HBSS−MES (pH 5.5) + 10% FBS buffers at 37 ºC. Error bars represent mean ± s.d. (n ≥ 3). (C−D) In vitro antiproliferative effect of pure SFB, SFB@UnTHCPSi, SFB@UnCPP and SFB@UnAuCPP on MDA-MD-231 breast cancer cells. The cells were exposed to different concentrations of the nanoparticles suspended in 10 mM of HBSS−HEPES (pH 7.4) + 10% FBS buffer for 6h (C) and 24 h (D) at 37 ºC. The pure SFB samples were prepared by suspending the correspondent amount of the bulk drug in 10 mM of HBSS−HEPES (pH 7.4) + 10% FBS buffer, followed by the corresponding dilution with the same solution. All the datasets were compared to the negative control, equivalent to the cell viability in 10 mM of HBSS−HEPES (pH 7.4) + 10% FBS buffer. Error bars denote mean ± s.d. (n ≥ 3). Copyright © (2017) Future Medicine. Adapted and reprinted with permission from ref.*[383].

The pure SFB did not affect the proliferation of MDA-MB-231 cancer cells in the experimental conditions and exposure times tested, possibly due to the very low drug aqueous solubility, and consequent incapacity to penetrate the cell membranes. Nevertheless, the same outcome was observed when formulating SFB into UnTHCPSi nanoparticles. Despite enhancing the drug's dissolution rate, the limited cellular interactions and internalization of the UnTHCPSi nanoparticles by cancer cells appeared to be a relevant factor limiting the delivery of the chemotherapeutic agent to the intracellular site of action, therefore also hindering the antiproliferative effect. In contrast, the SFB@UnCPP and SFB@UnAuCPP nanocomposites showed to considerably inhibit the proliferation of the breast cancer cells after 24 h, with remarkably low IC_{50} values of approximately 1.9 and 2.2 μM, respectively. The superior antiproliferative effect of the nanocomposites could be possibly explained by a combination between the attractive physicochemical properties and the biological performance of these nanoplatforms. Initially, the high cellular association and endocytosis observed for these nanocomposites, as well as their endosomolytic properties, enabled the efficient delivery of the nanoencapsulated SFB@UnTHCPSi nanoparticles to the cells' cytoplasm. Thereafter, the enhanced SFB's dissolution rate, resulting from the loading into the UnTHCPSi nanoparticles, played a key role on the achieved antiproliferative effect of the malignant cells, even at low concentrations of the nanocomposites and SFB. These results provided a robust evidence of the potential of the developed UnCPP and UnAuCPP nanocomposites to formulate poorly-water soluble anticancer agents and efficiently enhance their cytoplasmic delivery to the targeted cancer cells, ultimately improving the chemotherapeutic effect.

5.4 Endosomolytic nanocomplexes carrying DNA-anchored porous silicon nanoparticles for multiresponsive dual drug delivery (IV)

Despite the attractive and promising features of PSi nanoparticles for cancer nanomedicine, particularly when considering the formulation of chemotherapeutic agents with very limited aqueous solubility, their successful application in cancer drug delivery is still defied by several bottlenecks. Although the previous studies of this thesis have focused on different strategies for improving the limited receptor-specific and non-specific cellular interactions, cellular uptake and endosomolytic properties of PSi nanoparticles by developing surface-modified or multistage PSi-based nanocomposites, other challenging drawbacks of these nanocarriers include their leaky nature, burst and uncontrolled release of the therapeutic cargo, as well as the restraint of loading a single class of drug molecules. For addressing these hurdles, numerous strategies have been explored, involving the engineering of surface gate capped porous nanoparticles, aiming at developing advanced controlled drug delivery systems. In this regard, different biomolecular and supramolecular compounds have been anchored on the surface of porous nanoparticles for triggering the release of the active payload upon different internal and/or external stimuli, such as changes in the pH, light, redox potential, temperature and concentration of certain ions, enzymes or biomolecules.[266,388-390] However, it is still challenging to engineer a versatile drug delivery

platform capable of encapsulating large amounts of various therapeutic/imaging molecules without leakage or interference, and of efficiently delivering these active payloads intracellularly in a bioresponsive and controlled manner. Therefore, the fourth work of this dissertation contemplated the development of an innovative multifunctional nano-in-nano platform, idealized for controlled combination drug therapy or for theranostic applications. The developed nanocomposite was designed for the triggered and controlled intracellular delivery of both hydrophilic and hydrophobic molecules, by simultaneously endorsing endosomolytic properties and bioresponsiveness to intracellular reduction gradients through chemically defined mechanisms. For materializing this strategy, redox-responsive DNA-gated UnTHCPSi nanoparticles were encapsulated as a core nanocarrier within the previously developed CPP polymeric nanocomplexes. The DNA-capped UnTHCPSi nanoparticles were evaluated as redox and DNase responsive nanovehicle for both hydrophobic (SFB) and hydrophilic (calcein) model molecules, while being encapsulated within the CPP nanocomplexes covalently loaded with FITC *via* click chemistry, as a model drug or imaging agent. In addition, the engineered multifunctional nanocomposites, designated here as UnCAD@CPP, were investigated for the intracellular drug release by DNA cleavage and redox triggered mechanisms, as well as for the cellular association, internalization and capacity to escape the endosomal pathway.

5.4.1 Dual drug loading and multiresponsive drug release

In order to demonstrate the versatility of the developed multifunctional nanocomposites for combined drug delivery or theranostic purposes, SFB and calcein were separately loaded as hydrophobic and hydrophilic model cargos within the porous structure of the UnTHCPSi nanoparticles, as described in the *Section 4.3.1*. While the loading degree of SFB was 9.3 ± 0.2% (*w/w*), a loading value of 29 ± 3 $\mu mol.g^{-1}$ was attained for calcein. Despite the suitability of UnTHCPSi nanoparticles for loading desirable amounts of both model molecules, the direct exposure of the porous matrix to the dissolution medium results in an uncontrolled burst release of these payloads. In this case, cystine and 9-aminoacridine were consecutively conjugated onto the surface of bare UnTHCPSi nanoparticles, as a redox responsive cross-linker and DNA intercalating agent, respectively, prior the loading of the active agents. The drug-loaded UnCA nanoparticles were subsequently coated with DNA, for controlling the release of the payloads from the nanocarrier through both redox and DNase responsive mechanisms. Importantly, a negligible SFB leakage (i.e., <1%) was detected during the process of DNA coating, due to the large discrepancy between the polarities of the aqueous solution used and the drug molecules. Furthermore, the resulting DNA-anchored UnCAD nanoparticles were encapsulated within the CPP nanocomplexes, aiming at improving the cell penetrating and endosomolytic properties, as well as enabling the application of the assembled UnCAD@CPP nanocomposite for co-drug delivery or theranostics purposes. Thus, the sulfhydryl groups of the L-cysteine support the straightforward reaction of a wide variety of other functional moieties *via* thiol-click chemistry.[391] Here, FITC was used as a model compound to validate the integration into the nanocomplexes by a thiol-isothiocyanate click reaction. In addition, the electrostatic interaction of isothiocyanate with the amine groups of PEI and L-cysteine contributed to a

very efficient and stable encapsulation of these molecules. Therefore, the encapsulation efficiency of FITC in both the CPP and UnCAD@CPP nanocomplexes was evaluated and compared for different initial amounts of this fluorescent dye (**Figure 19A**). The results showed encapsulation efficiency values above 90% for the initial amounts of FITC lower than 45 μg. When the FITC amount was increased to 60 and 90 μg, the encapsulation efficiency of the fluorescent dye was significantly decreased to *ca*. 80 and 60%, respectively. Moreover, identical values of the encapsulation efficiency were obtained for both the CPP and UnCAD@CPP nanocomplexes, demonstrating that the simultaneous encapsulation of both UnCAD and FITC into the CPP nanocomplexes did not interfere with the loading efficiency of FITC.

Next, the release of SFB and calcein from the different nanoparticulate systems was investigated under simulated physiological conditions, namely at pH 7.4 and in the presence or absence of GSH or DNase. No dissolution of pure SFB was detected in the release medium, independently of the presence of GSH or DNase (**Figure 19B**). The SFB dissolution was significantly increased in PBS + 10% FBS (pH 7.4), after the loading into the UnTHCPSi nanoparticles (**Figure 19B**). Despite the enhanced SFB dissolution, the direct aperture and exposure of the pores to the release medium prevented the control over the SFB release rate from the UnTHCPSi nanoparticles. Therefore, the DNA capping was performed for enabling GSH and DNase responsive control over the drug release rate. Consequently, no SFB was released from the DNA-anchored UnCAD and UnCAD@CPP nanocomposites, after 6 h of incubation in PBS (pH 7.4) lacking the GSH. Contrarily, the SFB release occurred after supplementing the release medium with GSH, as a consequence of the cap removal through the cleavage of disulphide bond in the cystine chemical structure (**Figure 19C**). The slower SFB release rate observed for the UnCAD@CPP nanocomposites, in comparison with the UnCAD, could be explained by the slower diffusion of the hydrophilic GSH molecules through the CPP polymeric matrix for reducing the disulphide bonds of cystine conjugated at the UnCAD surface. Additionally, after being released, some drug molecules may have interacted and be retained within the nanocomplex matrix.

In addition to the GSH responsiveness, the SFB release from the UnCAD and UnCAD@CPP nanocomposites could be triggered by the presence of DNase (**Figure 19D**), due to the capability of this enzyme for breaking the DNA structure down to its constituting oligonucleotides, thus mediating the drug release. The DNase mediated drug release resulted in similar release rates than those corresponding to GSH-triggered drug release, despite the slightly higher percentage of SFB released when DNase was present in the medium. This phenomenon could be explained by the direct destructive effect of DNase over the DNA capping of the UnTHCPSi pores, comparative to the GSH treatment, which in turn resulted in the detachment of intact DNA molecules that were still electrostatically interacting with the pores surface. Moreover, in the case of UnCAD@CPP nanocomposites, a fraction of the DNA coating might have remained at the interface between the UnCAD nanoparticles and the CPP nanocomplexes, reducing the SFB release.

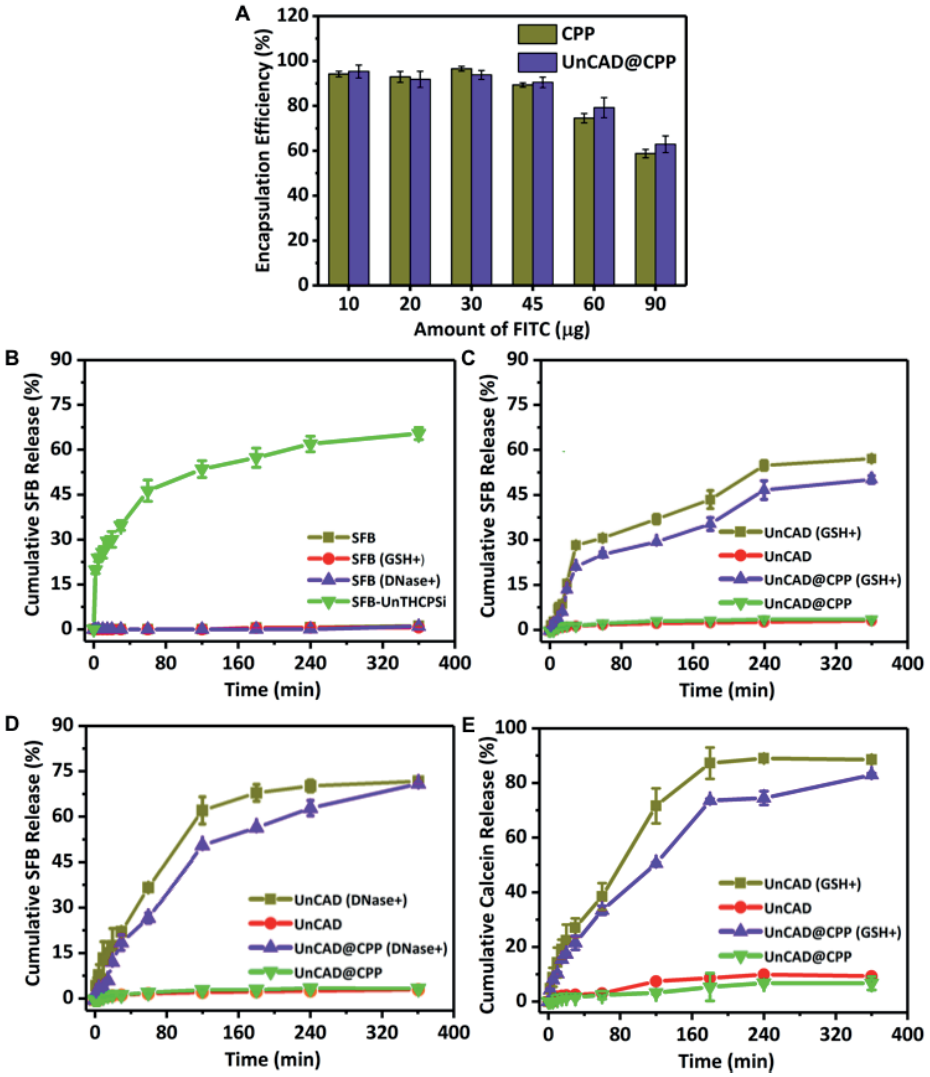

Figure 19. *(A) Encapsulation efficiency of FITC into CPP and UnCAD@CPP nanocomplexes, as a function of the initial FITC amount used for loading. (B) Dissolution profiles of free SFB and SFB-loaded UnTHCPSi nanoparticles in PBS + 10% FBS (pH 7.4) supplemented or not with 10 mM of GSH or 25 U.mL^{-1} of DNase. (C) GSH-responsive drug release profiles of SFB-loaded UnCAD and UnCAD@CPP nanocomposites in PBS + 10% FBS (pH 7.4) in the presence or absence of 10 mM of GSH. (D) DNase-responsive drug release profiles of SFB-loaded UnCAD and UnCAD@CPP nanocomposites in PBS + 10% FBS (pH 7.4), in the presence or absence of 25 U.mL^{-1} of DNase. (E) GSH-responsive drug release profiles of calcein-loaded UnCAD and UnCAD@CPP nanocomposites in PBS + 10% FBS (pH 7.4) in the presence or absence of 10 mM of GSH. All the error bars represent mean ± s.d. (n ≥ 3). Copyright © (2017) Elsevier B.V. Adapted and reprinted with permission from ref.*[392].

For confirming the feasibility of loading hydrophilic cargos within the developed nanocomposites, in addition to the hydrophobic payloads, the release of calcein was also investigated in the presence and absence of GSH (**Figure 19E**). The calcein loading degree and release profiles were determined by fluorescence spectroscopy after developing a linear calibration curve for calcein in PBS solution. No fluorescence was detected in the supernatant samples after calcein loading into the UnCAD nanoparticles and subsequent encapsulation into the CPP nanocomplexes, indicating the absence of compound release during this process. Contrarily, the washing steps of bare UnTHCPSi nanoparticles performed after calcein loading resulted in more than 95% of calcein release, dropping the loaded amount to 3 $\mu mol.g^{-1}$. For this reason, the calcein release was not studied for the bare UnTHCPSi nanoparticles. In the case of both the UnCAD and UnCAD@CPP nanocomposites, no premature calcein release was observed in the absence of GSH, as more than 93% of the loaded calcein remained entrapped within the nanoplatforms after the 6 h time period tested (**Figure 19E**). When adding GSH to the release medium, both UnCAD and UnCAD@CPP nanocomposites showed remarkable bioresponsive properties by sustaining the release of calcein during the same time period.

Overall, these results demonstrated that the DNA capping of PSi nanoparticles can be considered an effective strategy for controlling the intracellular release of different types of therapeutic and diagnostic cargos loaded within the PSi pores, through the bioresponsive cleavage of disulphide bonds or DNA disintegration.

5.4.2 Time dependent cellular association and endosomal escape

In order to verify the potential of the developed nanocomplexes for the intracellular delivery of the encapsulated materials, interactions of bare CPP nanocomplexes with MDA-MB-231 breast cancer cells were investigated as a function of time, using confocal fluorescence microscopy. In **Figure 20A**, the merged and magnified confocal images corresponding to the CPP nanocomplexes demonstrated that these nanoplatforms could extensively interact with the cancer cells within 1 h of incubation, and be internalized into the cells over the remaining period of time tested. These observations corroborated the results presented in the previous study (*Section 5.3*), and are in line with numerous reports in the literature demonstrating the high cellular affinity of nanoparticles containing PEI, owing to the high surface positive charge rendered by this polymer.[393,394] Furthermore, as previously explained, the bioadhesiveness of both PMVE-MA and L-cysteine may importantly contribute for the synergistic effects on the superior cellular interactions of the CPP nanocomplexes.[368,395]

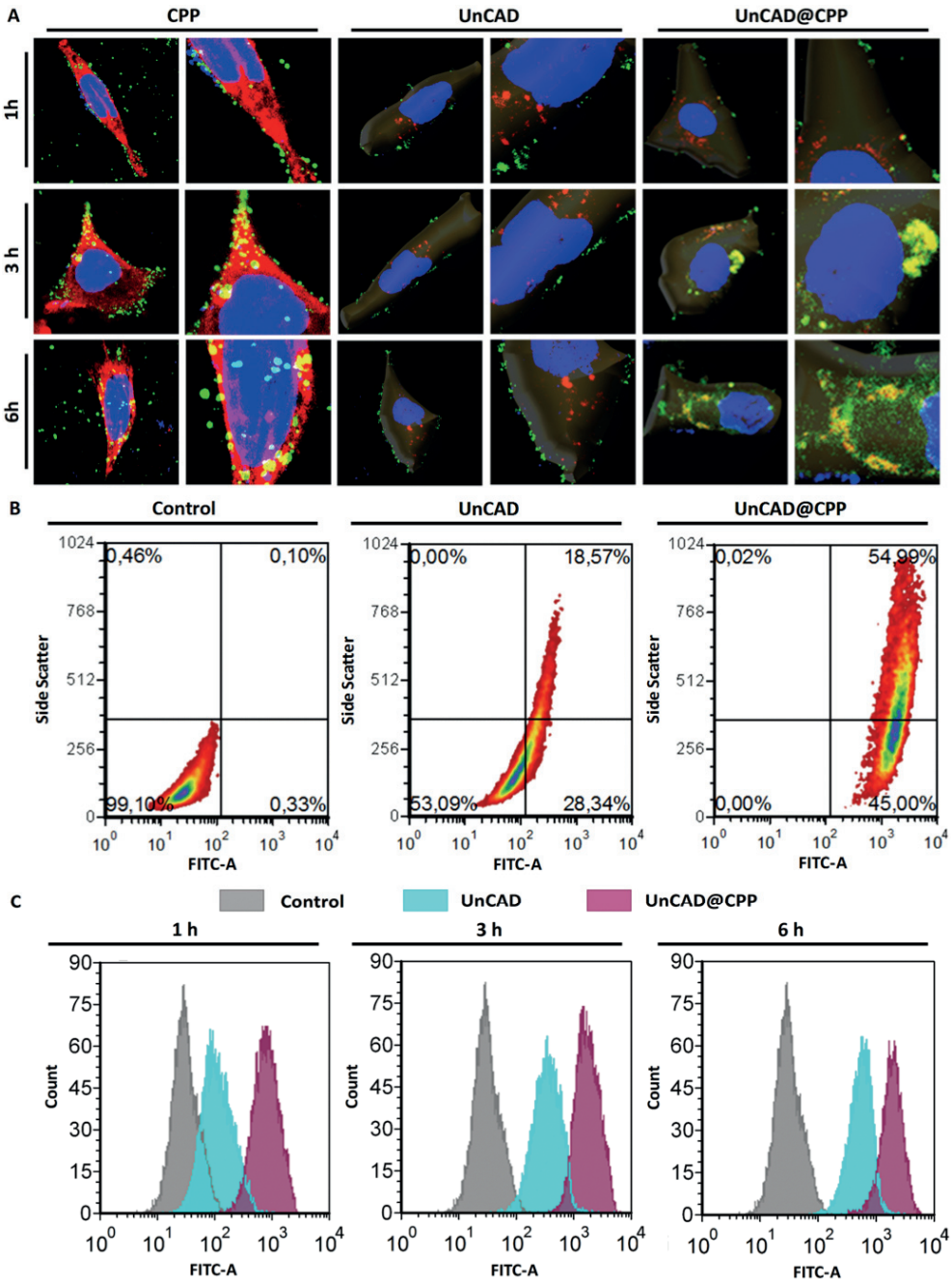

Figure 20. *Time dependent cellular association, internalization, and intracellular distribution of CPP, UnCAD and UnCAD@CPP nanoparticles. (A) Confocal fluorescence microscopy analysis of MDA-MB-231 breast cancer cells after incubation with CPP nanocomplexes at the concentration of 20 μg.mL^{-1}, and UnCAD and UnCAD@CPP*

nanocomposites at the concentration equivalent to 20 μg.mL^{-1} of UnTHCPSi for 1, 3 and 6 h at 37 ºC. Cells incubated with CPP were stained with CellMask™ Deep Red® and DAPI for their cell membrane and nucleus, presented in red and blue colours, respectively. FITC-labelled CPP nanocomplexes located at the cell surface are displayed in green colour, while the internalized counterparts are shown in yellow colour. The cells incubated with UnCAD and UnCAD@CPP were stained with LysoTracker® Red DND-99 and DAPI for their acidic compartments and the nucleus, and are presented in red and blue colours, respectively. The cystine of UnCAD was covalently conjugated to NHS-FITC, for fluorescently labelling both UnCAD and UnCAD@CPP nanoparticles. The nanocomposites interacting at the cell surface or located in the cytosol of the cells can be identified by the green colour, while the nanoparticles co-localized with the early endosomes and lysosomes are displayed in yellow colour. (B) Flow cytometry of the intracellular localization of the UnCAD and UnCAD@CPP nanocomposites in MDA-MB-231 breast cancer cells. The cells were incubated with the nanoparticles at the concentration equivalent to 10 μg.mL^{-1} of UnTHCPSi, for 3 h at 37 ºC. Cells incubated with HBSS buffer (pH 7.4) were used as controls. For labelling the nanoparticles, the amine groups of cystine in UnCAD were covalently conjugated to NHS-FITC. The increased SSC concurrent with enhanced FITC fluorescence intensity is representative of an increased intracellular granularity. (C) Flow cytometry of the time dependent cellular association of UnCAD and UnCAD@CPP nanoparticles with MDA-MB-231 breast cancer cells. The cells were exposed to the nanoparticles at the concentration equivalent to 20 μg.mL^{-1} of UnTHCPSi, for 1, 3 and 6 h at 37 ºC. Cells incubated with HBSS buffer (pH 7.4) + 10% FBS were used as controls. The cystine of UnCAD was covalently labelled with NHS-FITC fluorescent dye in both UnCAD and UnCAD@CPP nanocomposites. The percentage of cell−nanoparticles interactions was significantly higher after encapsulation of UnCAD into the CPP nanocomplexes, in a time-dependent manner. The results presented are representative of three independent experiments. Copyright © (2017) Elsevier B.V. Adapted and reprinted with permission from ref.[392].

In addition, as supportive evidence of the performance of CPP nanocomplexes to deliver the encapsulated bioresponsive UnCAD into the cells, the intracellular granularity of MDA-MB-231 breast cancer cells was measured by side scatter (SSC) flow cytometry, after 3 h of exposure to fluorescently labelled UnCAD and UnCAD@CPP nanocomposites (**Figure 20B**). The performance of this experiment correlated the intracellular granularity and cellular uptake depending on the nanoparticle type, size, and the cytosolic dispersity and aggregation.[396-398] Therefore, this approach could not be considered as conclusive for all types of nanoparticulate systems, with preliminary experimental data needed for discerning the suitability of SSC analysis for investigating the cellular internalization of nanoparticles. The SSC patterns displayed in **Figure 20B** showed a significant increase in the percentage of cells with high SSC, from 18.6% to 55.0%, after encapsulation of the formulation of UnCAD nanoparticles into UnCAD@CPP nanocomposites. The observed high localization of UnCAD nanoparticles within the intracellular compartments could be considered as an important aspect for the design and development of novel advanced multifunctional nanosystems with the capability of favourably localizing inside the cells, while

simultaneously incorporating different drug molecules, imaging agents, and/or biomacromolecules for multiple theranostic purposes.

The time-dependent association, internalization and cytosolic localization of the UnCAD nanoparticles was assessed by flow cytometry before and after encapsulation within the CPP nanocomplexes. In this experiment, MDA-MB-231 cells were incubated with fluorescently labelled UnCAD and UnCAD@CPP nanoparticles at the concentration equivalent to 20 $mg.mL^{-1}$ for 1, 3 and 6 h at 37 ºC (**Figure 20C**). The results evidenced different time-dependencies on the cellular associations of the UnCAD and UnCAD@CPP nanocomplexes. While the percentage of cells interacting with bare UnCAD nanoparticles was increased from 37 ± 6% in 1 h to 98 ± 1% after 6 h, the encapsulation within the CPP nanocomplexes resulted in over 99% of the cells being associated with the nanocomposites immediately within 1 h of exposure. Moreover, when comparing the fluorescence intensity of the cells exposed to UnCAD and UnCAD@CPP nanocomposites, after each individual incubation timepoint, it was possible to infer that the cellular interaction was significantly augmented after the loading of UnCAD nanoparticles into the CPP nanocomplexes. Despite the value of this data for understanding the impact of formulating UnCAD into UnCAD@CPP nanocomposites, it did not provide comparative information about the amount of nanoparticulate systems interacting per cell. Therefore, the MFI of the samples was compared for each time point (data not shown), showing that the amount of FITC-labelled UnCAD nanoparticles interacting with the cancer cells was 9.0 ± 0.6, 3.6 ± 0.1 and 3.3 ± 0.1 fold higher after 1, 3 and 6 h, respectively, when encapsulated into the CPP nanocomplexes.

Nevertheless, the findings obtained from the flow cytometry experiments did not still clarify the localization of the UnCAD nanoparticles within the cell, *i.e.*, whether the enhanced fluorescent signal had its origin from the nanoparticles located outside of the cellular membrane, inside the acidic compartments or in the cytosol of the cells. Therefore, confocal fluorescence microscopy was used for scrutinizing the intracellular trafficking of the UnCAD nanoparticles over time, and to further comprehend the impact of the CPP shell on their cellular penetration and endosomal escape (**Figure 20A**). The merged and magnified images corresponding to UnCAD nanoparticles showed that these nanocarriers remained extensively associated with the outer side of the cell membrane of MDA-MB-231 cells, without considerable cellular uptake occurring even after 6 h of incubation, thus indicating that the augmented fluorescence signal detected for the UnCAD nanoparticles in the flow cytometry tests originated from cell−particle interactions at the cell membrane. In contrast, the UnCAD@CPP nanocomposites showed internalization by the cancer cells within 3 h of exposure. Interestingly, the UnCAD nanoparticles encapsulated within the CPP nanocomplexes were mainly localized inside the endosomal compartments and moderately spotted in the cytoplasms of the cells, as evidenced by the yellow and green colours, respectively, in the related merged and magnified panels in the **Figure 20A**. After 6 h, the CPP shell of the UnCAD@CPP nanocomposites demonstrated to efficiently breach the membrane of the acidic organelles in which they were confined, owing to the cationic amine groups of the hyperbranched PEI and consequent "proton-sponge" effect,[168,399,400] resulting in the release the encapsulated UnCAD nanoparticles in the cytoplasm of the cells.

In summary, these finding allowed to conclude that the remarkably improved cellular uptake and cytosolic delivery of the developed nanocomposites stemmed from the synergistic role of the functional polymers used in the CPP formulation, namely the cell membrane binding affinity and intrinsic endosomolytic properties of PEI, as well as the bioadhesiveness of L-cysteine and PMVE-MA. Considering the GSH responsiveness of these nanocarriers, the higher GSH concentration in reducing intracellular compartments of tumour tissues compared to the extracellular environment,[401,402] as well as the endosomal breaching effect of the CPP nanocomplex shell, it was demonstrated that different chemotherapeutic agents can be efficiently delivered to the cytosol of cancer cells when simultaneously formulated into the developed multifunctional nanocomposites.

6 Summary and conclusions

In this dissertation, multifunctional PSi-based nanocomposites were designed, developed, characterised and investigated *in vitro* for their biological performance at the cellular level. The main aim of this work was to circumvent some of the deadlocks of PSi nanoparticles. including colloidal and plasma instabilities, poor cell-targeting efficiency, limited cellular association, internalization and intracellular trafficking, as well as premature and uncontrolled release of the therapeutic agents, which overall still defy the successful application of these nanoplatforms in cancer nanomedicine.

In the first study, taking advantage of the surface stabilizing properties and CD44 targeting specificity of HA, an amine-modified HA derivative was synthesised and covalently conjugated to the surface of UnTHCPSi nanoparticles. The HA biofunctionalization of the PSi nanoparticles was demonstrated to considerably improve the colloidal and plasma stability, and to remarkably enhance the cellular interaction and uptake by breast cancer cells. Importantly, the developed HA-modified PSi nanoplatforms showed a significantly higher affinity to CD44 overexpressing cancer cells, thus providing a clear evidence of the capacity to target these cells by a CD44 receptor mediated mechanism.

The second study reported the development of a bilayered zwitterionic PSi nanocomposite with high potential for intracellular drug delivery, by successively conjugating PEI and PMVE-MA polymers onto the surface of UnTHCPSi nanoparticles. In addition to a satisfactory cytocompatibility profile, the polymer-modified PSi nanoparticles showed augmented non-specific cellular association and internalization in the breast cancer cells, owing to the biocompatibility and bioadhesivevess of PMVE-MA, as well as improved intracellular trafficking. Moreover, the polymeric modification of the PSi nanoparticles contributed to increased loading of the anticancer agent MTX, as a consequence of drug confinement within the polymeric network, and sustained release, ultimately resulting in a potent *in vitro* antiproliferative effect in breast cancer cells.

In the third study, a novel PSi-based multifunctional nanocomposite was engineered by encapsulating both UnTHCPSi and Au nanoparticles into a self-assembling polymeric nanocomplex. This nanoencapsulation strategy not only rendered the PSi nanoparticles with superior cytocompatibility, but significantly enhanced the cellular association and endocytosis in breast cancer cells. Furthermore, the developed nanocomposites exhibited a remarkable endosomolytic effect, enabling the cytoplasmic delivery of the encapsulated PSi nanoparticles. In addition, the efficient loading of the chemotherapeutic drug SFB within the pores of the encapsulated PSi nanocarriers resulted in a dramatic increase of the drug's aqueous dissolution. Ultimately, the SFB-loaded nanosystems prevented the *in vitro* proliferation of breast cancer cells at very low SFB inhibitory concentrations, thus providing a robust evidence of the great promise of these multifunctional nanoplatforms for the intracellular delivery of chemotherapeutics.

In the fourth study, the aforementioned nanocomplexes were used to carry DNA-anchored UnTHCPSi nanoparticles, as an innovative strategy to fabricate a bioresponsive multifunctional PSi-based nanoplatform, envisioned for multidrug delivery or theranostic purposes. The potential of the engineered nanocomposites stems from both the versatility to load a vast combination of nanoparticulate systems, hydrophilic and hydrophobic drug

molecules, as well as fluorescent dyes within the nanostructure, and from the capability to efficiently deliver the encapsulated drug-loaded nanoparticles into the cytoplasms of the cells, which in turn bioresponsively release the therapeutic cargo in a controlled manner.

In conclusion, the multifunctional PSi-based nanocomposites engineered and evaluated here *in vitro* have proven to circumvent some of the drawbacks inherent to PSi nanoparticles and hold great promise for cancer targeting, (multi)drug delivery, and theranostic applications. However, in spite of providing important insights on the interactions of the developed nanoparticulate systems at the cellular level, the *in vitro* models used lack the complexity of biological barriers and tumour tissues. Therefore, the full realization of the potential of these nanomedicines critically depends on the future evaluation of their performance in more complex systems that closely mimic the *in vivo* scenario of human tumours, such as three-dimensional tumour-like spheroids, recently conceptualized "organ-on-a-chip" systems, or, preferentially, pre-clinical tumour animal models. In addition, from the nanotechnological perspective, it would be extremely exciting and challenging to design and engineer a more advanced multifunctional nanoplatform integrating the individual attractive features of each of the developed nanocomposites, including superior biocompatibility, high stability, active targeting capability, controllable/bioresponsive drug release and potential for cancer combined therapeutics and/or theranostics. Regardless of these future prospects, this dissertation introduces innovative strategies and, overall, represents an advanced and novel contribution for the envisioned future implementation of PSi nanoparticles as the next generation of cancer nanomedicines.

References

1. Ferlay J, Soerjomataram I, Dikshit R, et al. Cancer incidence and mortality worldwide: sources, methods and major patterns in GLOBOCAN 2012. Int J Cancer 2015;136:E359-86.
2. Hanahan D, Weinberg RA. Hallmarks of cancer: the next generation. Cell 2011;144:646-74.
3. Edwards BK, Noone AM, Mariotto AB, et al. Annual Report to the Nation on the status of cancer, 1975-2010, featuring prevalence of comorbidity and impact on survival among persons with lung, colorectal, breast, or prostate cancer. Cancer 2014;120:1290-314.
4. Gillet JP, Gottesman MM. Mechanisms of multidrug resistance in cancer. Methods Mol Biol 2010;596:47-76.
5. Housman G, Byler S, Heerboth S, et al. Drug resistance in cancer: an overview. Cancers (Basel) 2014;6:1769-92.
6. Creixell M, Peppas NA. Co-delivery of siRNA and therapeutic agents using nanocarriers to overcome cancer resistance. Nano Today 2012;7:367-79.
7. Ohyanagi F, Yanagitani N, Kudo K, et al. Phase II study of docetaxel-plus-bevacizumab combination therapy in patients previously treated for advanced non-squamous non-small cell lung cancer. Anticancer Res 2014;34:5153-8.
8. Stegemann S, Leveiller F, Franchi D, de Jong H, Linden H. When poor solubility becomes an issue: from early stage to proof of concept. Eur J Pharm Sci 2007;31:249-61.
9. Owen SC, Doak AK, Wassam P, Shoichet MS, Shoichet BK. Colloidal aggregation affects the efficacy of anticancer drugs in cell culture. ACS Chem Biol 2012;7:1429-35.
10. Torchilin VP, Lukyanov AN. Peptide and protein drug delivery to and into tumors: challenges and solutions. Drug Discov Today 2003;8:259-66.
11. Ferrari M. Cancer nanotechnology: opportunities and challenges. Nat Rev Cancer 2005;5:161-71.
12. Peer D, Karp JM, Hong S, Farokhzad OC, Margalit R, Langer R. Nanocarriers as an emerging platform for cancer therapy. Nat Nanotechnol 2007;2:751-60.
13. Sun T, Zhang YS, Pang B, Hyun DC, Yang M, Xia Y. Engineered nanoparticles for drug delivery in cancer therapy. Angew Chem Int Ed Engl 2014;53:12320-64.
14. Shi J, Kantoff PW, Wooster R, Farokhzad OC. Cancer nanomedicine: progress, challenges and opportunities. Nat Rev Cancer 2017;17:20-37.
15. Wang R, Billone PS, Mullett WM. Nanomedicine in Action: An Overview of Cancer Nanomedicine on the Market and in Clinical Trials. Journal of Nanomaterials 2013;2013:12.
16. Salonen J, Kaukonen AM, Hirvonen J, Lehto VP. Mesoporous silicon in drug delivery applications. J Pharm Sci 2008;97:632-53.
17. Haidary SM, Córcoles EP, Ali NK. Nanoporous Silicon as Drug Delivery Systems for Cancer Therapies. Journal of Nanomaterials 2012;2012:15.
18. Shahbazi MA, Herranz B, Santos HA. Nanostructured porous Si-based nanoparticles for targeted drug delivery. Biomatter 2012;2:296-312.

19. Santos HA, Mäkila E, Airaksinen AJ, Bimbo LM, Hirvonen J. Porous silicon nanoparticles for nanomedicine: preparation and biomedical applications. Nanomedicine (Lond) 2014;9:535-54.
20. Canham LT. Handbook of porous silicon: Springer; 2014.
21. Santos HA. Porous silicon for biomedical applications: Elsevier; 2014.
22. Bimbo LM, Sarparanta M, Santos HA, et al. Biocompatibility of thermally hydrocarbonized porous silicon nanoparticles and their biodistribution in rats. ACS Nano 2010;4:3023-32.
23. Shabir Q. Biodegradability of Porous Silicon. In: Canham L, ed. Handbook of Porous Silicon. Cham: Springer International Publishing; 2014:395-401.
24. Shahbazi MA, Hamidi M, Mäkila EM, et al. The mechanisms of surface chemistry effects of mesoporous silicon nanoparticles on immunotoxicity and biocompatibility. Biomaterials 2013;34:7776-89.
25. Barnes TJ, Jarvis KL, Prestidge CA. Recent advances in porous silicon technology for drug delivery. Ther Deliv 2013;4:811-23.
26. Alhmoud H, Delalat B, Elnathan R, et al. Porous Silicon Nanodiscs for Targeted Drug Delivery. Advanced Functional Materials 2015;25:1137-45.
27. Bimbo LM, Makila E, Raula J, et al. Functional hydrophobin-coating of thermally hydrocarbonized porous silicon microparticles. Biomaterials 2011;32:9089-99.
28. Jarvis KL, Barnes TJ, Prestidge CA. Surface chemistry of porous silicon and implications for drug encapsulation and delivery applications. Adv Colloid Interface Sci 2012;175:25-38.
29. Santos HA, Bimbo LM, Lehto VP, Airaksinen AJ, Salonen J, Hirvonen J. Multifunctional porous silicon for therapeutic drug delivery and imaging. Curr Drug Discov Technol 2011;8:228-49.
30. Yokoi K, Godin B, Oborn CJ, et al. Porous silicon nanocarriers for dual targeting tumor associated endothelial cells and macrophages in stroma of orthotopic human pancreatic cancers. Cancer Lett 2013;334:319-27.
31. Chou LY, Ming K, Chan WC. Strategies for the intracellular delivery of nanoparticles. Chem Soc Rev 2011;40:233-45.
32. Barenholz Y. Doxil(R)--the first FDA-approved nano-drug: lessons learned. J Control Release 2012;160:117-34.
33. Allen TM, Cullis PR. Drug delivery systems: entering the mainstream. Science 2004;303:1818-22.
34. Allen TM, Cullis PR. Liposomal drug delivery systems: from concept to clinical applications. Adv Drug Deliv Rev 2013;65:36-48.
35. Petersen GH, Alzghari SK, Chee W, Sankari SS, La-Beck NM. Meta-analysis of clinical and preclinical studies comparing the anticancer efficacy of liposomal versus conventional non-liposomal doxorubicin. J Control Release 2016;232:255-64.
36. Gabizon A, Catane R, Uziely B, et al. Prolonged circulation time and enhanced accumulation in malignant exudates of doxorubicin encapsulated in polyethylene-glycol coated liposomes. Cancer Res 1994;54:987-92.

37. Lyass O, Uziely B, Ben-Yosef R, et al. Correlation of toxicity with pharmacokinetics of pegylated liposomal doxorubicin (Doxil) in metastatic breast carcinoma. Cancer 2000;89:1037-47.
38. Gabizon AA. Pegylated liposomal doxorubicin: metamorphosis of an old drug into a new form of chemotherapy. Cancer Invest 2001;19:424-36.
39. Gabizon A, Shmeeda H, Barenholz Y. Pharmacokinetics of pegylated liposomal Doxorubicin: review of animal and human studies. Clin Pharmacokinet 2003;42:419-36.
40. Gradishar WJ, Tjulandin S, Davidson N, et al. Phase III trial of nanoparticle albumin-bound paclitaxel compared with polyethylated castor oil-based paclitaxel in women with breast cancer. J Clin Oncol 2005;23:7794-803.
41. Hawkins MJ, Soon-Shiong P, Desai N. Protein nanoparticles as drug carriers in clinical medicine. Adv Drug Deliv Rev 2008;60:876-85.
42. Guarneri V, Dieci MV, Conte P. Enhancing intracellular taxane delivery: current role and perspectives of nanoparticle albumin-bound paclitaxel in the treatment of advanced breast cancer. Expert Opin Pharmacother 2012;13:395-406.
43. Couvreur P. Nanoparticles in drug delivery: past, present and future. Adv Drug Deliv Rev 2013;65:21-3.
44. Ahn HK, Jung M, Sym SJ, et al. A phase II trial of Cremorphor EL-free paclitaxel (Genexol-PM) and gemcitabine in patients with advanced non-small cell lung cancer. Cancer Chemother Pharmacol 2014;74:277-82.
45. Kato K, Chin K, Yoshikawa T, et al. Phase II study of NK105, a paclitaxel-incorporating micellar nanoparticle, for previously treated advanced or recurrent gastric cancer. Invest New Drugs 2012;30:1621-7.
46. Clark AJ, Wiley DT, Zuckerman JE, et al. CRLX101 nanoparticles localize in human tumors and not in adjacent, nonneoplastic tissue after intravenous dosing. Proc Natl Acad Sci U S A 2016;113:3850-4.
47. Hrkach J, Von Hoff D, Mukkaram Ali M, et al. Preclinical development and clinical translation of a PSMA-targeted docetaxel nanoparticle with a differentiated pharmacological profile. Sci Transl Med 2012;4:128ra39.
48. Avramis VI, Tiwari PN. Asparaginase (native ASNase or pegylated ASNase) in the treatment of acute lymphoblastic leukemia. Int J Nanomedicine 2006;1:241-54.
49. Elazar V, Adwan H, Bauerle T, Rohekar K, Golomb G, Berger MR. Sustained delivery and efficacy of polymeric nanoparticles containing osteopontin and bone sialoprotein antisenses in rats with breast cancer bone metastasis. Int J Cancer 2010;126:1749-60.
50. Tolcher AW, Rodrigueza WV, Rasco DW, et al. A phase 1 study of the BCL2-targeted deoxyribonucleic acid inhibitor (DNAi) PNT2258 in patients with advanced solid tumors. Cancer Chemother Pharmacol 2014;73:363-71.
51. Gordon EM, Hall FL. Rexin-G, a targeted genetic medicine for cancer. Expert Opin Biol Ther 2010;10:819-32.
52. Davis ME, Zuckerman JE, Choi CH, et al. Evidence of RNAi in humans from systemically administered siRNA via targeted nanoparticles. Nature 2010;464:1067-70.

53. Schultheis B, Strumberg D, Santel A, et al. First-in-human phase I study of the liposomal RNA interference therapeutic Atu027 in patients with advanced solid tumors. J Clin Oncol 2014;32:4141-8.
54. Maier-Hauff K, Ulrich F, Nestler D, et al. Efficacy and safety of intratumoral thermotherapy using magnetic iron-oxide nanoparticles combined with external beam radiotherapy on patients with recurrent glioblastoma multiforme. J Neurooncol 2011;103:317-24.
55. Wang YX, Hussain SM, Krestin GP. Superparamagnetic iron oxide contrast agents: physicochemical characteristics and applications in MR imaging. Eur Radiol 2001;11:2319-31.
56. Hirsch LR, Stafford RJ, Bankson JA, et al. Nanoshell-mediated near-infrared thermal therapy of tumors under magnetic resonance guidance. Proc Natl Acad Sci U S A 2003;100:13549-54.
57. Maggiorella L, Barouch G, Devaux C, et al. Nanoscale radiotherapy with hafnium oxide nanoparticles. Future Oncol 2012;8:1167-81.
58. Garbuzenko OB, Saad M, Pozharov VP, Reuhl KR, Mainelis G, Minko T. Inhibition of lung tumor growth by complex pulmonary delivery of drugs with oligonucleotides as suppressors of cellular resistance. Proc Natl Acad Sci U S A 2010;107:10737-42.
59. Liechty WB, Caldorera-Moore M, Phillips MA, Schoener C, Peppas NA. Advanced molecular design of biopolymers for transmucosal and intracellular delivery of chemotherapeutic agents and biological therapeutics. J Control Release 2011;155:119-27.
60. Yu M, Wu J, Shi J, Farokhzad OC. Nanotechnology for protein delivery: Overview and perspectives. J Control Release 2016;240:24-37.
61. Matsumura Y, Maeda H. A new concept for macromolecular therapeutics in cancer chemotherapy: mechanism of tumoritropic accumulation of proteins and the antitumor agent smancs. Cancer Res 1986;46:6387-92.
62. Gerlowski LE, Jain RK. Microvascular permeability of normal and neoplastic tissues. Microvasc Res 1986;31:288-305.
63. Bertrand N, Wu J, Xu X, Kamaly N, Farokhzad OC. Cancer nanotechnology: the impact of passive and active targeting in the era of modern cancer biology. Adv Drug Deliv Rev 2014;66:2-25.
64. Maeda H. Toward a full understanding of the EPR effect in primary and metastatic tumors as well as issues related to its heterogeneity. Adv Drug Deliv Rev 2015;91:3-6.
65. Cedervall T, Lynch I, Lindman S, et al. Understanding the nanoparticle-protein corona using methods to quantify exchange rates and affinities of proteins for nanoparticles. Proc Natl Acad Sci U S A 2007;104:2050-5.
66. Nel AE, Madler L, Velegol D, et al. Understanding biophysicochemical interactions at the nano-bio interface. Nat Mater 2009;8:543-57.
67. Mahmoudi M, Lynch I, Ejtehadi MR, Monopoli MP, Bombelli FB, Laurent S. Protein-nanoparticle interactions: opportunities and challenges. Chem Rev 2011;111:5610-37.
68. Monopoli MP, Aberg C, Salvati A, Dawson KA. Biomolecular coronas provide the biological identity of nanosized materials. Nat Nanotechnol 2012;7:779-86.

69. Wolfram J, Yang Y, Shen J, et al. The nano-plasma interface: Implications of the protein corona. Colloids Surf B Biointerfaces 2014;124:17-24.
70. Walkey CD, Chan WC. Understanding and controlling the interaction of nanomaterials with proteins in a physiological environment. Chem Soc Rev 2012;41:2780-99.
71. Lundqvist M, Stigler J, Elia G, Lynch I, Cedervall T, Dawson KA. Nanoparticle size and surface properties determine the protein corona with possible implications for biological impacts. Proc Natl Acad Sci U S A 2008;105:14265-70.
72. Casals E, Pfaller T, Duschl A, Oostingh GJ, Puntes V. Time evolution of the nanoparticle protein corona. ACS Nano 2010;4:3623-32.
73. Bregoli L, Movia D, Gavigan-Imedio JD, Lysaght J, Reynolds J, Prina-Mello A. Nanomedicine applied to translational oncology: A future perspective on cancer treatment. Nanomedicine 2016;12:81-103.
74. Frank MM, Fries LF. The role of complement in inflammation and phagocytosis. Immunol Today 1991;12:322-6.
75. Owens DE, 3rd, Peppas NA. Opsonization, biodistribution, and pharmacokinetics of polymeric nanoparticles. Int J Pharm 2006;307:93-102.
76. Walkey CD, Olsen JB, Guo H, Emili A, Chan WC. Nanoparticle size and surface chemistry determine serum protein adsorption and macrophage uptake. J Am Chem Soc 2012;134:2139-47.
77. Ritz S, Schottler S, Kotman N, et al. Protein corona of nanoparticles: distinct proteins regulate the cellular uptake. Biomacromolecules 2015;16:1311-21.
78. Ogawara K, Furumoto K, Nagayama S, et al. Pre-coating with serum albumin reduces receptor-mediated hepatic disposition of polystyrene nanosphere: implications for rational design of nanoparticles. J Control Release 2004;100:451-5.
79. Lesniak A, Fenaroli F, Monopoli MP, Aberg C, Dawson KA, Salvati A. Effects of the presence or absence of a protein corona on silica nanoparticle uptake and impact on cells. ACS Nano 2012;6:5845-57.
80. Lesniak A, Salvati A, Santos-Martinez MJ, Radomski MW, Dawson KA, Aberg C. Nanoparticle adhesion to the cell membrane and its effect on nanoparticle uptake efficiency. J Am Chem Soc 2013;135:1438-44.
81. Byrne JD, Betancourt T, Brannon-Peppas L. Active targeting schemes for nanoparticle systems in cancer therapeutics. Adv Drug Deliv Rev 2008;60:1615-26.
82. Salvati A, Pitek AS, Monopoli MP, et al. Transferrin-functionalized nanoparticles lose their targeting capabilities when a biomolecule corona adsorbs on the surface. Nat Nanotechnol 2013;8:137-43.
83. Dong Y, Love KT, Dorkin JR, et al. Lipopeptide nanoparticles for potent and selective siRNA delivery in rodents and nonhuman primates. Proc Natl Acad Sci U S A 2014;111:3955-60.
84. Schaffler M, Sousa F, Wenk A, et al. Blood protein coating of gold nanoparticles as potential tool for organ targeting. Biomaterials 2014;35:3455-66.
85. Chen N, Li Y, Ye Y, Palmisano M, Chopra R, Zhou S. Pharmacokinetics and pharmacodynamics of nab-paclitaxel in patients with solid tumors: disposition kinetics and pharmacology distinct from solvent-based paclitaxel. J Clin Pharmacol 2014;54:1097-107.

86. Nie S. Understanding and overcoming major barriers in cancer nanomedicine. Nanomedicine (Lond) 2010;5:523-8.
87. Zamboni WC, Torchilin V, Patri AK, et al. Best practices in cancer nanotechnology: perspective from NCI nanotechnology alliance. Clin Cancer Res 2012;18:3229-41.
88. Longmire M, Choyke PL, Kobayashi H. Clearance properties of nano-sized particles and molecules as imaging agents: considerations and caveats. Nanomedicine (Lond) 2008;3:703-17.
89. Choi HS, Liu W, Misra P, et al. Renal clearance of quantum dots. Nat Biotechnol 2007;25:1165-70.
90. Tsoi KM, MacParland SA, Ma XZ, et al. Mechanism of hard-nanomaterial clearance by the liver. Nat Mater 2016;15:1212-21.
91. Tenzer S, Docter D, Kuharev J, et al. Rapid formation of plasma protein corona critically affects nanoparticle pathophysiology. Nat Nanotechnol 2013;8:772-81.
92. Wang H, Wu L, Reinhard BM. Scavenger receptor mediated endocytosis of silver nanoparticles into J774A.1 macrophages is heterogeneous. ACS Nano 2012;6:7122-32.
93. Qie Y, Yuan H, von Roemeling CA, et al. Surface modification of nanoparticles enables selective evasion of phagocytic clearance by distinct macrophage phenotypes. Sci Rep 2016;6:26269.
94. Ballou B, Ernst LA, Andreko S, et al. Sentinel lymph node imaging using quantum dots in mouse tumor models. Bioconjug Chem 2007;18:389-96.
95. Moghimi SM, Hunter AC, Murray JC. Long-circulating and target-specific nanoparticles: theory to practice. Pharmacol Rev 2001;53:283-318.
96. Deen WM, Lazzara MJ, Myers BD. Structural determinants of glomerular permeability. Am J Physiol Renal Physiol 2001;281:F579-96.
97. Kettiger H, Schipanski A, Wick P, Huwyler J. Engineered nanomaterial uptake and tissue distribution: from cell to organism. Int J Nanomedicine 2013;8:3255-69.
98. Duan X, Li Y. Physicochemical characteristics of nanoparticles affect circulation, biodistribution, cellular internalization, and trafficking. Small 2013;9:1521-32.
99. Zhou C, Long M, Qin Y, Sun X, Zheng J. Luminescent gold nanoparticles with efficient renal clearance. Angew Chem Int Ed Engl 2011;50:3168-72.
100. Harris JM, Chess RB. Effect of pegylation on pharmaceuticals. Nat Rev Drug Discov 2003;2:214-21.
101. Kamaly N, Xiao Z, Valencia PM, Radovic-Moreno AF, Farokhzad OC. Targeted polymeric therapeutic nanoparticles: design, development and clinical translation. Chem Soc Rev 2012;41:2971-3010.
102. Xia X, Yang M, Wang Y, et al. Quantifying the coverage density of poly(ethylene glycol) chains on the surface of gold nanostructures. ACS Nano 2012;6:512-22.
103. Rodriguez PL, Harada T, Christian DA, Pantano DA, Tsai RK, Discher DE. Minimal "Self" peptides that inhibit phagocytic clearance and enhance delivery of nanoparticles. Science 2013;339:971-5.
104. Takizawa H, Manz MG. Macrophage tolerance: CD47-SIRP-alpha-mediated signals matter. Nat Immunol 2007;8:1287-9.

105. Hu CM, Zhang L, Aryal S, Cheung C, Fang RH, Zhang L. Erythrocyte membrane-camouflaged polymeric nanoparticles as a biomimetic delivery platform. Proc Natl Acad Sci U S A 2011;108:10980-5.
106. Parodi A, Quattrocchi N, van de Ven AL, et al. Synthetic nanoparticles functionalized with biomimetic leukocyte membranes possess cell-like functions. Nat Nanotechnol 2013;8:61-8.
107. Hu CM, Fang RH, Wang KC, et al. Nanoparticle biointerfacing by platelet membrane cloaking. Nature 2015;526:118-21.
108. Hu Q, Sun W, Qian C, Wang C, Bomba HN, Gu Z. Anticancer Platelet-Mimicking Nanovehicles. Adv Mater 2015;27:7043-50.
109. Strebhardt K, Ullrich A. Paul Ehrlich's magic bullet concept: 100 years of progress. Nat Rev Cancer 2008;8:473-80.
110. Farokhzad OC, Langer R. Impact of nanotechnology on drug delivery. ACS Nano 2009;3:16-20.
111. Nicolas J, Mura S, Brambilla D, Mackiewicz N, Couvreur P. Design, functionalization strategies and biomedical applications of targeted biodegradable/biocompatible polymer-based nanocarriers for drug delivery. Chem Soc Rev 2013;42:1147-235.
112. Maeda H, Nakamura H, Fang J. The EPR effect for macromolecular drug delivery to solid tumors: Improvement of tumor uptake, lowering of systemic toxicity, and distinct tumor imaging in vivo. Adv Drug Deliv Rev 2013;65:71-9.
113. Bergers G, Benjamin LE. Tumorigenesis and the angiogenic switch. Nat Rev Cancer 2003;3:401-10.
114. McDonald DM, Foss AJ. Endothelial cells of tumor vessels: abnormal but not absent. Cancer Metastasis Rev 2000;19:109-20.
115. Baban DF, Seymour LW. Control of tumour vascular permeability. Adv Drug Deliv Rev 1998;34:109-19.
116. Haley B, Frenkel E. Nanoparticles for drug delivery in cancer treatment. Urol Oncol 2008;26:57-64.
117. Jain RK, Stylianopoulos T. Delivering nanomedicine to solid tumors. Nat Rev Clin Oncol 2010;7:653-64.
118. Hashizume H, Baluk P, Morikawa S, et al. Openings between defective endothelial cells explain tumor vessel leakiness. Am J Pathol 2000;156:1363-80.
119. Jin-Wook Y, Elizabeth C, Samir M. Factors that Control the Circulation Time of Nanoparticles in Blood: Challenges, Solutions and Future Prospects. Current Pharmaceutical Design 2010;16:2298-307.
120. Padera TP, Stoll BR, Tooredman JB, Capen D, di Tomaso E, Jain RK. Pathology: cancer cells compress intratumour vessels. Nature 2004;427:695.
121. Heldin CH, Rubin K, Pietras K, Ostman A. High interstitial fluid pressure - an obstacle in cancer therapy. Nat Rev Cancer 2004;4:806-13.
122. Jiang W, von Roemeling CA, Chen Y, et al. Designing nanomedicine for immuno-oncology. Nature Biomedical Engineering 2017;1:0029.
123. Dreher MR, Liu W, Michelich CR, Dewhirst MW, Yuan F, Chilkoti A. Tumor vascular permeability, accumulation, and penetration of macromolecular drug carriers. J Natl Cancer Inst 2006;98:335-44.

124. Sawant RR, Torchilin VP. Challenges in development of targeted liposomal therapeutics. AAPS J 2012;14:303-15.
125. Allen TM. Ligand-targeted therapeutics in anticancer therapy. Nat Rev Cancer 2002;2:750-63.
126. Shi J, Xiao Z, Kamaly N, Farokhzad OC. Self-assembled targeted nanoparticles: evolution of technologies and bench to bedside translation. Acc Chem Res 2011;44:1123-34.
127. Lammers T, Kiessling F, Hennink WE, Storm G. Drug targeting to tumors: principles, pitfalls and (pre-) clinical progress. J Control Release 2012;161:175-87.
128. Yu B, Tai HC, Xue W, Lee LJ, Lee RJ. Receptor-targeted nanocarriers for therapeutic delivery to cancer. Mol Membr Biol 2010;27:286-98.
129. Piktel E, Niemirowicz K, Watek M, Wollny T, Deptula P, Bucki R. Recent insights in nanotechnology-based drugs and formulations designed for effective anti-cancer therapy. J Nanobiotechnology 2016;14:39.
130. Ferreira M, Vingadas Almeida P, Shahbazi M-A, Correia A, Santos H. Chapter 5: Current Trends and Developments for Nanotechnology in Cancer2015.
131. Wang J, Byrne JD, Napier ME, DeSimone JM. More effective nanomedicines through particle design. Small 2011;7:1919-31.
132. Taurin S, Nehoff H, Greish K. Anticancer nanomedicine and tumor vascular permeability; Where is the missing link? J Control Release 2012;164:265-75.
133. Gratton SE, Ropp PA, Pohlhaus PD, et al. The effect of particle design on cellular internalization pathways. Proc Natl Acad Sci U S A 2008;105:11613-8.
134. Joyce JA. Therapeutic targeting of the tumor microenvironment. Cancer Cell 2005;7:513-20.
135. Arap W, Pasqualini R, Ruoslahti E. Cancer treatment by targeted drug delivery to tumor vasculature in a mouse model. Science 1998;279:377-80.
136. Sugahara KN, Teesalu T, Karmali PP, et al. Tissue-penetrating delivery of compounds and nanoparticles into tumors. Cancer Cell 2009;16:510-20.
137. Neri D, Bicknell R. Tumour vascular targeting. Nat Rev Cancer 2005;5:436-46.
138. Pasqualini R, Arap W, McDonald DM. Probing the structural and molecular diversity of tumor vasculature. Trends Mol Med 2002;8:563-71.
139. Ruoslahti E. Specialization of tumour vasculature. Nat Rev Cancer 2002;2:83-90.
140. Teesalu T, Sugahara KN, Kotamraju VR, Ruoslahti E. C-end rule peptides mediate neuropilin-1-dependent cell, vascular, and tissue penetration. Proc Natl Acad Sci U S A 2009;106:16157-62.
141. Ruoslahti E, Bhatia SN, Sailor MJ. Targeting of drugs and nanoparticles to tumors. J Cell Biol 2010;188:759-68.
142. Messerschmidt SK, Musyanovych A, Altvater M, et al. Targeted lipid-coated nanoparticles: delivery of tumor necrosis factor-functionalized particles to tumor cells. J Control Release 2009;137:69-77.
143. Weissleder R, Nahrendorf M, Pittet MJ. Imaging macrophages with nanoparticles. Nat Mater 2014;13:125-38.
144. Zhang B, Shen S, Liao Z, et al. Targeting fibronectins of glioma extracellular matrix by CLT1 peptide-conjugated nanoparticles. Biomaterials 2014;35:4088-98.

145. Kim H, Jeong H, Han S, et al. Hyaluronate and its derivatives for customized biomedical applications. Biomaterials 2017;123:155-71.
146. Dosio F, Arpicco S, Stella B, Fattal E. Hyaluronic acid for anticancer drug and nucleic acid delivery. Adv Drug Deliv Rev 2016;97:204-36.
147. Swierczewska M, Han HS, Kim K, Park JH, Lee S. Polysaccharide-based nanoparticles for theranostic nanomedicine. Adv Drug Deliv Rev 2016;99:70-84.
148. Mattheolabakis G, Milane L, Singh A, Amiji MM. Hyaluronic acid targeting of CD44 for cancer therapy: from receptor biology to nanomedicine. J Drug Target 2015;23:605-18.
149. Goodison S, Urquidi V, Tarin D. CD44 cell adhesion molecules. Molecular pathology : MP 1999;52:189-96.
150. Aruffo A, Stamenkovic I, Melnick M, Underhill CB, Seed B. CD44 is the principal cell surface receptor for hyaluronate. Cell 1990;61:1303-13.
151. Entwistle J, Hall CL, Turley EA. HA receptors: regulators of signalling to the cytoskeleton. Journal of cellular biochemistry 1996;61:569-77.
152. Toole BP. Hyaluronan: from extracellular glue to pericellular cue. Nat Rev Cancer 2004;4:528-39.
153. Girish KS, Kemparaju K. The magic glue hyaluronan and its eraser hyaluronidase: a biological overview. Life sciences 2007;80:1921-43.
154. Hiscox S, Baruha B, Smith C, et al. Overexpression of CD44 accompanies acquired tamoxifen resistance in MCF7 cells and augments their sensitivity to the stromal factors, heregulin and hyaluronan. BMC Cancer 2012;12:458.
155. Hiraga T, Ito S, Nakamura H. Cancer stem-like cell marker CD44 promotes bone metastases by enhancing tumorigenicity, cell motility, and hyaluronan production. Cancer Res 2013;73:4112-22.
156. Birch M, Mitchell S, Hart IR. Isolation and characterization of human melanoma cell variants expressing high and low levels of CD44. Cancer Res 1991;51:6660-7.
157. Sy MS, Guo YJ, Stamenkovic I. Distinct effects of two CD44 isoforms on tumor growth in vivo. The Journal of experimental medicine 1991;174:859-66.
158. Conner SD, Schmid SL. Regulated portals of entry into the cell. Nature 2003;422:37-44.
159. Canton I, Battaglia G. Endocytosis at the nanoscale. Chem Soc Rev 2012;41:2718-39.
160. Sahay G, Alakhova DY, Kabanov AV. Endocytosis of nanomedicines. J Control Release 2010;145:182-95.
161. Mousavi SA, Malerod L, Berg T, Kjeken R. Clathrin-dependent endocytosis. Biochem J 2004;377:1-16.
162. Bareford LM, Swaan PW. Endocytic mechanisms for targeted drug delivery. Adv Drug Deliv Rev 2007;59:748-58.
163. Verma A, Stellacci F. Effect of surface properties on nanoparticle-cell interactions. Small 2010;6:12-21.
164. Herd H, Daum N, Jones AT, Huwer H, Ghandehari H, Lehr CM. Nanoparticle geometry and surface orientation influence mode of cellular uptake. ACS Nano 2013;7:1961-73.
165. Huang C, Zhang Y, Yuan H, Gao H, Zhang S. Role of nanoparticle geometry in endocytosis: laying down to stand up. Nano Lett 2013;13:4546-50.

166. Petros RA, DeSimone JM. Strategies in the design of nanoparticles for therapeutic applications. Nat Rev Drug Discov 2010;9:615-27.
167. Stuart LM, Ezekowitz RA. Phagocytosis: elegant complexity. Immunity 2005;22:539-50.
168. Varkouhi AK, Scholte M, Storm G, Haisma HJ. Endosomal escape pathways for delivery of biologicals. J Control Release 2011;151:220-8.
169. Boussif O, Lezoualc'h F, Zanta MA, et al. A versatile vector for gene and oligonucleotide transfer into cells in culture and in vivo: polyethylenimine. Proc Natl Acad Sci U S A 1995;92:7297-301.
170. Jager M, Schubert S, Ochrimenko S, Fischer D, Schubert US. Branched and linear poly(ethylene imine)-based conjugates: synthetic modification, characterization, and application. Chem Soc Rev 2012;41:4755-67.
171. Neuberg P, Kichler A. Recent developments in nucleic acid delivery with polyethylenimines. Adv Genet 2014;88:263-88.
172. Lin C, Zhong Z, Lok MC, et al. Novel bioreducible poly(amido amine)s for highly efficient gene delivery. Bioconjug Chem 2007;18:138-45.
173. Lin C, Blaauboer CJ, Timoneda MM, et al. Bioreducible poly(amido amine)s with oligoamine side chains: synthesis, characterization, and structural effects on gene delivery. J Control Release 2008;126:166-74.
174. Mateos-Timoneda MA, Lok MC, Hennink WE, Feijen J, Engbersen JF. Poly(amido amine)s as gene delivery vectors: effects of quaternary nicotinamide moieties in the side chains. ChemMedChem 2008;3:478-86.
175. Patil ML, Zhang M, Taratula O, Garbuzenko OB, He H, Minko T. Internally cationic polyamidoamine PAMAM-OH dendrimers for siRNA delivery: effect of the degree of quaternization and cancer targeting. Biomacromolecules 2009;10:258-66.
176. Midoux P, Monsigny M. Efficient gene transfer by histidylated polylysine/pDNA complexes. Bioconjug Chem 1999;10:406-11.
177. Li Y, Wang J, Wientjes MG, Au JL. Delivery of nanomedicines to extracellular and intracellular compartments of a solid tumor. Adv Drug Deliv Rev 2012;64:29-39.
178. Pack DW, Hoffman AS, Pun S, Stayton PS. Design and development of polymers for gene delivery. Nat Rev Drug Discov 2005;4:581-93.
179. Moghimi SM, Symonds P, Murray JC, Hunter AC, Debska G, Szewczyk A. A two-stage poly(ethylenimine)-mediated cytotoxicity: implications for gene transfer/therapy. Mol Ther 2005;11:990-5.
180. Beyerle A, Irmler M, Beckers J, Kissel T, Stoeger T. Toxicity pathway focused gene expression profiling of PEI-based polymers for pulmonary applications. Mol Pharm 2010;7:727-37.
181. Kwon EJ, Liong S, Pun SH. A truncated HGP peptide sequence that retains endosomolytic activity and improves gene delivery efficiencies. Mol Pharm 2010;7:1260-5.
182. Kwon EJ, Bergen JM, Pun SH. Application of an HIV gp41-derived peptide for enhanced intracellular trafficking of synthetic gene and siRNA delivery vehicles. Bioconjug Chem 2008;19:920-7.

183. Wagner E, Plank C, Zatloukal K, Cotten M, Birnstiel ML. Influenza virus hemagglutinin HA-2 N-terminal fusogenic peptides augment gene transfer by transferrin-polylysine-DNA complexes: toward a synthetic virus-like gene-transfer vehicle. Proc Natl Acad Sci U S A 1992;89:7934-8.
184. Kumar S, Aaron J, Sokolov K. Directional conjugation of antibodies to nanoparticles for synthesis of multiplexed optical contrast agents with both delivery and targeting moieties. Nat Protoc 2008;3:314-20.
185. Plank C, Oberhauser B, Mechtler K, Koch C, Wagner E. The influence of endosome-disruptive peptides on gene transfer using synthetic virus-like gene transfer systems. J Biol Chem 1994;269:12918-24.
186. Wadia JS, Stan RV, Dowdy SF. Transducible TAT-HA fusogenic peptide enhances escape of TAT-fusion proteins after lipid raft macropinocytosis. Nat Med 2004;10:310-5.
187. Lewin M, Carlesso N, Tung CH, et al. Tat peptide-derivatized magnetic nanoparticles allow in vivo tracking and recovery of progenitor cells. Nat Biotechnol 2000;18:410-4.
188. Lo SL, Wang S. An endosomolytic Tat peptide produced by incorporation of histidine and cysteine residues as a nonviral vector for DNA transfection. Biomaterials 2008;29:2408-14.
189. Kwon EJ, Bergen JM, Park IK, Pun SH. Peptide-modified vectors for nucleic acid delivery to neurons. J Control Release 2008;132:230-5.
190. Kamper N, Day PM, Nowak T, et al. A membrane-destabilizing peptide in capsid protein L2 is required for egress of papillomavirus genomes from endosomes. J Virol 2006;80:759-68.
191. Li W, Nicol F, Szoka FC, Jr. GALA: a designed synthetic pH-responsive amphipathic peptide with applications in drug and gene delivery. Adv Drug Deliv Rev 2004;56:967-85.
192. Kakudo T, Chaki S, Futaki S, et al. Transferrin-modified liposomes equipped with a pH-sensitive fusogenic peptide: an artificial viral-like delivery system. Biochemistry 2004;43:5618-28.
193. Sasaki K, Kogure K, Chaki S, et al. An artificial virus-like nano carrier system: enhanced endosomal escape of nanoparticles via synergistic action of pH-sensitive fusogenic peptide derivatives. Anal Bioanal Chem 2008;391:2717-27.
194. Wyman TB, Nicol F, Zelphati O, Scaria PV, Plank C, Szoka FC, Jr. Design, synthesis, and characterization of a cationic peptide that binds to nucleic acids and permeabilizes bilayers. Biochemistry 1997;36:3008-17.
195. Lee H, Jeong JH, Park TG. A new gene delivery formulation of polyethylenimine/DNA complexes coated with PEG conjugated fusogenic peptide. J Control Release 2001;76:183-92.
196. Min SH, Lee DC, Lim MJ, et al. A composite gene delivery system consisting of polyethylenimine and an amphipathic peptide KALA. J Gene Med 2006;8:1425-34.
197. Heitz F, Morris MC, Divita G. Twenty years of cell-penetrating peptides: from molecular mechanisms to therapeutics. Br J Pharmacol 2009;157:195-206.
198. Uhlir A. Electrolytic Shaping of Germanium and Silicon. Bell System Technical Journal 1956;35:333-47.

199. Watanabe YS, T. Application of a thinck anode film to semiconductor devices. Review of the Electrical Communications Laboratories 1971;19:899.
200. Canham LT. Silicon quantum wire array fabrication by electrochemical and chemical dissolution of wafers. Applied Physics Letters 1990;57:1046-8.
201. Canham LT. Bioactive silicon structure fabrication through nanoetching techniques. Advanced Materials 1995;7:1033-7.
202. Makila E, Ferreira MP, Kivela H, et al. Confinement effects on drugs in thermally hydrocarbonized porous silicon. Langmuir 2014;30:2196-205.
203. Anglin EJ, Cheng L, Freeman WR, Sailor MJ. Porous silicon in drug delivery devices and materials. Adv Drug Deliv Rev 2008;60:1266-77.
204. Xu W, Thapa R, Liu D, et al. Smart Porous Silicon Nanoparticles with Polymeric Coatings for Sequential Combination Therapy. Mol Pharm 2015;12:4038-47.
205. Wang CF, Makila EM, Kaasalainen MH, et al. Copper-free azide-alkyne cycloaddition of targeting peptides to porous silicon nanoparticles for intracellular drug uptake. Biomaterials 2014;35:1257-66.
206. Salonen J, Lehto V-P. Fabrication and chemical surface modification of mesoporous silicon for biomedical applications. Chemical Engineering Journal 2008;137:162-72.
207. Riikonen J, Salomaki M, van Wonderen J, et al. Surface chemistry, reactivity, and pore structure of porous silicon oxidized by various methods. Langmuir 2012;28:10573-83.
208. Frotscher U, Rossow U, Ebert M, et al. Investigation of different oxidation processes for porous silicon studied by spectroscopic ellipsometry. Thin Solid Films 1996;276:36-9.
209. Halimaoui A, Oules C, Bomchil G, et al. Electroluminescence in the visible range during anodic oxidation of porous silicon films. Applied Physics Letters 1991;59:304-6.
210. Salonen J, Lehto V-P, Laine E. Thermal oxidation of free-standing porous silicon films. Applied Physics Letters 1997;70:637-9.
211. Mawhinney DB, Glass JA, Yates JT. FTIR Study of the Oxidation of Porous Silicon. The Journal of Physical Chemistry B 1997;101:1202-6.
212. Santos HA, Riikonen J, Salonen J, et al. In vitro cytotoxicity of porous silicon microparticles: effect of the particle concentration, surface chemistry and size. Acta Biomater 2010;6:2721-31.
213. Boukherroub R, Morin S, Wayner DDM, et al. Ideal Passivation of Luminescent Porous Silicon by Thermal, Noncatalytic Reaction with Alkenes and Aldehydes. Chemistry of Materials 2001;13:2002-11.
214. Buriak JM. Silicon-Carbon Bonds on Porous Silicon Surfaces. Advanced Materials 1999;11:265-7.
215. Salonen J, Laine E, Niinistö L. Thermal analysis of hydrosilylation of 1-dodecene on porous silicon surface. physica status solidi (a) 2003;197:246-50.
216. Bateman JE, Eagling RD, Worrall DR, Horrocks BR, Houlton A. Alkylation of Porous Silicon by Direct Reaction with Alkenes and Alkynes. Angewandte Chemie International Edition 1998;37:2683-5.
217. Salonen J, Björkqvist M, Laine E, Niinistö L. Stabilization of porous silicon surface by thermal decomposition of acetylene. Applied Surface Science 2004;225:389-94.

218. Salonen J, Laine E, Niinistö L. Thermal carbonization of porous silicon surface by acetylene. Journal of Applied Physics 2002;91:456-61.
219. Kovalainen M, Monkare J, Mäkila E, et al. Mesoporous silicon (PSi) for sustained peptide delivery: effect of psi microparticle surface chemistry on peptide YY3-36 release. Pharm Res 2012;29:837-46.
220. Jalkanen T, Makila E, Sakka T, Salonen J, Ogata YH. Thermally promoted addition of undecylenic acid on thermally hydrocarbonized porous silicon optical reflectors. Nanoscale Res Lett 2012;7:311.
221. Ferreira MP, Ranjan S, Correia AM, et al. In vitro and in vivo assessment of heart-homing porous silicon nanoparticles. Biomaterials 2016;94:93-104.
222. Correia A, Shahbazi MA, Makila E, et al. Cyclodextrin-Modified Porous Silicon Nanoparticles for Efficient Sustained Drug Delivery and Proliferation Inhibition of Breast Cancer Cells. ACS Appl Mater Interfaces 2015;7:23197-204.
223. Low SP, Voelcker NH, Canham LT, Williams KA. The biocompatibility of porous silicon in tissues of the eye. Biomaterials 2009;30:2873-80.
224. Tasciotti E, Godin B, Martinez JO, et al. Near-infrared imaging method for the in vivo assessment of the biodistribution of nanoporous silicon particles. Mol Imaging 2011;10:56-68.
225. Tolli MA, Ferreira MP, Kinnunen SM, et al. In vivo biocompatibility of porous silicon biomaterials for drug delivery to the heart. Biomaterials 2014;35:8394-405.
226. Riikonen J, Correia A, Kovalainen M, et al. Systematic in vitro and in vivo study on porous silicon to improve the oral bioavailability of celecoxib. Biomaterials 2015;52:44-55.
227. Shahbazi MA, Fernandez TD, Makila EM, et al. Surface chemistry dependent immunostimulative potential of porous silicon nanoplatforms. Biomaterials 2014;35:9224-35.
228. Sarparanta M, Makila E, Heikkila T, et al. (1)(8)F-labeled modified porous silicon particles for investigation of drug delivery carrier distribution in vivo with positron emission tomography. Mol Pharm 2011;8:1799-806.
229. Sarparanta M, Bimbo LM, Rytkonen J, et al. Intravenous delivery of hydrophobin-functionalized porous silicon nanoparticles: stability, plasma protein adsorption and biodistribution. Mol Pharm 2012;9:654-63.
230. Park JH, Gu L, von Maltzahn G, Ruoslahti E, Bhatia SN, Sailor MJ. Biodegradable luminescent porous silicon nanoparticles for in vivo applications. Nat Mater 2009;8:331-6.
231. Shrestha N, Shahbazi MA, Araujo F, et al. Chitosan-modified porous silicon microparticles for enhanced permeability of insulin across intestinal cell monolayers. Biomaterials 2014;35:7172-9.
232. Araujo F, Shrestha N, Shahbazi MA, et al. Microfluidic Assembly of a Multifunctional Tailorable Composite System Designed for Site Specific Combined Oral Delivery of Peptide Drugs. ACS Nano 2015;9:8291-302.
233. Jugdaohsingh R, Anderson SH, Tucker KL, et al. Dietary silicon intake and absorption. Am J Clin Nutr 2002;75:887-93.

234. Shabir Q, Pokale A, Loni A, et al. Medically Biodegradable Hydrogenated Amorphous Silicon Microspheres. Silicon 2011;3:173-6.
235. Anderson SHC, Elliott H, Wallis DJ, Canham LT, Powell JJ. Dissolution of different forms of partially porous silicon wafers under simulated physiological conditions. physica status solidi (a) 2003;197:331-5.
236. Godin B, Gu J, Serda RE, et al. Tailoring the degradation kinetics of mesoporous silicon structures through PEGylation. J Biomed Mater Res A 2010;94:1236-43.
237. Chiappini C, Liu X, Fakhoury JR, Ferrari M. Biodegradable porous silicon barcode nanowires with defined geometry. Adv Funct Mater 2010;20:2231-9.
238. McInnes SJ, Irani Y, Williams KA, Voelcker NH. Controlled drug delivery from composites of nanostructured porous silicon and poly(L-lactide). Nanomedicine (Lond) 2012;7:995-1016.
239. Kayahan E. The role of surface oxidation on luminescence degradation of porous silicon. Applied Surface Science 2011;257:4311-6.
240. Frohlich E. The role of surface charge in cellular uptake and cytotoxicity of medical nanoparticles. Int J Nanomedicine 2012;7:5577-91.
241. Huang X, Teng X, Chen D, Tang F, He J. The effect of the shape of mesoporous silica nanoparticles on cellular uptake and cell function. Biomaterials 2010;31:438-48.
242. Kulkarni SA, Feng SS. Effects of particle size and surface modification on cellular uptake and biodistribution of polymeric nanoparticles for drug delivery. Pharm Res 2013;30:2512-22.
243. Maxfield FR, McGraw TE. Endocytic recycling. Nat Rev Mol Cell Biol 2004;5:121-32.
244. Maeda Y, Pittella F, Nomoto T, et al. Fine-tuning of charge-conversion polymer structure for efficient endosomal escape of siRNA-loaded calcium phosphate hybrid micelles. Macromol Rapid Commun 2014;35:1211-5.
245. Pittella F, Zhang M, Lee Y, et al. Enhanced endosomal escape of siRNA-incorporating hybrid nanoparticles from calcium phosphate and PEG-block charge-conversional polymer for efficient gene knockdown with negligible cytotoxicity. Biomaterials 2011;32:3106-14.
246. Zhang M, Xu R, Xia X, et al. Polycation-functionalized nanoporous silicon particles for gene silencing on breast cancer cells. Biomaterials 2014;35:423-31.
247. Tong WY, Sweetman MJ, Marzouk ER, Fraser C, Kuchel T, Voelcker NH. Towards a subcutaneous optical biosensor based on thermally hydrocarbonised porous silicon. Biomaterials 2016;74:217-30.
248. Irani YD, Tian Y, Wang M, et al. A novel pressed porous silicon-polycaprolactone composite as a dual-purpose implant for the delivery of cells and drugs to the eye. Exp Eye Res 2015;139:123-31.
249. Balasubramanian V, Correia A, Zhang H, et al. Biomimetic Engineering Using Cancer Cell Membranes for Designing Compartmentalized Nanoreactors with Organelle-Like Functions. Adv Mater 2017;29.
250. Wang CF, Sarparanta MP, Makila EM, et al. Multifunctional porous silicon nanoparticles for cancer theranostics. Biomaterials 2015;48:108-18.
251. Joo J, Liu X, Kotamraju VR, Ruoslahti E, Nam Y, Sailor MJ. Gated Luminescence Imaging of Silicon Nanoparticles. ACS Nano 2015;9:6233-41.

252. Santos HA. Chemotherapy with Porous Silicon. In: Canham L, ed. Handbook of Porous Silicon. Cham: Springer International Publishing; 2016:1-15.
253. Haidary SM, Corcoles EP, Ali NK. Nanoporous Silicon as Drug Delivery Systems for Cancer Therapies. Journal of Nanomaterials 2012.
254. Fontana F, Shahbazi MA, Liu D, et al. Multistaged Nanovaccines Based on Porous Silicon@Acetalated Dextran@Cancer Cell Membrane for Cancer Immunotherapy. Adv Mater 2017;29.
255. Bauleth-Ramos T, Shahbazi MA, Liu DF, et al. Nutlin-3a and Cytokine Co-loaded Spermine-Modified Acetalated Dextran Nanoparticles for Cancer Chemo-Immunotherapy. Advanced Functional Materials 2017;27.
256. Shahbazi M-A, Shrestha N, Mäkilä E, et al. A prospective cancer chemo-immunotherapy approach mediated by synergistic CD326 targeted porous silicon nanovectors. Nano Research 2015;8:1505-21.
257. Shrestha N, Shahbazi MA, Araujo F, et al. Multistage pH-responsive mucoadhesive nanocarriers prepared by aerosol flow reactor technology: A controlled dual protein-drug delivery system. Biomaterials 2015;68:9-20.
258. Araujo F, Shrestha N, Shahbazi MA, et al. The impact of nanoparticles on the mucosal translocation and transport of GLP-1 across the intestinal epithelium. Biomaterials 2014;35:9199-207.
259. Ferreira MPA, Ranjan S, Kinnunen S, et al. Drug-Loaded Multifunctional Nanoparticles Targeted to the Endocardial Layer of the Injured Heart Modulate Hypertrophic Signaling. Small 2017.
260. Zhang H, Liu D, Shahbazi MA, et al. Fabrication of a multifunctional nano-in-micro drug delivery platform by microfluidic templated encapsulation of porous silicon in polymer matrix. Adv Mater 2014;26:4497-503.
261. Zhang F, Correia A, Makila E, et al. Receptor-Mediated Surface Charge Inversion Platform Based on Porous Silicon Nanoparticles for Efficient Cancer Cell Recognition and Combination Therapy. ACS Appl Mater Interfaces 2017;9:10034-46.
262. Janoniene A, Liu Z, Baranauskiene L, et al. A Versatile Carbonic Anhydrase IX Targeting Ligand-Functionalized Porous Silicon Nanoplatform for Dual Hypoxia Cancer Therapy and Imaging. ACS Appl Mater Interfaces 2017;9:13976-87.
263. Liu ZH, Balasubramanian V, Bhat C, et al. Quercetin-Based Modified Porous Silicon Nanoparticles for Enhanced Inhibition of Doxorubicin-Resistant Cancer Cells. Advanced Healthcare Materials 2017;6.
264. Liu D, Zhang H, Herranz-Blanco B, et al. Microfluidic assembly of monodisperse multistage pH-responsive polymer/porous silicon composites for precisely controlled multi-drug delivery. Small 2014;10:2029-38.
265. Herranz-Blanco B, Liu DF, Makila E, et al. On-Chip Self-Assembly of a Smart Hybrid Nanocomposite for Antitumoral Applications. Adv Funct Mater 2015;25:1488-97.
266. Tamarov K, Xu W, Osminkina L, et al. Temperature responsive porous silicon nanoparticles for cancer therapy - spatiotemporal triggering through infrared and radiofrequency electromagnetic heating. J Control Release 2016;241:220-8.

267. Wang CF, Makila EM, Kaasalainen MH, et al. Dual-drug delivery by porous silicon nanoparticles for improved cellular uptake, sustained release, and combination therapy. Acta Biomater 2015;16:206-14.
268. Liu D, Zhang H, Makila E, et al. Microfluidic assisted one-step fabrication of porous silicon@acetalated dextran nanocomposites for precisely controlled combination chemotherapy. Biomaterials 2015;39:249-59.
269. Secret E, Smith K, Dubljevic V, et al. Antibody-functionalized porous silicon nanoparticles for vectorization of hydrophobic drugs. Adv Healthc Mater 2013;2:718-27.
270. Cifuentes-Rius A, Ivask A, Sporleder E, et al. Dual-Action Cancer Therapy with Targeted Porous Silicon Nanovectors. Small 2017;13.
271. Kinnari PJ, Hyvonen ML, Makila EM, et al. Tumour homing peptide-functionalized porous silicon nanovectors for cancer therapy. Biomaterials 2013;34:9134-41.
272. Gu L, Ruff LE, Qin Z, Corr M, Hedrick SM, Sailor MJ. Multivalent porous silicon nanoparticles enhance the immune activation potency of agonistic CD40 antibody. Adv Mater 2012;24:3981-7.
273. Shahbazi MA, Shrestha N, Makila E, et al. A prospective cancer chemo-immunotherapy approach mediated by synergistic CD326 targeted porous silicon nanovectors. Nano Res 2015;8:1505-21.
274. Xiao L, Gu L, Howell SB, Sailor MJ. Porous silicon nanoparticle photosensitizers for singlet oxygen and their phototoxicity against cancer cells. ACS Nano 2011;5:3651-9.
275. Secret E, Maynadier M, Gallud A, et al. Anionic porphyrin-grafted porous silicon nanoparticles for photodynamic therapy. Chem Commun (Camb) 2013;49:4202-4.
276. Secret E, Maynadier M, Gallud A, et al. Two-photon excitation of porphyrin-functionalized porous silicon nanoparticles for photodynamic therapy. Adv Mater 2014;26:7643-8.
277. Hong C, Lee J, Zheng H, Hong SS, Lee C. Porous silicon nanoparticles for cancer photothermotherapy. Nanoscale Res Lett 2011;6:321.
278. Hong C, Lee C. In vitro cell tests of pancreatic malignant tumor cells by photothermotherapy based on DMSO porous silicon colloids. Lasers Med Sci 2014;29:221-3.
279. Xia B, Wang B, Shi J, et al. Photothermal and biodegradable polyaniline/porous silicon hybrid nanocomposites as drug carriers for combined chemo-photothermal therapy of cancer. Acta Biomater 2017;51:197-208.
280. Zhang H, Zhu Y, Qu L, et al. Gold Nanorods Conjugated Porous Silicon Nanoparticles Encapsulated in Calcium Alginate Nano Hydrogels Using Microemulsion Templates. Nano Lett 2018;18:1448-53.
281. Xia B, Zhang Q, Shi J, Li J, Chen Z, Wang B. Co-loading of photothermal agents and anticancer drugs into porous silicon nanoparticles with enhanced chemo-photothermal therapeutic efficacy to kill multidrug-resistant cancer cells. Colloids Surf B Biointerfaces 2018;164:291-8.
282. Wan Y, Apostolou S, Dronov R, Kuss B, Voelcker NH. Cancer-targeting siRNA delivery from porous silicon nanoparticles. Nanomedicine (Lond) 2014;9:2309-21.

283. Gu L, Hall DJ, Qin Z, et al. In vivo time-gated fluorescence imaging with biodegradable luminescent porous silicon nanoparticles. Nat Commun 2013;4:2326.
284. Kim D, Kang J, Wang T, et al. Two-Photon In Vivo Imaging with Porous Silicon Nanoparticles. Adv Mater 2017;29.
285. Kallinen AM, Sarparanta MP, Liu D, et al. In vivo evaluation of porous silicon and porous silicon solid lipid nanocomposites for passive targeting and imaging. Mol Pharm 2014;11:2876-86.
286. Sinha S, Tong WY, Williamson NH, et al. Novel Gd-Loaded Silicon Nanohybrid: A Potential Epidermal Growth Factor Receptor Expressing Cancer Cell Targeting Magnetic Resonance Imaging Contrast Agent. ACS Appl Mater Interfaces 2017;9:42601-11.
287. Sviridov AP, Osminkina LA, Kharin AY, et al. Cytotoxicity control of silicon nanoparticles by biopolymer coating and ultrasound irradiation for cancer theranostic applications. Nanotechnology 2017;28:105102.
288. De Rosa E, Chiappini C, Fan DM, Liu XW, Ferrari M, Tasciotti E. Agarose Surface Coating Influences Intracellular Accumulation and Enhances Payload Stability of a Nano-delivery System. Pharm Res-Dordr 2011;28:1520-30.
289. Huotari A, Xu W, Monkare J, et al. Effect of surface chemistry of porous silicon microparticles on glucagon-like peptide-1 (GLP-1) loading, release and biological activity. Int J Pharm 2013;454:67-73.
290. Kilpelainen M, Monkare J, Vlasova MA, et al. Nanostructured porous silicon microparticles enable sustained peptide (Melanotan II) delivery. Eur J Pharm Biopharm 2011;77:20-5.
291. Kilpelainen M, Riikonen J, Vlasova MA, et al. In vivo delivery of a peptide, ghrelin antagonist, with mesoporous silicon microparticles. J Control Release 2009;137:166-70.
292. Kovalainen M, Monkare J, Kaasalainen M, et al. Development of porous silicon nanocarriers for parenteral peptide delivery. Mol Pharm 2013;10:353-9.
293. McInnes SJ, Voelcker NH. Porous silicon-based nanostructured microparticles as degradable supports for solid-phase synthesis and release of oligonucleotides. Nanoscale Res Lett 2012;7:385.
294. Rytkonen J, Arukuusk P, Xu W, et al. Porous silicon-cell penetrating peptide hybrid nanocarrier for intracellular delivery of oligonucleotides. Mol Pharm 2014;11:382-90.
295. Tanaka T, Mangala LS, Vivas-Mejia PE, et al. Sustained small interfering RNA delivery by mesoporous silicon particles. Cancer Res 2010;70:3687-96.
296. Shen H, Sun T, Ferrari M. Nanovector delivery of siRNA for cancer therapy. Cancer Gene Ther 2012;19:367-73.
297. Xu R, Huang Y, Mai J, et al. Multistage vectored siRNA targeting ataxia-telangiectasia mutated for breast cancer therapy. Small 2013;9:1799-808.
298. Hasanzadeh Kafshgari M, Alnakhli M, Delalat B, et al. Small interfering RNA delivery by polyethylenimine-functionalised porous silicon nanoparticles. Biomater Sci 2015;3:1555-65.

299. Salonen J, Laitinen L, Kaukonen AM, et al. Mesoporous silicon microparticles for oral drug delivery: loading and release of five model drugs. J Control Release 2005;108:362-74.
300. Prestidge CA, Barnes TJ. 15 - Nanoporous silicon to enhance drug solubility A2 - Santos, Hélder A. Porous Silicon for Biomedical Applications: Woodhead Publishing; 2014:356-73.
301. Lehto VP, Riikonen J. 14 - Drug loading and characterization of porous silicon materials A2 - Santos, Hélder A. Porous Silicon for Biomedical Applications: Woodhead Publishing; 2014:337-55.
302. Limnell T, Riikonen J, Salonen J, et al. Surface chemistry and pore size affect carrier properties of mesoporous silicon microparticles. Int J Pharm 2007;343:141-7.
303. Schwartz MP, Cunin F, Cheung RW, Sailor MJ. Chemical modification of silicon surfaces for biological applications. Phys Status Solidi A 2005;202:1380-4.
304. Wu EC, Park JH, Park J, Segal E, Cunin F, Sailor MJ. Oxidation-triggered release of fluorescent molecules or drugs from mesoporous Si microparticles. ACS Nano 2008;2:2401-9.
305. Fry NL, Boss GR, Sailor MJ. Oxidation-Induced Trapping of Drugs in Porous Silicon Microparticles. Chem Mater 2014;26:2758-64.
306. Kaukonen AM, Laitinen L, Salonen J, et al. Enhanced in vitro permeation of furosemide loaded into thermally carbonized mesoporous silicon (TCPSi) microparticles. Eur J Pharm Biopharm 2007;66:348-56.
307. Liu DF, Makila E, Zhang HB, et al. Nanostructured Porous Silicon-Solid Lipid Nanocomposite: Towards Enhanced Cytocompatibility and Stability, Reduced Cellular Association, and Prolonged Drug Release. Advanced Functional Materials 2013;23:1893-902.
308. Bimbo LM, Makila E, Laaksonen T, et al. Drug permeation across intestinal epithelial cells using porous silicon nanoparticles. Biomaterials 2011;32:2625-33.
309. Heikkila T, Salonen J, Tuura J, et al. Evaluation of mesoporous TCPSi, MCM-41, SBA-15, and TUD-1 materials as API carriers for oral drug delivery. Drug Deliv 2007;14:337-47.
310. Wang K, Wang H, Cheng YB. Synthesis of nanostructured silicon carbide spheres from mesoporous C-SiO2 nanocomposites. Chem Commun (Camb) 2010;46:303-5.
311. Kinnari P, Makila E, Heikkila T, Salonen J, Hirvonen J, Santos HA. Comparison of mesoporous silicon and non-ordered mesoporous silica materials as drug carriers for itraconazole. Int J Pharm 2011;414:148-56.
312. Vale N, Makila E, Salonen J, Gomes P, Hirvonen J, Santos HA. New times, new trends for ethionamide: In vitro evaluation of drug-loaded thermally carbonized porous silicon microparticles. Eur J Pharm Biopharm 2012;81:314-23.
313. Bimbo LM, Denisova OV, Makila E, et al. Inhibition of influenza A virus infection in vitro by saliphenylhalamide-loaded porous silicon nanoparticles. ACS Nano 2013;7:6884-93.
314. Park JS, Kinsella JM, Jandial DD, Howell SB, Sailor MJ. Cisplatin-loaded porous Si microparticles capped by electroless deposition of platinum. Small 2011;7:2061-9.

315. Xue M, Zhong X, Shaposhnik Z, et al. pH-Operated mechanized porous silicon nanoparticles. J Am Chem Soc 2011;133:8798-801.
316. McInnes SJ, Szili EJ, Al-Bataineh SA, et al. Fabrication and Characterization of a Porous Silicon Drug Delivery System with an Initiated Chemical Vapor Deposition Temperature-Responsive Coating. Langmuir 2016;32:301-8.
317. Bonanno LM, Segal E. Nanostructured porous silicon-polymer-based hybrids: from biosensing to drug delivery. Nanomedicine (Lond) 2011;6:1755-70.
318. Hernandez-Montelongo J, Naveas N, Degoutin S, et al. Porous silicon-cyclodextrin based polymer composites for drug delivery applications. Carbohydr Polym 2014;110:238-52.
319. Liu D, Herranz-Blanco B, Makila E, et al. Microfluidic templated mesoporous silicon-solid lipid microcomposites for sustained drug delivery. ACS Appl Mater Interfaces 2013;5:12127-34.
320. Herranz-Blanco B, Arriaga LR, Makila E, et al. Microfluidic assembly of multistage porous silicon-lipid vesicles for controlled drug release. Lab Chip 2014;14:1083-6.
321. Herranz-Blanco B, Liu D, Mäkilä E, et al. On-Chip Self-Assembly of a Smart Hybrid Nanocomposite for Antitumoral Applications. Advanced Functional Materials 2015;25:1488-97.
322. Kong F, Zhang X, Zhang H, et al. Inhibition of Multidrug Resistance of Cancer Cells by Co-Delivery of DNA Nanostructures and Drugs Using Porous Silicon Nanoparticles@Giant Liposomes. Advanced Functional Materials 2015;25:3330-40.
323. Chiappini C, Tasciotti E, Serda RE, Brousseau L, Liu X, Ferrari M. Mesoporous silicon particles as intravascular drug delivery vectors: fabrication, in-vitro, and in-vivo assessments. physica status solidi (c) 2011;8:1826-32.
324. Shen H, Rodriguez-Aguayo C, Xu R, et al. Enhancing chemotherapy response with sustained EphA2 silencing using multistage vector delivery. Clin Cancer Res 2013;19:1806-15.
325. Mann AP, Tanaka T, Somasunderam A, Liu X, Gorenstein DG, Ferrari M. E-selectin-targeted porous silicon particle for nanoparticle delivery to the bone marrow. Adv Mater 2011;23:H278-82.
326. Blanco E, Sangai T, Hsiao A, et al. Multistage delivery of chemotherapeutic nanoparticles for breast cancer treatment. Cancer Lett 2013;334:245-52.
327. Tasciotti E, Liu X, Bhavane R, et al. Mesoporous silicon particles as a multistage delivery system for imaging and therapeutic applications. Nat Nanotechnol 2008;3:151-7.
328. Gaur G, Koktysh DS, Weiss SM. Immobilization of Quantum Dots in Nanostructured Porous Silicon Films: Characterizations and Signal Amplification for Dual-Mode Optical Biosensing. Advanced Functional Materials 2013;23:3604-14.
329. Shen H, You J, Zhang G, et al. Cooperative, nanoparticle-enabled thermal therapy of breast cancer. Adv Healthc Mater 2012;1:84-9.
330. Gu L, Park JH, Duong KH, Ruoslahti E, Sailor MJ. Magnetic luminescent porous silicon microparticles for localized delivery of molecular drug payloads. Small 2010;6:2546-52.

331. Kinsella JM, Ananda S, Andrew JS, et al. Enhanced magnetic resonance contrast of Fe(3)O(4) nanoparticles trapped in a porous silicon nanoparticle host. Adv Mater 2011;23:H248-53.
332. Schneider A, Picart C, Senger B, Schaaf P, Voegel JC, Frisch B. Layer-by-layer films from hyaluronan and amine-modified hyaluronan. Langmuir 2007;23:2655-62.
333. Novo L, Rizzo LY, Golombek SK, et al. Decationized polyplexes as stable and safe carrier systems for improved biodistribution in systemic gene therapy. J Control Release 2014;195:162-75.
334. Shatsberg Z, Zhang X, Ofek P, et al. Functionalized nanogels carrying an anticancer microRNA for glioblastoma therapy. J Control Release 2016;239:159-68.
335. Tappertzhofen K, Weiser F, Montermann E, Reske-Kunz A, Bros M, Zentel R. Poly-L-Lysine-Poly[HPMA] Block Copolymers Obtained by RAFT Polymerization as Polyplex-Transfection Reagents with Minimal Toxicity. Macromol Biosci 2015;15:1159-73.
336. Brunauer S, Emmett PH, Teller E. Adsorption of Gases in Multimolecular Layers. Journal of the American Chemical Society 1938;60:309-19.
337. Hoyle CE, Lowe AB, Bowman CN. Thiol-click chemistry: a multifaceted toolbox for small molecule and polymer synthesis. Chem Soc Rev 2010;39:1355-87.
338. Yu T, Malugin A, Ghandehari H. Impact of silica nanoparticle design on cellular toxicity and hemolytic activity. ACS Nano 2011;5:5717-28.
339. Lynch I, Salvati A, Dawson KA. Protein-nanoparticle interactions: What does the cell see? Nat Nanotechnol 2009;4:546-7.
340. Karmali PP, Simberg D. Interactions of nanoparticles with plasma proteins: implication on clearance and toxicity of drug delivery systems. Expert Opin Drug Deliv 2011;8:343-57.
341. Blanco E, Shen H, Ferrari M. Principles of nanoparticle design for overcoming biological barriers to drug delivery. Nat Biotechnol 2015;33:941-51.
342. Swain S, Sahu PK, Beg S, Babu SM. Nanoparticles for Cancer Targeting: Current and Future Directions. Curr Drug Deliv 2016;13:1290-302.
343. Studart AR, Amstad E, Gauckler LJ. Colloidal stabilization of nanoparticles in concentrated suspensions. Langmuir 2007;23:1081-90.
344. Ayala V, Herrera AP, Latorre-Esteves M, Torres-Lugo M, Rinaldi C. Effect of surface charge on the colloidal stability and in vitro uptake of carboxymethyl dextran-coated iron oxide nanoparticles. J Nanopart Res 2013;15:1874.
345. French RA, Jacobson AR, Kim B, Isley SL, Penn RL, Baveye PC. Influence of ionic strength, pH, and cation valence on aggregation kinetics of titanium dioxide nanoparticles. Environ Sci Technol 2009;43:1354-9.
346. Almeida PV, Shahbazi MA, Makila E, et al. Amine-modified hyaluronic acid-functionalized porous silicon nanoparticles for targeting breast cancer tumors. Nanoscale 2014;6:10377-87.
347. Haxaire K, Marechal Y, Milas M, Rinaudo M. Hydration of polysaccharide hyaluronan observed by IR spectrometry. I. Preliminary experiments and band assignments. Biopolymers 2003;72:10-20.

348. Liut G, Cui K. Carboxyl-reduced hyaluronan: preparation and enzymatic assay. Carbohydr Res 1996;285:167-72.
349. Aggarwal P, Hall JB, McLeland CB, Dobrovolskaia MA, McNeil SE. Nanoparticle interaction with plasma proteins as it relates to particle biodistribution, biocompatibility and therapeutic efficacy. Adv Drug Deliv Rev 2009;61:428-37.
350. Wang LS, Wu LC, Lu SY, et al. Biofunctionalized phospholipid-capped mesoporous silica nanoshuttles for targeted drug delivery: improved water suspensibility and decreased nonspecific protein binding. ACS Nano 2010;4:4371-9.
351. Upadhyay KK, Bhatt AN, Castro E, et al. In vitro and in vivo evaluation of docetaxel loaded biodegradable polymersomes. Macromol Biosci 2010;10:503-12.
352. Upadhyay KK, Mishra AK, Chuttani K, et al. The in vivo behavior and antitumor activity of doxorubicin-loaded poly(gamma-benzyl l-glutamate)-block-hyaluronan polymersomes in Ehrlich ascites tumor-bearing BalB/c mice. Nanomedicine 2012;8:71-80.
353. Peer D, Margalit R. Tumor-targeted hyaluronan nanoliposomes increase the antitumor activity of liposomal Doxorubicin in syngeneic and human xenograft mouse tumor models. Neoplasia 2004;6:343-53.
354. Veiseh M, Turley EA. Hyaluronan metabolism in remodeling extracellular matrix: probes for imaging and therapy of breast cancer. Integr Biol (Camb) 2011;3:304-15.
355. Chan CL, Majzoub RN, Shirazi RS, et al. Endosomal escape and transfection efficiency of PEGylated cationic liposome-DNA complexes prepared with an acid-labile PEG-lipid. Biomaterials 2012;33:4928-35.
356. Ke JH, Young TH. Multilayered polyplexes with the endosomal buffering polycation in the core and the cell uptake-favorable polycation in the outer layer for enhanced gene delivery. Biomaterials 2010;31:9366-72.
357. Rennert R, Wespe C, Beck-Sickinger AG, Neundorf I. Developing novel hCT derived cell-penetrating peptides with improved metabolic stability. Biochim Biophys Acta 2006;1758:347-54.
358. Haas AK, Maisel D, Adelmann J, von Schwerin C, Kahnt I, Brinkmann U. Human-protein-derived peptides for intracellular delivery of biomolecules. Biochem J 2012;442:583-93.
359. Huhn D, Kantner K, Geidel C, et al. Polymer-coated nanoparticles interacting with proteins and cells: focusing on the sign of the net charge. ACS Nano 2013;7:3253-63.
360. Bhattacharyya S, Wang H, Ducheyne P. Polymer-coated mesoporous silica nanoparticles for the controlled release of macromolecules. Acta Biomater 2012;8:3429-35.
361. Appelhans D, Komber H, Quadir MA, et al. Hyperbranched PEI with various oligosaccharide architectures: synthesis, characterization, ATP complexation, and cellular uptake properties. Biomacromolecules 2009;10:1114-24.
362. Lee SY, Huh MS, Lee S, et al. Stability and cellular uptake of polymerized siRNA (poly-siRNA)/polyethylenimine (PEI) complexes for efficient gene silencing. J Control Release 2010;141:339-46.

363. Aravindan L, Bicknell KA, Brooks G, Khutoryanskiy VV, Williams AC. Effect of acyl chain length on transfection efficiency and toxicity of polyethylenimine. Int J Pharm 2009;378:201-10.
364. Florea BI, Meaney C, Junginger HE, Borchard G. Transfection efficiency and toxicity of polyethylenimine in differentiated Calu-3 and nondifferentiated COS-1 cell cultures. AAPS PharmSci 2002;4:E12.
365. Shahbazi MA, Almeida PV, Makila EM, et al. Augmented cellular trafficking and endosomal escape of porous silicon nanoparticles via zwitterionic bilayer polymer surface engineering. Biomaterials 2014;35:7488-500.
366. Ahmed M, Narain R. Cell line dependent uptake and transfection efficiencies of PEI-anionic glycopolymer systems. Biomaterials 2013;34:4368-76.
367. Fuller JE, Zugates GT, Ferreira LS, et al. Intracellular delivery of core-shell fluorescent silica nanoparticles. Biomaterials 2008;29:1526-32.
368. Shahbazi MA, Almeida PV, Makila E, et al. Poly(methyl vinyl ether-alt-maleic acid)-functionalized porous silicon nanoparticles for enhanced stability and cellular internalization. Macromol Rapid Commun 2014;35:624-9.
369. Irache JM, Huici M, Konecny M, Espuelas S, Campanero MA, Arbos P. Bioadhesive properties of Gantrez nanoparticles. Molecules 2005;10:126-45.
370. Cho EC, Xie J, Wurm PA, Xia Y. Understanding the role of surface charges in cellular adsorption versus internalization by selectively removing gold nanoparticles on the cell surface with a I2/KI etchant. Nano Lett 2009;9:1080-4.
371. Villanueva A, Canete M, Roca AG, et al. The influence of surface functionalization on the enhanced internalization of magnetic nanoparticles in cancer cells. Nanotechnology 2009;20:115103.
372. Wilhelm C, Billotey C, Roger J, Pons JN, Bacri JC, Gazeau F. Intracellular uptake of anionic superparamagnetic nanoparticles as a function of their surface coating. Biomaterials 2003;24:1001-11.
373. Patil S, Sandberg A, Heckert E, Self W, Seal S. Protein adsorption and cellular uptake of cerium oxide nanoparticles as a function of zeta potential. Biomaterials 2007;28:4600-7.
374. Wang D, Huang J, Wang X, et al. The eradication of breast cancer cells and stem cells by 8-hydroxyquinoline-loaded hyaluronan modified mesoporous silica nanoparticle-supported lipid bilayers containing docetaxel. Biomaterials 2013;34:7662-73.
375. Bondar OV, Sagitova AV, Badeev YV, Shtyrlin YG, Abdullin TI. Conjugation of succinic acid to non-ionogenic amphiphilic polymers modulates their interaction with cell plasma membrane and reduces cytotoxic activity. Colloids Surf B Biointerfaces 2013;109:204-11.
376. Tu J, Wang T, Shi W, et al. Multifunctional ZnPc-loaded mesoporous silica nanoparticles for enhancement of photodynamic therapy efficacy by endolysosomal escape. Biomaterials 2012;33:7903-14.
377. Takemoto H, Miyata K, Hattori S, et al. Acidic pH-responsive siRNA conjugate for reversible carrier stability and accelerated endosomal escape with reduced IFNalpha-associated immune response. Angew Chem Int Ed Engl 2013;52:6218-21.

378. Rozema DB, Ekena K, Lewis DL, Loomis AG, Wolff JA. Endosomolysis by masking of a membrane-active agent (EMMA) for cytoplasmic release of macromolecules. Bioconjug Chem 2003;14:51-7.
379. Alexander C. Temperature- and pH-responsive smart polymers for gene delivery. Expert Opin Drug Deliv 2006;3:573-81.
380. Barros S, Mencia N, Rodriguez L, et al. The redox state of cytochrome c modulates resistance to methotrexate in human MCF7 breast cancer cells. PLoS One 2013;8:e63276.
381. Tian H, Cronstein BN. Understanding the mechanisms of action of methotrexate: implications for the treatment of rheumatoid arthritis. Bull NYU Hosp Jt Dis 2007;65:168-73.
382. Genestier L, Paillot R, Quemeneur L, Izeradjene K, Revillard JP. Mechanisms of action of methotrexate. Immunopharmacology 2000;47:247-57.
383. Almeida PV, Shahbazi MA, Correia A, et al. A multifunctional nanocomplex for enhanced cell uptake, endosomal escape and improved cancer therapeutic effect. Nanomedicine (Lond) 2017.
384. Leitner VM, Walker GF, Bernkop-Schnurch A. Thiolated polymers: evidence for the formation of disulphide bonds with mucus glycoproteins. Eur J Pharm Biopharm 2003;56:207-14.
385. Islam MA, Park TE, Singh B, et al. Major degradable polycations as carriers for DNA and siRNA. J Control Release 2014;193:74-89.
386. Kwon IK, Lee SC, Han B, Park K. Analysis on the current status of targeted drug delivery to tumors. J Control Release 2012;164:108-14.
387. Wilhelm SM, Carter C, Tang L, et al. BAY 43-9006 exhibits broad spectrum oral antitumor activity and targets the RAF/MEK/ERK pathway and receptor tyrosine kinases involved in tumor progression and angiogenesis. Cancer Res 2004;64:7099-109.
388. Sancenon F, Pascual L, Oroval M, Aznar E, Martinez-Manez R. Gated Silica Mesoporous Materials in Sensing Applications. ChemistryOpen 2015;4:418-37.
389. Wang X, Cui M, Zhou H, Zhang S. DNA-hybrid-gated functional mesoporous silica for sensitive DNA methyltransferase SERS detection. Chem Commun (Camb) 2015;51:13983-5.
390. Zhang B, Luo Z, Liu J, Ding X, Li J, Cai K. Cytochrome c end-capped mesoporous silica nanoparticles as redox-responsive drug delivery vehicles for liver tumor-targeted triplex therapy in vitro and in vivo. J Control Release 2014;192:192-201.
391. Gokmen MT, Brassinne J, Prasath RA, Du Prez FE. Revealing the nature of thio-click reactions on the solid phase. Chem Commun (Camb) 2011;47:4652-4.
392. Shahbazi MA, Almeida PV, Correia A, et al. Intracellular responsive dual delivery by endosomolytic polyplexes carrying DNA anchored porous silicon nanoparticles. J Control Release 2017;249:111-22.
393. Xia T, Kovochich M, Liong M, et al. Polyethyleneimine coating enhances the cellular uptake of mesoporous silica nanoparticles and allows safe delivery of siRNA and DNA constructs. ACS Nano 2009;3:3273-86.

394. Dempsey C, Lee I, Cowan KR, Suh J. Coating barium titanate nanoparticles with polyethylenimine improves cellular uptake and allows for coupled imaging and gene delivery. Colloids Surf B Biointerfaces 2013;112:108-12.
395. Suchaoin W, Bonengel S, Griessinger JA, et al. Novel bioadhesive polymers as intra-articular agents: Chondroitin sulfate-cysteine conjugates. Eur J Pharm Biopharm 2016;101:25-32.
396. Gamucci O, Bertero A, Malvindi MA, et al. Detection of fluorescent nanoparticle interactions with primary immune cell subpopulations by flow cytometry. J Vis Exp 2014.
397. Zucker RM, Daniel KM. Detection of TiO2 nanoparticles in cells by flow cytometry. Methods Mol Biol 2012;906:497-509.
398. Kumar A, Pandey AK, Singh SS, Shanker R, Dhawan A. A flow cytometric method to assess nanoparticle uptake in bacteria. Cytometry A 2011;79:707-12.
399. Shrestha R, Elsabahy M, Florez-Malaver S, Samarajeewa S, Wooley KL. Endosomal escape and siRNA delivery with cationic shell crosslinked knedel-like nanoparticles with tunable buffering capacities. Biomaterials 2012;33:8557-68.
400. Kim H, Kim WJ. Photothermally controlled gene delivery by reduced graphene oxide-polyethylenimine nanocomposite. Small 2014;10:117-26.
401. Wang J, Yang G, Guo X, Tang Z, Zhong Z, Zhou S. Redox-responsive polyanhydride micelles for cancer therapy. Biomaterials 2014;35:3080-90.
402. Hu H, Yuan W, Liu FS, Cheng G, Xu FJ, Ma J. Redox-responsive polycation-functionalized cotton cellulose nanocrystals for effective cancer treatment. ACS Appl Mater Interfaces 2015;7:8942-51.

Recent Publications in this Series

66/2017 Henri A. J. Puttonen
Neuropharmacological Properties of the Histaminergic System in the Zebrafish
67/2017 Mónica Ferreira
Multifunctional Nanoparticles for Targeted Drug Delivery and Imaging for Ischemic Myocardial Injury
68/2017 Prson Gautam
Chemical Systems Biology Studies of Triple Negative Breast Cancer Cell Lines
1/2018 Susanna Lallukka
Non-Alcoholic Fatty Liver Disease: The Role of Insulin Resistance, Inflammation and the PNPLA3 I148M Variant
2/2018 Anna Tikka
Characterization of ANGPTL3 Deficiency and Molecular Mechanisms of ANGPTL3 Deficiency-Induced Hypolipidemia
3/2018 Anna Parkkola
The Phenotype and Genotype of Children with Newly Diagnosed Type 1 Diabetes in Relation to Family History of Type 1 Diabetes and Other Autoimmune Diseases
4/2018 Erika Gucciardo
Mechanisms of Cell Invasion and Fibrovascular Complications in Cancer and Diabetic Retinopathy
5/2018 Maria Lume
Cellular Regulation of Glial Cell Line-Derived Neurotrophic Factor
6/2018 Jinghua Gui
BMP/Dpp Signaling and Epithelial Morphogenesis in *Drosophila* Development
7/2018 Petra Tauscher
Post-translational Regulation of TGF-β Signaling in *Drosophila* Development
8/2018 Agnieszka Szwajda
Bioinformatic Identification of Disease Driver Networks Using Functional Profiling Data
9/2018 Kärt Mätlik
Altering the 3'UTR to Increase Endogenous GDNF and BDNF Expression
10/2018 Arjen Gebraad
Tissue Engineering Approaches for the Treatment of Degenerated Intervertebral Discs
11/2018 Leena Arpalahti
The Proteasome-Associated Deubiquitinase UCHL5/UBH-4 in Proteasome Modulation and as a Prognostic Marker in Gastrointestinal Cancers
12/2018 Tiina Mattila
Airway Obstruction and Mortality
13/2018 Lauri Jouhi
Oropharyngael Cancer: Changing Management and the Role of Toll-like Receptors
14/2018 Jukka Saarinen
Non-linear Label-free Optical Imaging of Cells, Nanocrystal Cellular Uptake and Solid-State Analysis in Pharmaceutics
15/2018 Olena Santangeli
Sleep and Depression: Developmental and Molecular Mechanisms
16/2018 Shadia Rask
Diversity and Health in the Population: Findings on Russian, Somali and Kurdish Origin Populations in Finland
17/2018 Richa Gupta
Association and Interplay of Genetic and Epigenetic Variants in Smoking Behavior

Helsinki 2018 ISSN 2342-3161 ISBN 978-951-51-4149-1